universität wien

DISSERTATION

Titel der Dissertation

Artificial Biomimetic Sensor Materials for Folic Acid, its Metabolites and Phenyl Acetone

angestrebter akademischer Grad

Doktor der Naturwissenschaften (Dr. rer. nat.)

Verfasser:	M.Sc. Munawar Hussain
Matrikel-Nummer:	0713500
Dissertationsgebiet	Chemie
Betreuerin / Betreuer:	Ao. Univ. Prof. Peter A. Lieberzeit

Wien, 1. Juni 2011

Preface

This research has been done in the department of Chemical Sensors and Optical Molecular Spectroscopy from January 2009 to the present date under the supervision of *Ao. Univ. Prof. Peter A. Lieberzeit.* University of Vienna, Austria.

To My Family

Acknowledgements

I feel modest gratitude for honorable and praiseworthy research supervisor *Ao. Univ. Prof. Mag. Dr. Peter A. Lieberzeit* for providing exalted and noble ideas. The feedback and motivation are not merely a source of inspiration for this project, but launching pad for my future research. The practical knowledge along with theoretical concepts for developing artificial biomimetic sensing materials for chemical sensors shows his dedication and honesty to the field of science.

It would be dishonesty if the name of *O. Univ. Prof. Dr. Franz Ludwig Dickert,* would not be mentioned regarding his everlasting research experience. His assistance and guidance helped me removing the fundamental deficiencies, building problem solving approaches and creating ideas for practicing research independently.

I acknowledge the European Commission for the project of phenyl acetone imprinting that became the part of my thesis.

I acknowledge all the group fellows for valuable discussions about the research topics within the group. It was nice to talk with the people from different ethnics, cultures and regions of the world. Their affectionate and pleasant behavior made my stay in Austria a prodigious and awesome.

I thank the Higher Education Commission of Pakistan for financing my life expanses in Austria. Without the stipend from HEC, doing PhD from prestigious department of Uni-Wien would have remained a dream of my life. The role of Austrian Exchange Service (OeAD) regarding admission in Uni-Wien, stipend processing, visa and health insurance is appreciable.

My stay in Austria added a lot of honest friends in the list of my friendship. Although it is impossible to mention every one, yet for simplicity I would remember special ones from rainy Graz and blooming Vienna. Thanks to all the friends from Pakistan especially from my home town “FORT ABBAS”, their prayers were always a gratification source for me.

I have the strongest feelings for my dear ones, Naheed, Farhan, Noman and Farheen along with my mom and sisters. Their prayers and best wishes always accompanied me to achieve the goal of PhD.

Table of Contents

Chapter 1
Fundamentals

1.1 Sensor

The term "*chemical sensor*" in current chemistry literature is used in broad context and not always as unambiguous expression. Chemical sensor is defined, for example, as "*measurement device which uses chemical or biological reactions as tool to sense and quantify a specific analyte or an event*" or "*miniaturized analytical device which can produce real-time and on-line information in the presence of specific compounds or ions in complex media*." [1]

According to definitions of Analytical Division of IUPAC "a chemical sensor is a device that converts chemical information into analytically valuable signal dealing from the concentration of a specific sample component to total composition analysis. The chemical information described above may be attributed due to a chemical reaction of the analyte or to a physical property of the system investigated."[2] Fundamental configuration of sensor in general is shown in figure 1.1.

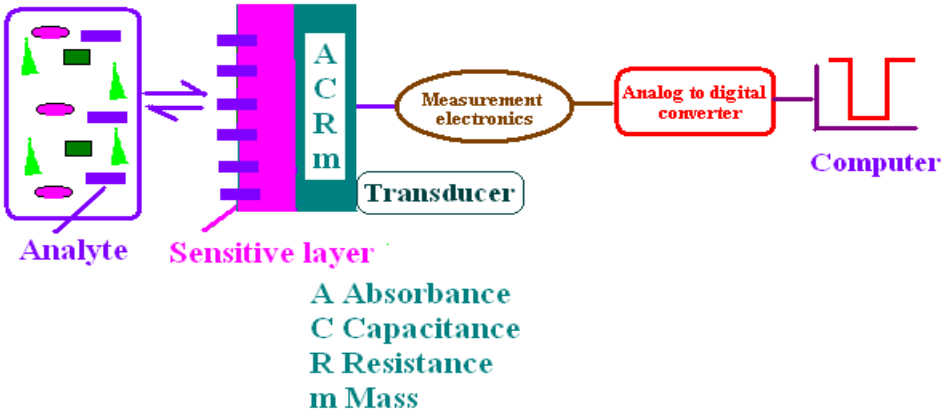

Figure 1.1 Fundamental configuration of a sensor

Classification

Classification of Chemical sensors can also be done on the basis of how they transduce the presence of chemical species into an electrical signal. Table 1.1 shows the classification of sensor on the basis of transduction properties.

Table 1.1 The chemical sensors classification proposed in 1991 by Analytical IUPAC chemistry division

Class of Sensors	Operating Principle
Optical devices (optodes)	Absorbance
	Reflectance
	Luminescence
	Refractive index
	Optothermal effect
	Light scattering
Electrochemical	Voltammetry (including amperometry)
	Potentiometry
	Chemically sensitized field effect transistor
	Potentiometry with solid electrolytes for gas sensing
Electrical	Metal oxide seminconductivity
	Organic semiconductivity
	Electrolytic conductivity
	Electric permittivity
Mass sensitive	Piezoelectric
	Surface acoustic wave propagation
Magnetic	Changes of paramagnetic gas properties
Thermometric	Heat effects of a specific chemical reaction
Others	Emission of α, β or γ radiation

1.2 Mass Sensitive Sensors

Bulk Acoustic Wave Sensors

Mass sensitive sensors (also called as oscillator sensors) measurements are based on piezoelectricity of crystals often appropriately cut quartz crystals. The fundamental crystal frequency is measured in part by crystal mass while the resonance frequency changes with the variation in the crystal mass. QCM wafer portion located between the electrodes oscillates at its fundamental frequency when kept in an oscillator circuit. Extremely thin films or layers on

oscillating piezoelectric crystal produce frequency change proportional to the deposited mass on the crystal surface in bulk acoustic wave (BAW) mode. The most common piezoelectric application is the so called Quartz Crystal Microbalance (QCM). [3,4,5] QCM is the most famous acoustic sensors representative based on transduction between electrical and mechanical energies. The quartz crystal microbalance is the most popular BAW and its fundamental frequency is determined by the thickness of the plate. QCM measurements are widely employed both for sensing in gaseous and liquid phases.[6,7,8,9,10] A variety of techniques are applied for coating applications to piezoelectric crystals for example spin coating, chopping, sputtering, dipping, spraying, and Langmuir–Blodgett etc. Various applications are used for gas/vapor and aerosol sensing. The oscillating quartz thickness is the key parameter determining its resonance frequency. QCMs frequencies up to 50 MHz are commercially available but QCM plates become too unstable mechanically to practically apply for sensor technology above 50 MHz. 5-10 MHz frequency range is commonly employed in sensor generation. [11,12,13] Figure 1.2 shows a 10 MHz AT cut QCM with gold electrodes.

Figure 1.2 A 10 MHz AT cut QCM with gold electrodes

The crystals are coated by chemical sensitive layers to give selectivity. The resonance frequency change with respect to the deposited analyte mass on QCM is demonstrated in Sauerbrey equation.

$$\Delta f = -f_{\circ}^{2} \frac{2}{A_{cr}(\rho_m C_q)^{1/2}} \Delta m$$

The Sauerbrey equation describes the frequency change (Δf), to the mass change (Δm) involving other parameters i.e. the chemical film density (ρ_m), the quartz crystal shear modulus (C_q), the crystal fundamental resonance frequency ($f_{\circ}$) and crystal area (A_{cr}). The equation demonstrates frequency decrease with increase in mass on QCM in gas phase. While sensing in liquid phase liquids properties make the equation in the following form.

$$\Delta f = -f_{\circ}^{2} \frac{2}{(\rho_m C_q)^{1/2}} \sqrt{\frac{\rho_l \eta_l}{4\pi f_{\circ}}}$$

The additional parameters involved are the surrounding liquid density (ρ_l) and viscosity (η_l). According to Sauerbrey equation frequency change from air to aqueous solution is around 2 - 4 kHz for 10 MHz QCM. But in actual practice the frequency shift is usually 1.5 to 3 folds higher to that of expected value. The enhanced effect can be assigned to the differences between the surface and bulk values of viscosity, density along with contribution from hydrophilic or hydrophobic properties, intermolecular interactions, electric double layer structure and surface roughness of the film.

SAW Sensors

The surface acoustic wave (SAW) piezoelectric devices are based on Rayleigh wave propagation at solid thin-film boundaries. Interdigitated electrodes (two sets) are coated on a piezoelectric crystal surface, one acting as transmitter and other as receiver. A synchronous mechanical stress in the crystal generates acoustic wave along longitudinal and vertical shear components when radio-wave frequencies are applied to the transmitter

electrodes. Like BAW, SAW sensors are applied in both gaseous and liquid phases by using chemically or biochemically modified sensitive interfaces. The wave velocity in the sensitive surface layer may be more or less the same as compared to that in the piezoelectric material.[14]

1.3 Chemical Sensing Mechanism

In chemical sensors, sensor response is based on analyte interaction with a modified transducer (discussed above). Selectivity and sensitivity are the key parameters of this process. Recognition can be based on different mechanisms, e.g. incorporation of the analyte into a material, chemically modifying active surface or by additional selective chemical reaction of analyte on/in the sensor. Modification in amperometric sensors selectivity and signal magnitude is achieved by altering electrode material e.g. by using different composition carbon pastes or different material composites, along with active surface modification. Sensor surface modification can be done by direct polymer layers generation on the surface or spin or dip coating. Metallocyanates coating may produce strong size-charge selectivity towards incorporated counter ions. Additionally in amperometric sensors self-assembled structures are generated for example self-assembled monolayers (SAM) on solid supports or bilayer lipid membranes (BLM) on different supports.[15] SAMs possessing redox active and inactive receptors are applied for ion recognition self-assembled monolayers.[16] Various same surface coating methods are applied for piezoelectric sensors and voltammetric sensors. Molecularly imprinted polymers (MIPs) are attractive technique for piezoelectric sensors. Electropolymerization can be carried out on conducting surfaces. A polymer layer on a flat surface can be generated by using sandwich techniques for surface imprinting of template. MIPs nano or microparticles can be interfaced with the transducer surface by different

layers for example electrodeposited conducting polymers. MIPs can be applied on other transducers including voltammetric or impedometric.[17]

1.4 Molecular Imprinting

Molecular imprinting has received increasing interest to solve selectivity problems in various chemistry disciplines. Particularly, their selectivity and robustness are attractive. In the last decade, molecular imprinting has established into a mature discipline generating polymeric receptors for small and recently large molecules for large range of molecular recognition-based applications.

Molecular imprinting involves the following key steps (Figure 1.3)

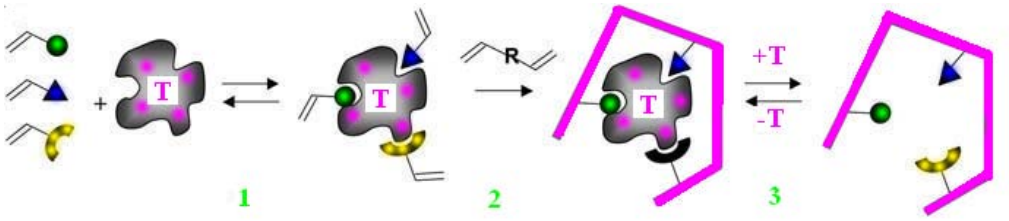

Figure 1.3 Molecular imprinting fundamental principle T= template

A template molecule (or target molecule), is mixed with functional monomer(s) in solution.[18] Polymerization is initiated in excess of a cross-linking monomer producing a three-dimensional cross-linked porous polymer network. The template is washed or removed from the polymer matrix resulting in the molecularly imprinted polymer (MIP). A popular technique for MIP generation binding sites is depicted by the noncovalent route. This uses template' noncovalent self-assembly with the functional monomer(s) before polymerization. After polymerization and template removal, rebinding is possible due to noncovalent interactions. Sometime MIP is achieved by adding a pore-forming solvent (porogen) to enhance the sensitivity due to effective template removal and accessibility of recognition sites. For

stabilization of electrostatic interactions between the template and functional monomers, the porogen is usually aprotic and has low to moderate polarity. Addition of porogen limits polymer morphology control and excludes the possibility of beads or nanoparticles generation from MIPs.[19] This practice has to compromise between the two aspects: polymer morphology and molecular detection. The template should be stable and soluble in the mixture prior and during polymerization. Different parameters are optimized to achieve high sensitivity, LoD and selectivity for template. The factors affecting the binding site characteristics are demonstrated in Figure 1.4.

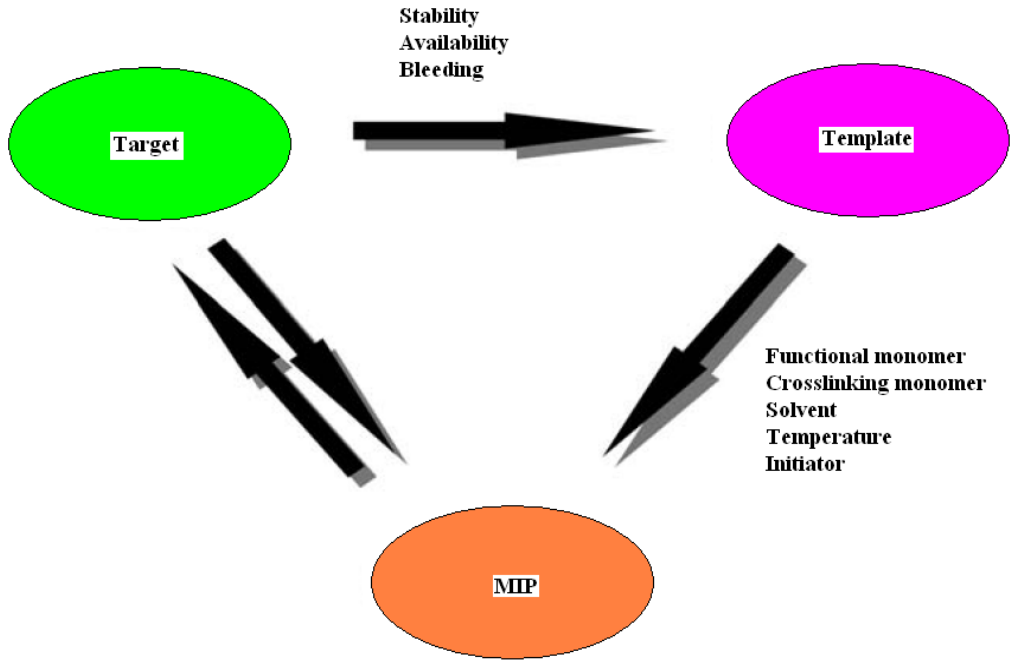

Figure 1.4 Factors affecting the quality of the molecular recognition by MIPs

The MIP properties are affected by the polymer morphology, cross-linking monomer type and amount, functional monomer type and amount and porogenic solvent type and amount along with solvent nature.

Molecular Imprinting vs Biomolecules

Although the biomolecules applications like enzymes as sensor materials are popular due to their high selectivity towards the target, yet these

are fragile.[20] The biomolecules manufacturing from animals is extremely difficult, technically complicated and expensive. MIPs advantageous features make them better alternatives of biomolecules for different sensors applications.[21]

Parameters Affecting MIP Performance

The self-assembly approach suggests that monomer–template assemblies (i.e. solution parameters) determine the subsequently binding sites generation. The extent and quality of MIP recognition sites are based on the strength and number of selective interactions between the template and the monomers in the pre-formed polymerization mixture. The details are explained in Figure 1.5. These parameters are further affected by the solvent nature, cross-linking monomer, temperature and pressure applied during polymerization. The fundamental criterion is the stability enhancement of these interactions. This will lead to minimization of nonspecific binding sites because the end result will be reduction in free non-associated functional monomer. However, parameter optimization will also change the polymer morphology at meso and macroscopic level, which ultimately change the kinetics parameters like diffusion mass transfer limitations, size exclusion effects and bleeding etc.[22]

The Template

The templates and their structural analogues mainly employed possess moderate to high solubility in the final MIP media and thus can be used directly in the traditional procedure.

Functional Monomers

The fundamental principle in the functional monomer selection is functional group complementarity. (Figure 1.5)

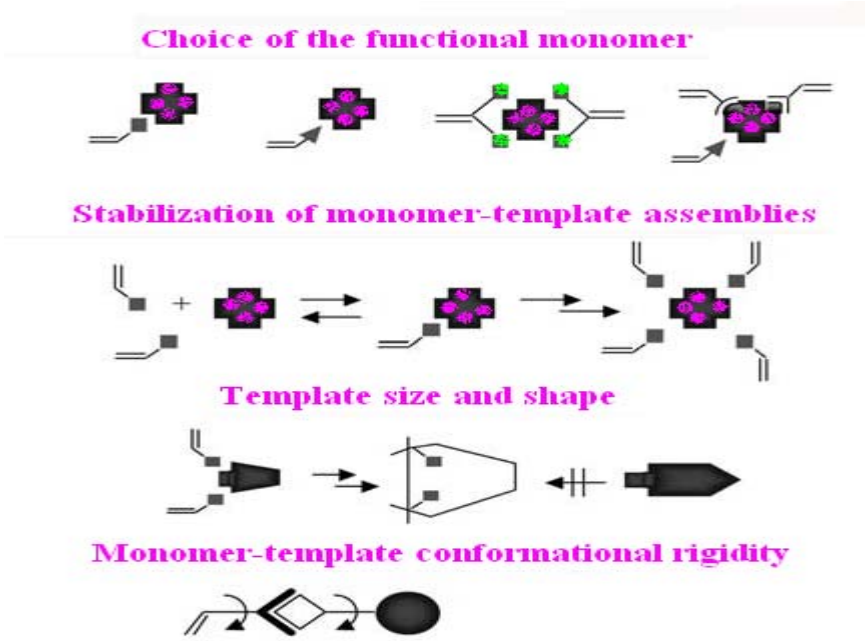

Figure 1.5 Factors affecting the quality of the imprinted sites associated with the monomer–template assemblies

Thus, for templates containing acidic groups, Bronsted basic functional monomers (e.g., 2- or 4-vinyl pyridine (VPy)); diethyl amino ethyl methacrylate (DEAEMA) are preferably selected whereas acidic functional monomers (e.g., methacrylic acid (MAA), trifluoro methylacrylic acid (TFM), itaconic acid (ITA)) are employed to target Bronsted bases. For amides and carboxylic acids, appreciable selectivities are proposed with primary amide possessing monomers (e.g., methacryl amide (MAAM)). Neutral solvating monomers that normally have positive effect on imprinting are *N*-vinyl pyrrolidone (NVP) and hydroxyl ethyl methacrylate (HEMA). For less polar to apolar templates having few polar interaction sites, amphiphilic monomers are proposed. This will stabilize the monomer-template assemblies by hydrophobic and van der Waals interactions or, for extended π-systems, by means of charge transfer. Thus, using co-monomers that may orthogonally target various subunits in a complex template is affective popular strategy.[23]

Polymerizable host monomers for strongly complexation of a guest in solution are employed for imprinting similar guests.[24]

Cross-Linking Monomer and Solvent

EGDMA is mostly used as cross-linker especially in methacrylate polymers because of providing mechanical, thermal stability and wettability in most rebinding media and rapid mass transfer for recognition characteristics. No other cross-linker generates such recognition characteristics for a huge variety of templates except trimethacrylate monomers e.g. trimethylol propane trimethacrylate (TRIM).[25] DVB is good for some templates in different polymerization formats e.g., emulsion, suspension or precipitation. In peptides imprinting TRIM is applied for producing resins containing a better loading capacity and better functioning than that of prepared with EGDMA. Polar protic crosslinkers for example methylene diacrylamide (MDA) and pentaerythritoltrimethacrylate (PETRA) are good for imprinting and MIPs applications in relevantly polar solvents. Furthermore the amide-based cross linking monomers for example methylene diacrylamide (MDA) are better for such applications because they generate a polar and more protein like microenvironment. This is good for polar templates imprinting having low solubility in organic solvents. The solvent should completely solubilize the monomers, template and radical initiator. Nonprotic less polar solvents are used for monomer–template interactions stabilized by polar forces because they will not compete with the monomers for the template. The functional monomer–template complexes in polymerization are commonly based on hydrogen bonding. If the solvent has the properties of hydrogen bond donor or acceptor, it will undergo competition with the monomers and ultimately destabilize the complexes. High polar solvents with higher temperatures for polymerization are suitable for monomer–template interactions containing solvatophobic forces.[26]

Temperature and Initiator

For electrostatic interactions based systems, lower temperatures increase the stability of monomer–template assemblies producing efficient MIPs. Low temperature initiators are normally employed or the polymerization is carried out using photolabile initiators. Thermal polymerization is applied and preferred in certain monomer–template systems.[27] For example for caffeine and theophylline imprinting thermal polymerization is better option.[28]

Recent Advancements in MIPs

Most of the advancements are based on the cross linked MIPs while there are a few applications of non-cross linked MIPs. In phase inversion molecular imprinting linear polymer is used as matrix and template molecules are imprinted by phase inversion process.[29] Aromatic polyimide is an example of non cross linked MIP which is thermally stable and mechanically rigid. The urethane bond between template and polyimide matrix is stable at room temperature and can be easily broken at high temperature. These sorts of interactions are useful for the development of successful sensors.[30] Another method involves radio frequency glow discharge plasma deposition to generate polymeric thin film around protein molecules coated with disaccharide layer. Disaccharide molecules covalently attach to polymer containing imprinting sites for a variety of protein molecules.[31] Normally, the template removal produces pores in MIPs exhibiting nano scale binding sites. The controlling of pores size is a difficult task but another alternative is template immobilization on disposable solid material (mold).[32] The imprinting strategies have been developed mostly for small molecules like drugs, amino acids, metal ions or nucleotides. The applications for larger molecules are in the stage of development and need challenging experimental conditions.[33]

a) Separation of Structurally Related Compounds

Mostly MIPs are applied for pharmaceuticals like enantiomeric molecules using MIPs as stationary phases in HPLC or in capillary electro chromatography.[34] The separation of specific species from complex matter of biological and foods like milk, serum or urine are the other MIPs applications.[35] MIPs applications are extended to natural contaminants or environmental pollutants on vegetables, fruit or decaying foods for example ochratoxin.[36,37] Biomedical and pharmaceutical species can be separated by using ultrathin MIPs films.[38] MIP microspheres are gaining popularity over the particles approach.[39] Different polymerization techniques are applied for MIPs generation for example suspension, core shell emulsion or precipitation/dispersion. The particles morphology is important parameter for these sorts of polymerization. Another approach is the use of MIPs on different supports like grafted coatings on silica supports, organic polymer supports or on walls of fused silica capillaries.[40]

b) Separation and Screening of Bioactive Compounds

The direct extraction of bioactive pharmacophoric compounds from the herbs can be done by using imprints of different templates e.g. quercetin for the extraction of structural related compounds from the hydrolyzate of gingko leaves.[41] The screening of drugs by using MIPs offers cheap and robust methods as compared to those which involve the use of expensive and highly sensitive bio macro molecules. The bioactive molecules can be synthesized using template guided MIPs.[42]

c) Sensor Technology

MIPs are appreciable alternatives of enzymes, antibodies and receptors for biosensors because of their stability, robustness and other advantageous features. For example sensors have been developed for sensing atrazine like QCM and conductometric sensors.[43] Microsystin LR, a highly toxic compound produced by freshwater cyanobacteria can be sensed by

piezoelectric sensor.[44] Chloramphenicol sensing has been possible by using MIP generated from vinyl pyrrolidone. Epinephrine analysis is possible via MIPs generated from polymerization of 3- aminophenylboronic acid as a functional monomer in the presence of ammonium persulfate coated on microplate wells an ELISA plate assay format.[45] Successful sensor for corticosteroid has been developed by generation of MIPs from poly methacrylate and EGDMA using acetone or THF as porogens. MIPs have been used as artificial antibodies for sensing microbial cells and tobacco mosaic virus (TMV).[46] For sensing chloropropanol (a carcinogen in foods), 3-MCPD imprints have been successfully developed using 4-vinyl phenylboronic acid as the functional monomer.[47] Direct sensing of molecules is convenient by using fluorescence based sensors via the use of fluorescent tags. A change of fluorescent intensity is seen on binding of sample molecule.[48]

d) Catalysis

The synthetic biomimetic catalytic counterparts can be substitutes of enzymes and catalytic antibodies.[49] The catalytically active MIPs can be synthesized by creating cavity relevant to the substrate shape. During the synthesis of the cavity, binding sites are created by different groups in a well defined stereo specific pattern. The exact mimic of enzymes can be possible due to new polymer systems and new ideas.[50]

Chapter 2
Folic Acid and Metabolites

2.1 Introduction

The isolation, structure identification, and synthesis of folic acid, which took place in the 1940s, led to the widespread therapeutic use of this water-soluble vitamin for the treatment of megaloblastic anemia. During the next 50 years, the basic aspects of folate metabolism and the biochemical functions were investigated and the key role of folate coenzymes in one carbon metabolism established. Since the early 1990s, the links between folate intake and birth outcome or chronic disease risk were explored. One of the most important public health discoveries of this century is that daily supplemental folic acid taken periconceptionally significantly reduces the risk of neural tube defects (NTDs).

Nomenclature and Structure

Word 'folic' is taken from a Latin word *folium* means leaves because folic acid was originally isolated from spinach leaves.[51] Folate consists of a family of compounds (more than 100 compounds) that differ in a variety of ways including the oxidation state of the molecule, the length of the glutamate side chain, and the specific one carbon units attached to the molecule. The folate molecule, tetrahydrofolate, is derived from 5, 6, 7, 8-tetrahydropteroylglutamate, which consists of a 2-amino-4- hydroxy-pteridine (pterin) moiety linked via a methylene group at the C-6 position to a p-aminobenzoylglutamic acid (pABG). The pyrazine ring in tetrahydrofolate is fully reduced at the 5, 6, 7, and 8 positions and reduction at positions 7 and 8 only yields dihydrofolate.

The monoglutamate form of the vitamin contains one glutamic acid molecule, which can be converted to a glutamate chain by the addition of glutamate residues by g-peptide linkage. In the majority of naturally occurring folates, the number of glutamate units in the side chain varies from 5 to 8. The fully oxidized monoglutamate form of the vitamin is referred to as folic acid and is the form used commercially in supplements and fortified foods. In contrast to polyglutamyl folate, folic acid rarely occurs naturally in food. Specific one carbon units that can be added at either or both of the N-5 or N-10 positions of the polyglutamyl form of the tetrahydrofolate molecule include methyl (CH_3), methylene (-CH_2-), methenyl (-CH=), formyl (-CH=), or formimino (-CH=NH) groups.[52] The structure of folic acid shown in figure 2.1

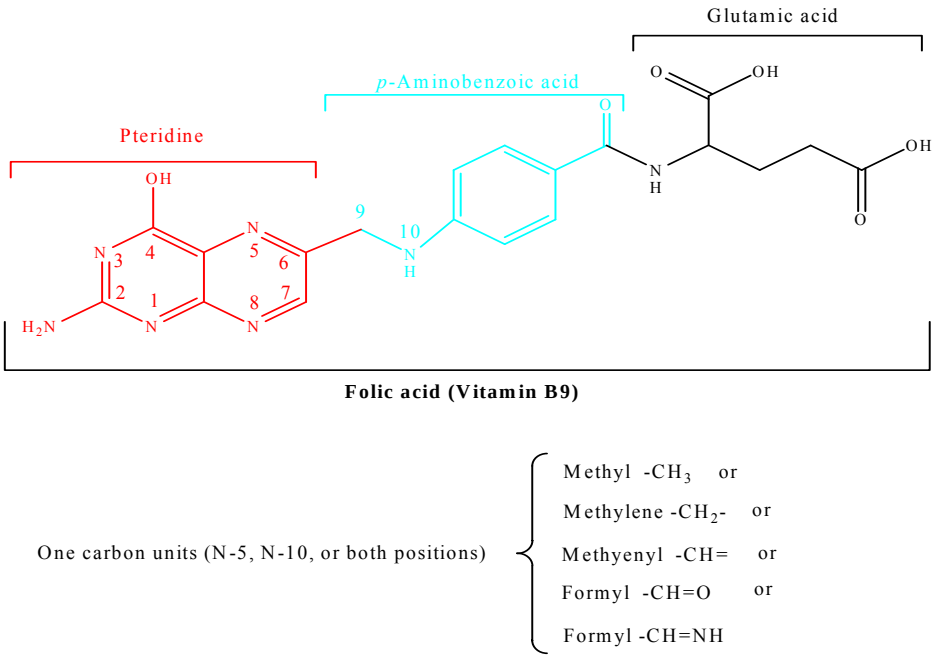

Figure 2.1 Folic acid structure, Folic acid consists of a pteridine ring linked to p-aminobenzoic acid joined at the other end to a molecule of glutamic acid. Food folates exist in various forms, containing different numbers of additional glutamate residues joined to the first glutamate. The folate or folic acid structure can vary by reduction of the pteridine moiety to form dihydrofolic acid and tetrahydrofolic acid, elongation of the glutamate chain, and substitution of one carbon units to the polyglutamated form of the tetrahydrofolic acid molecule

Properties

The molar mass of folic acid is 441.4, and although it is described as ‘‘water soluble,’’ the acid form is soluble 1.6 μg/ml (25 °C). The tetrahydrofolate molecule is labile in solution due to sensitivity to oxygen, light, and pH. In oxygenated solutions, tetrahydrofolate breaks down to form pterin-6-carboxaldehyde, H2 pterin, pterin, and xanthopterin. The molecule is rapidly cleaved at the C-9–N-10 bond forming pABG. In contrast to tetrahydrofolate and N-10-substituted tetrahydrofolate, which are unstable in the presence of oxygen, folic acid and tetrahydrofolate substituted at N-5 (or N-5, N-10) are relatively stable when exposed to oxygen. Instability to light is a consistent feature of all forms of folate.[53]

Natural Sources

Folate that occurs naturally in the diet, referred to in this chapter as food folate, is concentrated in select foods including orange juice, strawberries, dark green leafy vegetables, peanuts, and dried beans such as black beans and kidney beans. Meat in general is not a good source of folate, with the exception of liver.[54]

Fortified and Enriched Food Products

In addition to food folate, ready-to-eat breakfast cereals contribute significantly to folate intake in the United States since the majority of breakfast cereals in the United States marketplace contain ~100 mg per serving of folic acid and a smaller number contain 400 mg per serving.[55] Folic acid is an added ingredient in a large number of other food products including meal replacement and infant formulas, and an increasing number of ready-to-eat breakfast cereals, nutritional bars, and snack foods.[56]

Fortification Effects on Folate Intake

Folic acid fortification has had a significant impact on folate status in the United States and Canada.[57] The median serum folate concentration increased more than two fold (from 12.5 to 32.2 nmol/L) and the median red

blood cell (RBC) folate concentration increased from 392 to 625 nmol/L from NHANES III (1988–1994) to NHANES (1999–2000).[58]

2.2 Analysis

Food Samples

Several dozen forms of folate source in low concentrations in foods make the analysis complicated.[59] Food folate has historically been measured by a wide range of methods including microbiological assay, radiobinding or radiometric assay, and fluorometric, electrochemical, or spectrophotometric methods, with some methods in combination with high-performance liquid chromatography (HPLC).[60] Microbiological assay involving the use of three enzyme extraction in the order of *α*-amylase, protease, and conjugase along with the standard microbiological assay has been estimated.[61] Folate values using the microbiological assay are currently obtained after heat extraction to release folate from folate-binding protein or the food matrix in the presence of a reducing agent such as ascorbic acid, followed by trienzymatic extraction and deconjugation. Food folate can also be measured by HPLC methods and procedures are also available to either allow the identification of specific carbon derivatives of folate or characterize the length of the polypeptide chain.[62] To identify the carbon entities, folates are treated with folate conjugase to convert the polyglutamyl folates to monoglutamates and then separated by reverse phase HPLC.[63]

Biological Samples

Quantification of folate in biological specimens includes microbiological growth procedures, protein–ligand-binding methods, chromatographic and mass spectrometric methods.[64] Several liquid chromatography–tandem mass spectrometry methods have been developed for the analysis of clinical specimens.[65] The classical *L. casei* method for measurement of both serum and RBC folate concentrations has been used in

research laboratories for more than 50 years. In a clinical setting, radioassay procedures are most commonly used with variable cutoffs depending on the specific kit used. Improvement and standardization of methods for quantitation of folate in biological samples remains the focus of ongoing research efforts due to substantial differences between commonly used methods in different laboratories.[66]

2.3 Metabolism

Absorption and Transport

Dietary folate predominately occurs in a polyglutamate form, which must be first hydrolyzed to the monoglutamate form before intestinal epithelial cell uptake, which takes place primarily in the jejunum. When high doses of folic acid are given (>10 mM), intestinal uptake takes place by a nonsaturable mechanism involving a diffusion-like process.[67] Once internalized, folate is metabolized to 5-methyl tetrahydrofolate, although the degree of metabolism depends on the folate dose, with unmetabolized folic acid appearing in the portal circulation when pharmacological doses are given. With passage through the liver, folic acid is converted to 5-methyl tetrahydrofolate, however, large oral doses of folic acid result in a significant increase in urinary excretion of unmetabolized folic acid.[68] In the kidney, the folate receptor has a well-established role in receptor-mediated re-absorption of folate.[69]

Intracellular Storage

Tissue storage of folate in general is limited to the amounts required for metabolic function, which is estimated to be on average ~15–30 mg. Cellular folate accumulation displays saturation kinetics with the upper limit approximating the folate-binding capacity of the cell.[70] Within the cells, folate is bound by enzymes that catalyze folate-dependent reactions and by other folate proteins that sequester folate.[71]

Catabolism and Turnover

Folate is excreted in the urine primarily as breakdown products, with only a very small percentage as intact folate.[72] The percentage of ingested food folate that is excreted as intact urinary folate is estimated to be only 1%–2%, which indicates that folate is catabolized before urinary excretion.[73] Folate-binding proteins are not expressed in all tissues or are expressed to different degrees, which may explain the variability in different rates of tissue folate turnover since unbound folate is susceptible to catabolism.[74]

Excretion

The origins of folate excreted in feces include unabsorbed dietary folate, folate synthesized by colonic microbes, and folate contributed by endogenous secretions. It is estimated that the quantity of fecal folate excretion is comparable to that of urinary folate excretion.[75]

2.4 Biochemical Functions

One carbon metabolism is synonymous with folate-requiring reactions and includes those involved with different phases of amino acid metabolism, pyrimidine and purine synthesis, and methylation reactions following the formation of the body's primary methylating agent, S-adenosylmethionine (SAM) (Figure 2.2). In each of these folate-dependent pathways, a specific form of the folate coenzyme donates a one carbon unit to the reaction, resulting in regeneration of tetrahydrofolate, which is then free to accept other one carbon units from the folate pool and thus continue the cycle.[76]

Anhydroleucovorin Formation

In the final steps of histidine catabolism, the transfer of the formimino group of formiminoglutamate to tetrahydrofolate is catalyzed by formiminotransferase (Figure 2.2, Reaction 14). The formimino moiety is converted to 5, 10-methenyl tetrahydrofolate (anhydroleucovorin) in a formimidoyl tetrahydrofolate cyclodeaminase reaction.

Leucovorin Formation

Cells also contain leucovorin which acts as one carbon donor in the biochemical reactions producing nucleotides. Because of this important biochemical contribution leucovorin is used as rescue therapy for cancer treatment followed by methotrexate. Methenyltetrahydrofolate synthetase converts the leucovorin molecule to leucovorin coenzyme. The leucovorin coenzyme can be recycled back to leucovorin molecule by SHMT enzyme. The cyclic conversion called futile cycle is responsible for folic acid pathways.[77]

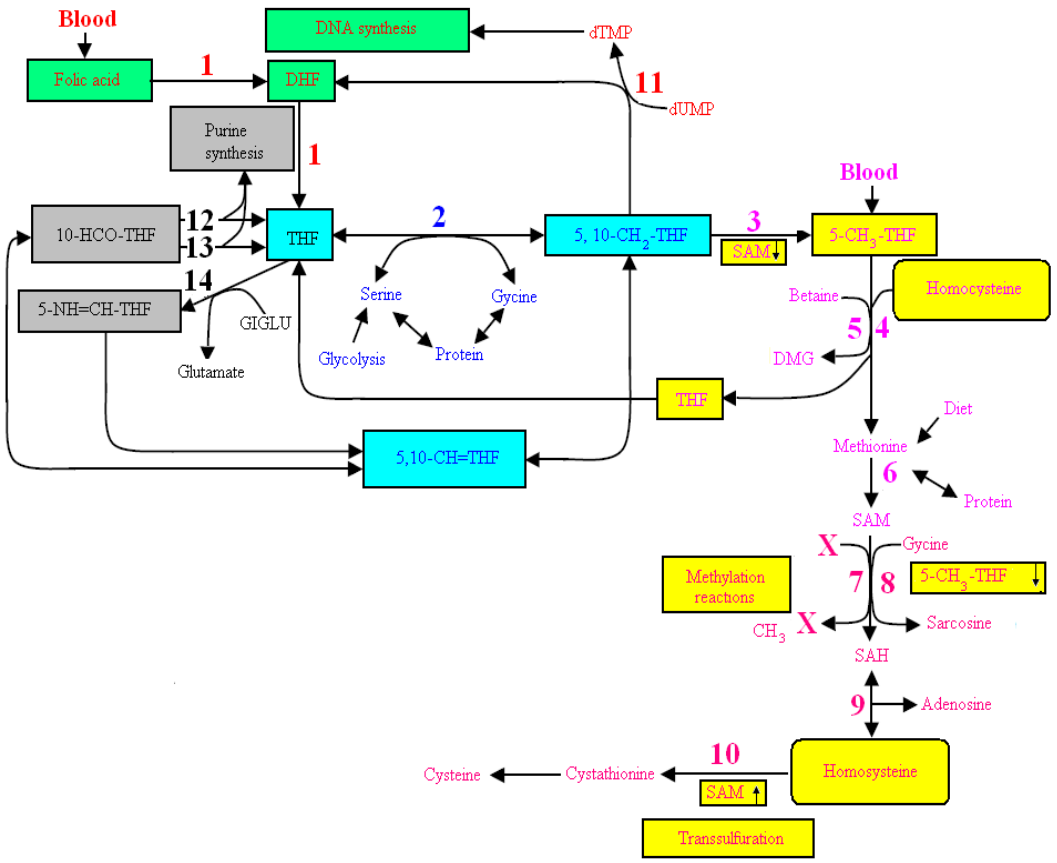

Figure 2.2 represents the major metabolic reactions and interconversions of folate coenzymes (polyglutamates). DHF, dihydrofolate; THF, tetrahydrofolate; DMG, dimethylglycine; SAM, S-adenosylmethionine; SAH, S-adenosylhomocysteine; FIGLU, formiminoglutamic acid. The enzymes and reaction numbers are noted in Table 2.1

Table 2.1

Reaction	*Enzyme Involved in One Carbon Metabolism Depicted in Figure 2.2*
1	Dihydrofolate reductase
2	Serine hydroxymethyltransferase
3	5,10-Methylene THF reductase
4	Methionine synthase
5	Betaine:homocysteine methyltransferase
6	Methionine adenosyltransferase
7	Variety methyltransferase reactions
8	Glycine N-methyltransferase
9	*S*-Adenosylhomocysteine hydrolase
10	Cystathionine β-synthase
11	Thymidylate synthase
12	Glycinamide ribonucleotide transformylase
13	Aminocarboxamide ribotide transformylase
14	Formiminotransferase

2.5 Deficiency

Serum and Red Blood Cell Folate Concentration

The deficiency of folic acid lead to reduction in *de novo* DNA and RNA biosynthesis necessary for normal cell division and protein/enzyme synthesis cause the prolongation of the synthesis phase of cell division. The outcome of this is abnormal red cell precursors and ultimately the cells are converted to megaloblastic (enlarged). Folates act as a carbon carrier in the manufacturing of heme, the iron containing nonprotein portion of hemoglobin. The body remains unable to produce new blood cells that result anemia due to deficiency of folates.[78]

Homocysteine Concentration

Elevated homocysteine concentration is considered a functional indicator of folate status in that it reflects a metabolic abnormality (insufficient 5-methyl tetrahydrofolate to convert homocysteine to methionine) and not just a reduction in blood folate concentration associated with folate inadequacy.[79,80]

DNA Methylation

Genomic DNA methylation, an epigenetic modification of DNA, is evolving as a sensitive biomarker of dietary folate intake. The primary methylating agent of the body, SAM, is dependent on an adequate supply of 5-methyl tetrahydrofolate (Figure 2.2).[81]

Hematological Indices

A folate deficiency leads to early hematological abnormalities in the bone marrow, which precede hypersegmentation of neutrophils in peripheral blood. Macrocytic cells are produced in the bone marrow when folate supply to the bone marrow becomes rate limiting for erythropoiesis.[82]

Abnormal Pregnancy Outcomes

Folate requirements are increased in pregnant women to meet the demands for DNA synthesis and one carbon transfer reactions in rapidly dividing fetal and maternal cells. When folate intake is restricted during pregnancy, impaired folate status has been associated with poor pregnancy outcomes including preterm delivery, low infant birth weight, and fetal growth retardation.[83]

Increased Risk of Birth Defects

a) Neural Tube Defects

The neural tube forms in the developing embryo from the neural plate during the first 28 days postconception and develops into the spinal cord and its protrusion that encases the brain. Incomplete closure of the neural tube

results in a group of birth defects collectively referred to as NTDs, which vary in severity depending on the location and size of the defect. Folic acid supplements taken periconceptionally significantly reduce the risk of NTDs, a major public health discovery based on findings from randomized controlled intervention trials supported by a large body of observational data.[84,85,86,87]

b) Congenital Heart Defects

Heart defects affect 1 in 110 newborns and account for a third or more of infant deaths due to birth defects, more than that for any other congenital anomaly including NTDs.[88] Periconceptional folic acid supplement use has also been associated with risk reduction for congenital heart defects in some but not all studies.[89]

Vascular Disease

Folic acid supplementation lowers plasma homocysteine concentration with the greatest homocysteine-lowering effect observed in individuals with the highest pretreatment homocysteine concentration.[90, 91] Ongoing randomized trials in European countries and Australia, which do not have mandatory folic acid fortification, are likely to provide a sustained homocysteine-lowering effect of folic acid thus increasing the probability of detecting vascular benefits.[92,93]

Cancer

Observational data provide population-based evidence for the conclusion that poor folate status is associated with an increase in cancer risk with the strongest support for colorectal cancer and its precancerous lesion, adenoma.[94,95] In addition to colorectal cancer, accumulating evidence from large prospective epidemiological studies suggests that folate has a protective role against breast cancer, especially among alcohol users.[96] It is hypothesized that a folate deficiency may alter the normal methylation patterns in

neoplastic cells, which could potentially be associated with inactivation of tumor suppressor genes.[97]

Depression

The folic acid deficiency creates several neurological defects like depression, stroke and Alzheimer's disease.[98]

Arsenic Genotoxicity

Methyltransferase is required for the detoxification of arsenic coming from pesticides or natural water component. Folic acid is needed for methyltransferase. The insufficient folic acid leaves chronic diseases in human body.[99]

Mental Agility and Brain Memory

The amount of folic acid in every day foods affects the mental health and memory.[100]

Allergy

A relationship has been found in allergic diseases and folic acid like atopy, wheeze, and asthma. Use of folic acid during pregnancy decreases the risks of allergic diseases in the children.[101]

Rheumatoid Arthritis

Protective affects have been seen against rheumatoid arthritis.[102]

Effect on Sex

Positive effects have been found on the fertility of both sexes, among men folic acid promotes to spermatogenesis while in women contributes to placentation, implantation and oocyte maturation.[103]

Macular Degeneration

The use of folic acid along with other vitamins like pyridoxine and cynocobaltamin reduces the macular degeneration.[104]

Chapter 3
Folic Acid & Metabolites Imprinting Literature and Experimental

3.1 Literature Review

The first imprinting approaches focus on substructure imprinting strategies, while more recent literature mainly demonstrates electrochemical approaches pertaining to modified electrode with different composites or by converting the MIPs into conducting materials. All work has been reported on folic acid sensing and no report is found for imprinting metabolites such as leucovorin and anhydroleucovorin in the literature. Furthermore, no report is found regarding using bulk MIP / NPs directly as sensing layer for QCM transducer. The literature can be divided into three main strategies 1) substructure imprinting approaches 2) optical based sensing 3) electrochemical approaches

Substructure imprinting strategy for dihydrofolate reductase inhibitors and *Z*-L-glutamic acid along with larger molecules has been applied. MIP has been generated for detection of *N*-*Z*-L-glutamic acid involving the use of bis-urea functional monomer.[105] Another substructure imprinting approach has been applied for detection of larger molecules like folic acid. Large number of 2-acrylamidopyridines has been employed as functional monomers in MIP generation demonstrating small differences in media for binding carboxylic acids. *N*-*Z*-L-glutamic acid imprinting using such monomer remained successful for MIP generation and for template recognition along with large molecules possessing glutamic acid residues e.g. folic acid. MIPs have been

compared with reported literature of urea-based MIPs for glutamic acid residue and pteridine substructure of folic acid.[106]

To the second strategy i.e. optical based sensing, folic acid analysis has been achieved by chemiluminescence sensor assimilated with flow injection technique. Luminol and hexacyanoferrate(III) were used in chemiluminescence and were immobilized on an anion-exchange column containing Amberlyst A-27 anion-exchange resin in flow injection. Luminol and hexacyanoferrate(III) reaction generated chemiluminescence signal, after elution from the column through sodium phosphate injection, that was reduced due to folic acid. Analysis is based on the folic acid inhibition in chemiluminescence reaction between luminol and hexacyanoferrate (III).[107] In another optical based sending, bovine milk-derived folate binding protein was measured while developing a ligand binding assay for the folic acid analysis. An inhibition assay format was optimized for optical biosensor comparison with an established assay employing a monoclonal antibody. Folic acid was immobilized to the sensor surface and optimal technique was used for folic acid analysis in milk and milk-based paediatric formulae. Samples were prepared directly by diluting in buffer via heating. Initial studies are satisfactory for a viable FBP-based biosensor assay for sensing total folate in paediatric stuffs and simpler substitute to the existing applied chromatographic, radioassay and microbiological techniques.[108]

To the third approach i.e. different electrochemical approaches have been developed for folic acid sensing recently. For example, immunoassay-based approach in electrochemical detection using magneto sensors for folic acid sensing in vitamin-fortified milk was applied. Better results were obtained with an indirect competitive immunoassay on comparing direct analysis to that of indirect competitive formats. The folic acid detection was achieved in immunochemical reaction on the magnetic bead solid support via

covalent immobilization of a protein conjugate BSA-FA on tosyl-activated magnetic bead. The transducer for the electrochemical detection was generated by modification of magnetic beads captured by a magneto sensor consisting of graphite–epoxy composite. The immunoassay-based analysis with electrochemical sensing via magneto sensors was performed on spiked-milk samples and compared with a novel magneto-ELISA based optical detection.[109]

In another electrochemical approach, folic acid has been selectively analyzed in solution containing ascorbic acid and uric acid at physiological pH employing electropolymerized film of 5-amino-2-mercapto-1,3,4-thiadiazole altered glass carbon electrode. Glass carbon electrode without any coating could not detect folic acid along with ascorbic acid and uric acid because of the surface fouling produced by the oxidized folic acid and ascorbic acid products. But 5-amino-2-mercapto-1,3,4-thiadiazole (p-AMT) film altered electrode can do voltammetric analysis with potential differences of 410 and 170 mV between uric acid-folic acid and ascorbic acid–uric acid, respectively in 0.2M PB solution.[110]

While in another electrochemical strategy, an amperometric sensor for 6-thioguanine and folic acid recognition has been developed by using multiwall carbon nanotubes modified electrode prepared by using ferrocenedicarboxylic acid as a mediator. Cyclic voltammetry, electrochemical impedance spectroscopy and differential pulse voltammetry were applied to study electrochemical response of the compounds at the electrode. The electrode possessed electrocatalytic activity for the oxidation of folic acid and 6-thioguanine at pH 9. Catalytic reaction rate constant was measured at 8.2*102 $(\text{mol } L^{-1})^{-1}s^{-1}$ by chronoamperometry and catalytic peak current depends on folic acid and 6-thioguanine concentrations. Although folic acid oxidation peak overlapped with that of 6-TG, yet the electrode

could differentiate the both for simultaneous measurements. The electrode gave better selectivity in voltammetric analysis for folic acid and 6-TG in mixture solution.[111]

Ardakani et al has applied carbon electrode altered by 2, 2' [1, 2 buthanediylbi (nitriloethylidyne)]-bis-hydroquinone along with TiO_2 nanoparticles. The altered electrode has shown response for electrocatalytic oxidization of folic acid, acetaminophene, and norepinephrine. Differential pulse voltammetry has been applied on the altered electrode for simultaneous measurement of folic acid, acetaminophene, and norepinephrine. Electrocatalytic and simultaneous sensing of folic acid, acetaminophene, and norepinephrine with TiO_2 nanoparticles altered carbon electrode is the first study by using differential pulse voltammetry. The measuring potential differences of 370 mV, 670 mV and 300 mV between acetaminophene–folic acid, norepinephrine–folic acid and norepinephrine–acetaminophene, respectively, are sufficient to measure folic acid, acetaminophene and norepinephrine cumulatively and individually.[112]

More recent electrochemical approaches have been developed by Prasad et al e.g. a hyphenated molecularly imprinted micro-solid phase extraction fiber and MIP composite fiber sensor was developed. A 'substrate-selective' MIP was prepared by using 2, 4, 6-trisacrylamido-1, 3, 5-triazine (TAT) as monomer, EGDMA as cross linking monomer and dimethylsulphoxide (DMSO) as porogen and merged with micro-solid phase extraction (MIMSPE) fiber. The ratio between the sample volume and solid phase was kept 5.3:102. Owing to extremely small solid phase, micro-solid phase extraction is suitable expression rather than SPME. MIMSPE and sensor possessing MIP with conductive carbon particles in the form of homogenous 'carbon strip' were coupled for measurements. The same MIP was employed in MIMSPE fiber to produce direct electronic conduction for

sensitivity measurements but not applied for selectivity pattern studies with structural analogues.[113] An electrochemical sensor was generated by using a preanodized sol–gel coated pencil graphite electrode with MIP coated on its external surface. MIP was generated for sol gel by stoichiometric imprinting keeping template/monomer molar ratio 1:3 using trifunctional monomer 2, 4, 6-trisacrylamido-1, 3, 5-triazine. PGE has been applied in stripping electrochemical analysis but modified PGEs are rarely applied in literature. PGEs offer enhanced electrode active surface area, rigidity, very low cost, low background current and better electrochemical properties like large potential window. MIP was spin coated to achieve the layer height and permeability. Carbon powder mixed in sol–gel texture made the film to work like a 'molecular wire' linking top MIP layer and electrode for electrical conductivity and enhanced transduction.[114] MIPs being electrically insulating, their coatings and electrode surface do not offer direct electrons conduction from the binding sites to the electrode for electrochemical measurements. MIPs are applied indirectly by designing substrate-selective MIP-fiber for combing traditional non conductor MIP and conducting carbon powder in consolidated phase. Conducting carbon powder layer in the form of 'carbon strip' is introduced to MIP for producing conductivity in the material. Composite material was generated by carbon (monolithic fiber) in polymerization by using 2, 4, 6-trisacrylamido-1, 3, 5-triazine TAT as functional monomer, EGDMA as cross linking monomer in the environment of carbon powder and folic acid as template. A new strategy has been followed to achieve close integration between MIP and transducer for generation of electrochemical sensor. Insulator phase has been merged with homogenous carbon conductive phase without using solid support for permitting fast electron conduction from binding sites to the transduction surface. The method promises the results without matrix effect or cross-reactivity.[115]

3.2 Experimental

3.2.1 Chemicals for MIPs Synthesis

Chemicals used for MIPs synthesis are shown in figures 3.1 and 3.2

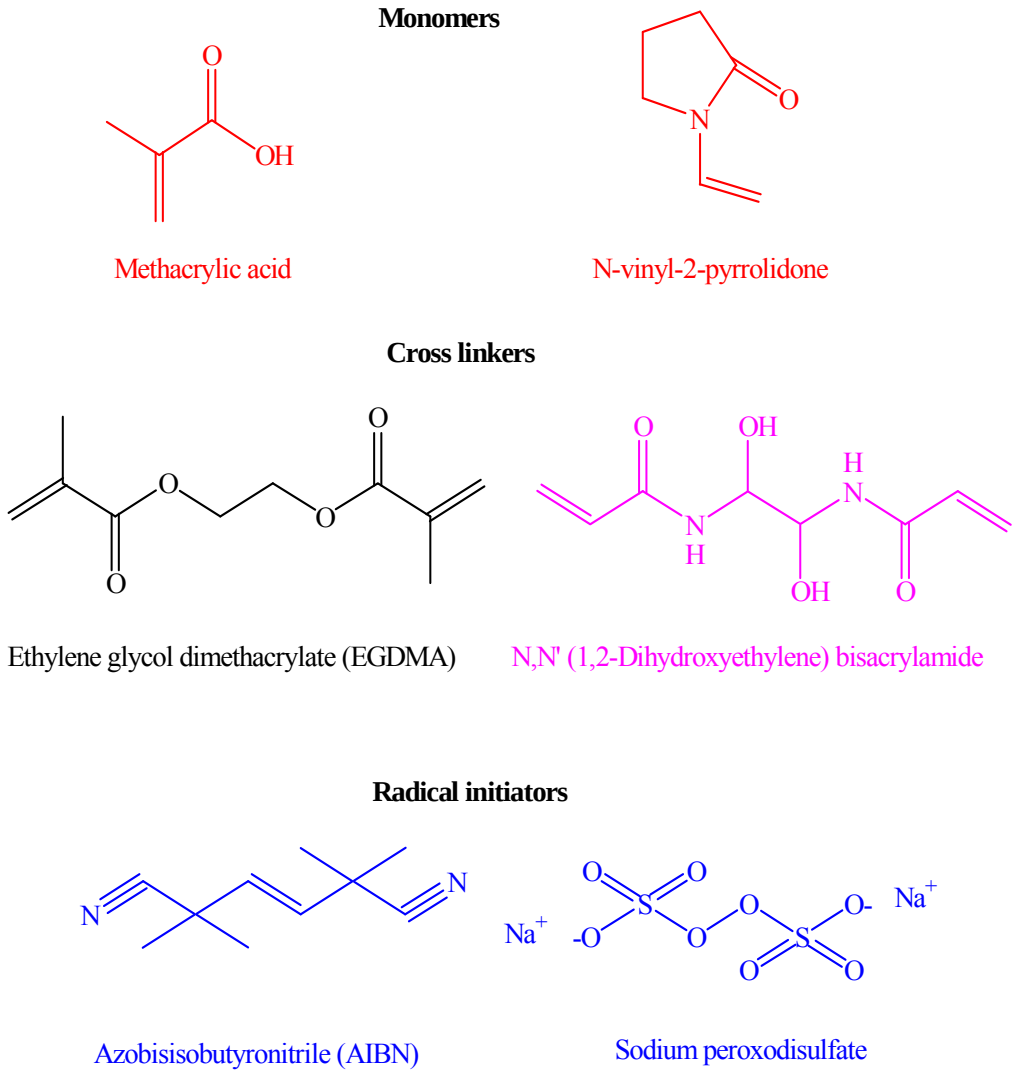

Figure 3.1 *Chemicals used for MIPs synthesis*

Chemicals were purchased from Merck, Aldrich or Fluka in highest available purity and used and stored according to the literature recommendations. Folic acid and anhydroleucovorin are insoluble in H_2O in ppm levels at room temperature but soluble in H_2O at pH 10 while leucovorin is soluble in H_2O. 1 mM ammonium phosphate aqueous buffer pH=10 was used to prepared

standards of folic acid and its metabolites while the buffer was used as blank solution in all mass sensitive measurements.

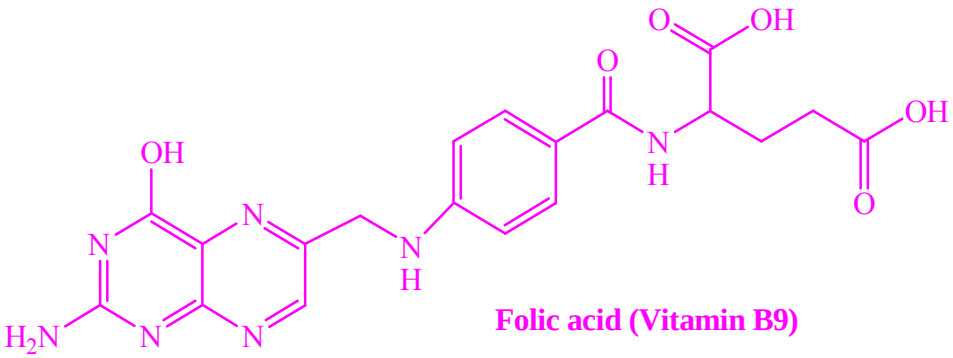

Folic acid (Vitamin B9)

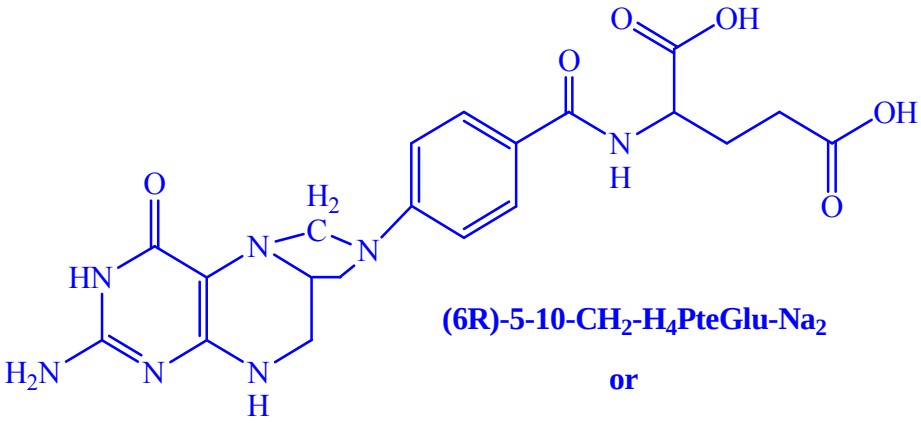

(6R)-5-10-CH_2-H_4PteGlu-Na_2

or

5, 10-Methenyltetrahydrofolate

(Anhydroleucovorin)

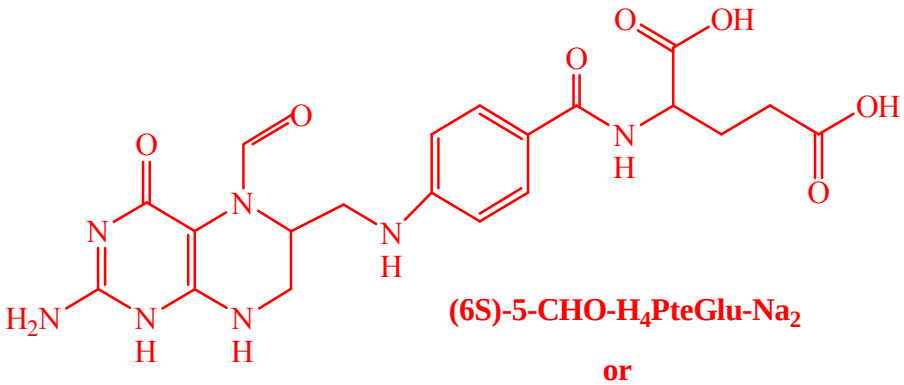

(6S)-5-CHO-H_4PteGlu-Na_2

or

5-Formyltetrahydrofolate (Leucovorin)

Figure 3.2 Templates used for bulk imprinting

All the solutions were prepared freshly every day via sonication of folic acid and its metabolites weighed in defined amounts. Concentrated aqueous buffers like 10 mM or higher buffer concentrations are unsuitable for the base line stability because they degenerate polymer layers while measuring. All the MIPs and NIPs have been prepared under UV source at room temperature because this approach proved much more effective than thermal polymerization for poly methacrylate and vinyl pyrrolidone systems. The reason behind this is the templates sensitivity towards heat above 55°C, air and visible light. The distance between the reaction tube and the UV source affects the polymerization time and ultimately the sensitivity and LoD of the polymers. The closer the distance of UV source from reaction tube, the shorter will be the polymerization time and vice versa. MIPs synthesized in shorter time remain unhardened gels thus unsuitable for coating onto the QCM electrodes. While, contrastingly longer distance between reaction tube and UV source generates extremely rigid MIPs. For MIP batches with longer polymerization time, the template cannot be properly removed, ultimately leading to low mass sensitivity. Different spin coating speeds have been applied to achieve homogenous layers of MIPs and NIP on QCM electrodes on the basis of rigidity, stickiness and nature of polymers. Various washing strategies have been adopted for efficient template removal from the MIPs depending on the template solubility.

3.2.2 Folic Acid Imprinting

a) Optimized Poly Methacrylate MIP

After the dissolving 5 mg folic acid in 500 µL DMF in the reaction tube, 20 mg methacrylic acid along with 30 mg EGDMA were mixed by stirring. After homogenous mixing, 5 mg AIBN was added in the solution to initialize the polymerization. Within this last step, 240 µL CH_2Cl_2 was added to achieve homogenous oligomer MIP at room temperature. The reaction tube was kept under UV light (λ_{max} 360 nm and 210 W) for 5 hours till the reach of

gel point. Non imprinted polymer (NIP) was prepared in the same way keeping all the parameters constant except for folic acid addition. After MIP synthesis, 5 µL MIP was spin coated at 3500 rpm onto the measuring electrode of QCM, while the second electrode was spin coated with NIP. The spin coated QCMs were kept overnight at room temperature for drying and hardening and washed with methanol for 4 hours prior to mass sensitive measurements.

b) Poly Methacrylate MIP-NPs

For generating NPs, synthesis was achieved based on the fact that acetonitrile is a poor solvent for methacrylate or vinyl pyrrolidone polymer. For NPs synthesis, 500 µL poly methacrylate bulk MIP oligomer solution was mixed with 10 mL acetonitrile and kept stirring overnight by using magnetic stirrer. The resultant homogenous NPs suspensions were centrifuged at 4000 rpm and solvent was removed to obtain the NPs. The NPs were mixed with 10 mL water (maintained at pH 10 by NH_3) and stirred for 1 hour. Water was removed via centrifugation and the washing process was repeated by using distilled water and methanol separately to achieve template free imprinted NPs. The NPs were again mixed in 500 µL acetonitrile in eppendorf tube. 5 µL NPs suspensions were spin coated at 2000 rpm on the unhardened layer of acrylic acid and EGDMA (2:1) on one electrode of QCM while the second electrode was spin coated with reference beads generated from NIP. The thin acrylic acid/EGDMA layers are used for immobilizing the NPs on the electrode surface even when immersed into liquids. The first electrode acts as measuring electrode while the second as reference electrode for reducing the non specific effects e.g. of temperature, viscosity of solution etc. The spin coated QCMs were kept overnight at room temperature for drying as well as for hardening NPs layers prior to mass sensitive measurements. After deposition, NP layer did not need washing, because the template had already

been removed during NP synthesis process, which means that template free NPs were used for spin-coating.

c) Optimized Poly Vinyl Pyrrolidone MIP

After the dissolving 5 mg folic acid in 500 µL DMF in the reaction tube, 20 mg N-vinyl 2-pyrrolidone and 30 mg EGDMA were mixed by stirring. Then afterwards, 5 mg AIBN was added in the solution to initialize the polymerization. While in the end, 240 µL CH_2Cl_2 was added to achieve homogenous oligomer MIP at room temperature. The reaction tube was kept under UV light (λ_{max} 360 nm and 210 W) for 6 hours till the reach of gel point. Non imprinted polymer (NIP) was prepared in the same pattern keeping all the parameters constant except folic acid addition. After MIP synthesis, 5 µL MIP was spin coated at 3500 rpm onto the measuring electrode of QCM, while the second electrode was spin coated with NIP. The spin coated QCMs were kept overnight at room temperature for drying and hardening and washed with methanol for 4 hours before mass sensitive measurements.

d) Poly Vinyl Pyrrolidone MIP-NPs

For NPs synthesis, 500 µL poly vinyl pyrrolidone bulk MIP oligomer solution was mixed with 10 mL acetonitrile and kept stirring for 24 hours by using magnetic stirrer. The resultant homogenous NPs suspensions were centrifuged at 4000 rpm and solvent was removed to obtain the NPs. The NPs were re-suspended in 10 mL water (maintained at pH 10 by NH_3) and stirred for 1 hour. Water was removed via centrifugation and the washing process was repeated by using distilled water and methanol separately to achieve template free imprinted NPs. The NPs were again re-suspended in 500 µL acetonitrile in eppendorf tube. After NPs synthesis, 5 µL NPs suspensions were spin coated at 2000 rpm on the unhardened layer of acrylic acid and EGDMA (2:1) on one electrode of QCM while the second electrode was spin coated with reference beads generated from NIP.

3.2.3 Leucovorin Imprinting

a) Poly Methacrylate MIP

A mixture of 20 mg methacrylic acid: N, N' (1, 2-Dihydorxyethylene) bisacrylamide (3.5: 1.5) was added to 200 μL of water in a reaction tube. After mixing thoroughly via stirring, 0.5 mg of sodium peroxidisulphate was added as radical initiator for polymerization. Finally 2 mg leucovorin was mixed and the resulting solution was kept under UV for 40 minutes till the reach of gel point. Non imprinted polymer was synthesized in the same manner except the addition of template. Then 5 μL MIP oligomer solution was spin coated at 2000 rpm onto the measuring electrode of QCM while NIP was spin coated onto the second electrode. The QCMs were kept overnight for drying as well as hardening and template was washed by keeping QCMs in warm water at 50°C for 1.5 hours.

b) Hardening and Drying of Thin Films

To improve the hardness of MIP, the spin coated QCMs were heated at 100°C for two hours that led to the evaporation of water from the spin coated polymer thin films. Afterwards, the heated QCM were washed with warm water (50°C) for 1.5 hours.

c) Optimized Poly Methacrylate MIP

The MIP synthesis was further modified by changing the monomer to cross linking monomer ratio to achieve better sensitivity and selectivity. In the optimized MIP synthesis, 200 μL of water was taken in a reaction tube and 16 mg methacrylic acid was added along with 4 mg of N, N' (1, 2-Dihydorxyethylene) bisacrylamide. After thoroughly mixing via stirring, 3 mg of sodium peroxidisulphate was added as radical initiator for polymerization. Finally 2 mg leucovorin was added and the resultant solution was kept under UV for 40 minutes till the reach of gel point. The NIP was prepared keeping all the components and parameters constant except the template addition. Then 5 μL MIP oligomer solution was spin coated at 2000 rpm onto the

measuring electrode of QCM while NIP was spin coated onto the second electrode. The QCMs were kept overnight for drying as well as hardening and were heated at 100°C in the oven for two hours. Finally the template was washed with warm water at 50°C for 1.5 hours prior to the mass sensitive measurements.

3.2.4 Anhydroleucovorin Imprinting

a) Poly Vinyl Pyrrolidone MIP

In the first step, 5 mg N-vinyl 2-pyrrolidone: EGDMA (2:3) was mixed with 50 µL DMF containing 0.5 mg anhydroleucovorin in a reaction tube. Then, 0.5 mg AIBN was added to the resulting solution and the reaction tube was kept under ultraviolet light to polymerize until reaching the gel point. The NIP was prepared in the same way by keeping all the parameters constant except adding template. The MIP was spin coated at 3500 rpm onto the measuring electrode of QCM while NIP was coated onto the second electrode and kept overnight at room temperature for drying and hardening. The dried QCM were washed in methanol: water (1:1) for 1.5 hours and measured in the cell. The spin coating and template washing procedure was adopted for all future mass sensitive measurements for anhydroleucovorin imprinting explained below.

b) Poly Vinyl Pyrrolidone MIP (Acryl Amide as Cross Linker)

Further modification in the MIP synthesis was done by changing the cross linker monomer i.e. N, N' (1, 2-Dihydroxyethylene) bisacrylamide. In the modified MIP synthesis, 5 mg N-vinyl 2-pyrrolidone: N, N' (1, 2-Dihydroxyethylene) bisacrylamide (3:2) was mixed with 50 µL DMF containing 0.5 mg anhydroleucovorin. Then, 0.5 mg AIBN was added to the resulting solution and mixed thoroughly. After homogenizing the mixture, the reaction tube was kept under ultraviolet light to achieve polymerization till

reaching the gel point. The NIP was also prepared in the same pattern keeping all the parameters constant except the addition of template.

c) MIP (Methacrylic Acid as Co-Monomer)

To achieve the structural stability of MIP after template removal for selectivity improvement, the MIP synthesis was further modified by adding methacrylic acid as co-monomer. In the modified synthesis, 5 mg of methacrylic acid: N-vinyl 2-pyrrolidone (1:1) / EGDMA (40 / 60) was mixed thoroughly in 50 µL methanol: DMF (1:9) containing 1 mg anhydroleucovorin by stirring. Then, 0.3 mg AIBN was added in the resulting solution to initialize the polymerization in the reaction tube. After homogenizing the mixture, reaction tube was kept under ultraviolet light for 3 hours to for polymerization till the reach of gel point.

d) Optimized MIP

In the final optimized MIP synthesis, 5 mg of methacrylic acid: N-vinyl 2-pyrrolidone (1:1) / EGDMA (40 / 60) was mixed thoroughly in 50 µL of methanol: DMF (3:2) containing 1 mg anhydroleucovorin via stirring. In the end, 0.3 mg AIBN was added in the resulting solution to initialize the polymerization. The reaction tube was kept under ultraviolet light for 3 hours to complete polymerization till the reach of gel point. After MIP synthesis, 5 µL MIP was spin coated at 3500 rpm on the measuring electrode of QCM while NIP was spin coated on the second electrode. QCMs were kept overnight at room temperature for drying and hardening. The dried QCM were washed in methanol: water (1:1) for 1.5 hour and mounted in the cell for mass sensitive measurements.

3.3 QCM Electrode Printing

AT-cut quartz crystals microbalances possessing 10 MHz fundamental resonance frequency were purchased from Zheijiang Quartz Crystal Electronics, Shanghai (China). The two electrode design was coated on the

quartz crystals by means of printing of the gold paste using a designed sieve. The structures of the designed sieves and electrodes are shown in figures 3.3 and 3.4.

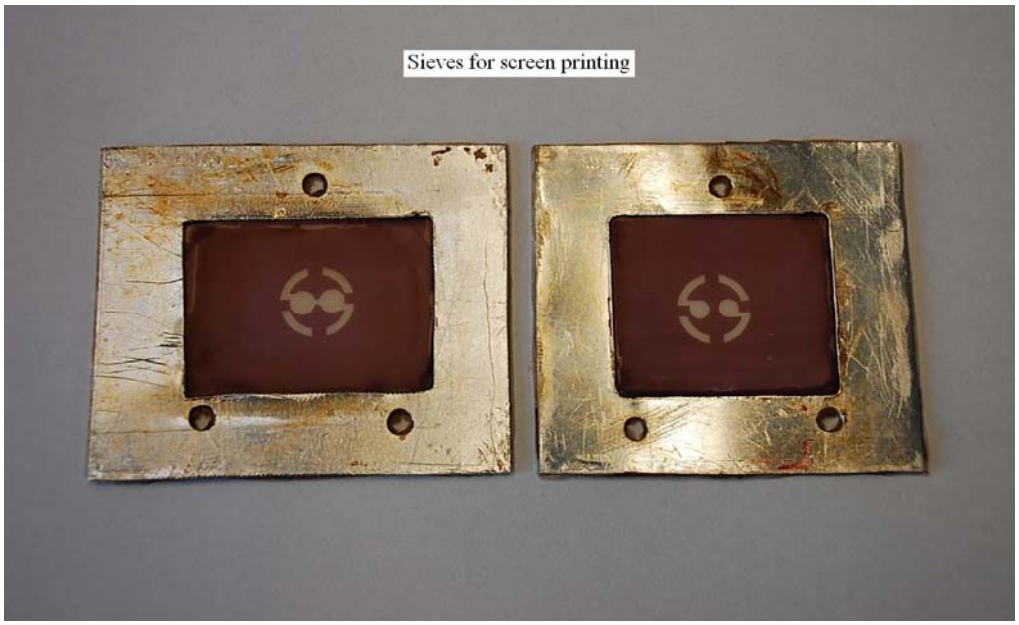

Figure 3.3 *Sieves for dual electrode screen printing*

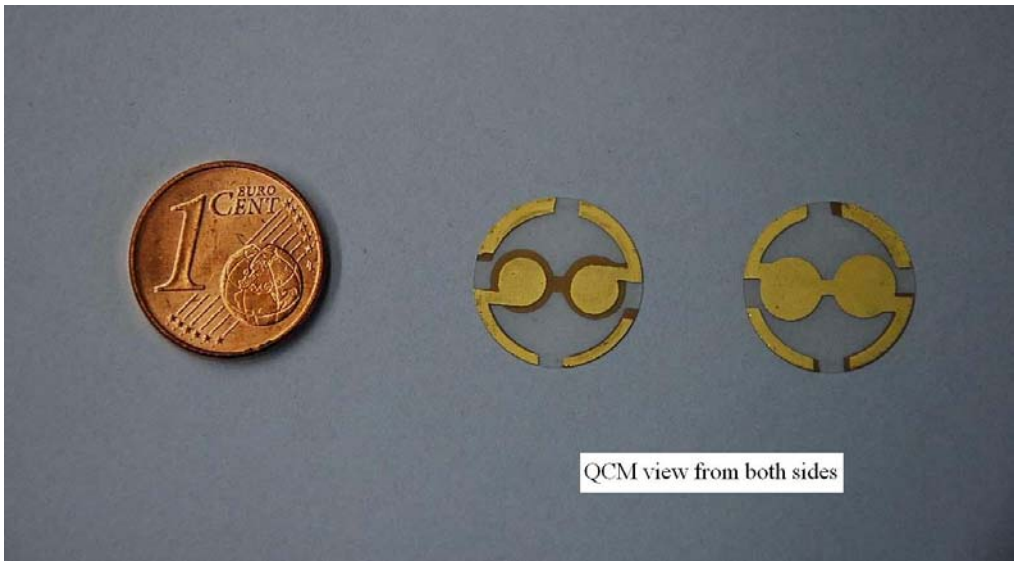

Figure 3.4 *QCM containing dual electrode structures after gold screen printing*

The designed sieves for gold paste screen printing on quartz crystals were made with 36μm mesh sized fabric stretched tightly by means of glue to

a metalloid rectangular shaped framework. The sieves were coated homogenously with a UV photo-resist lacquer (Azocol poly-plus s) and kept in the dark for half an hour for blocking mesh pores. The electrode design was generated by means of lithography on fabric by using a UV-printer. While the uncooked lacquered area was washed with hot water for generating the electrodes structures in this lithographic process.

3.4 Spin Coating

The MIPs were spin coated on one QCM gold electrode to generate thin layers for sensing. The second gold electrode was coated with non imprinted polymer (NIP) as reference layer. Polymers were spin coated on the electrode surface by means of spin coater shown in Figure 3.5.

Figure 3.5 Spin coater for MIP, NIP or NPs spin coating at different speeds (rpm)

QCM position is adjusted in spin coater centre and attached there by removable adhesive tape that covers the QCM surface expect the electrode for coating. Spin coater is turned on after fixing QCM and specific quantity of

polymer (in the µL range) is dropped on electrode surface using a micro pipette. Speed and spinning time can be easily optimized on the bases of nature of polymer viscosity parameters and according to layer height requirements.

The spin coated QCMs were kept overnight at room temperature for drying and hardening of the polymer layers. Different washing strategies on the basis of template solubility in the solvents were applied for template removal from MIPs. Homogeneous, robust and rigid MIP layers were achieved by these strategies. The MIP / NIP layer height was noted from the frequency difference before and after spin coating recorded by the means of a network analyzer. Usually no or minute layer height effect was noted for NIP coated electrode after washing. 40 nm layer hieght causes a 1 kHz frequency decrease at the gold electrode.

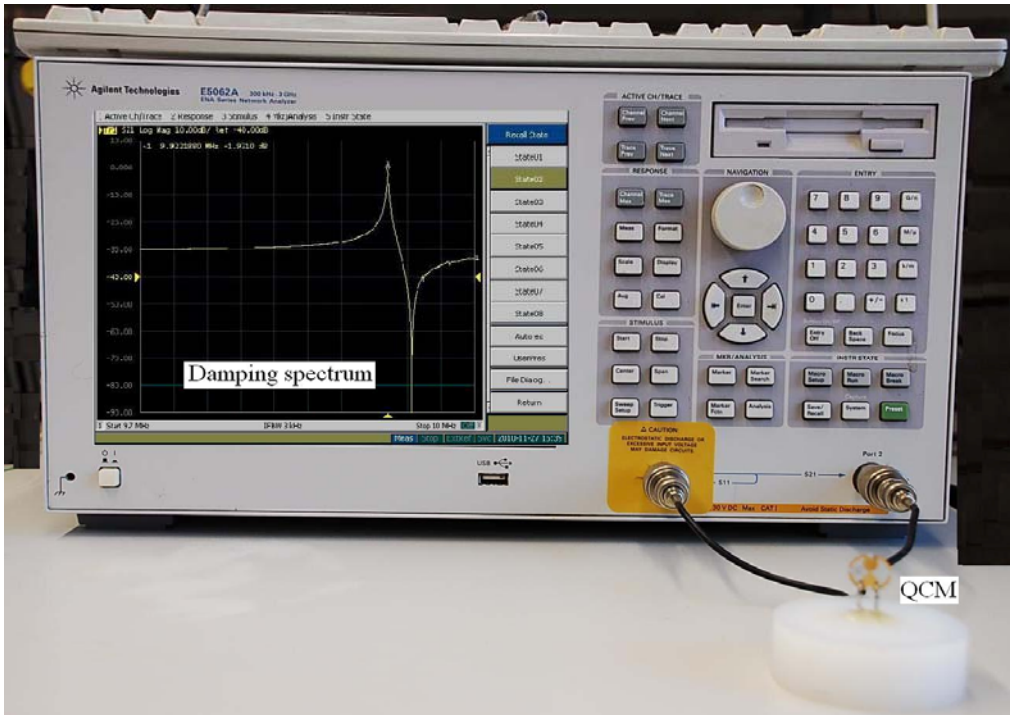

Figure 3.6 Network analyzer demonstrating QCM damping spectrum

An *ENA series of Agilent Technologies* network analyzer *(model no. E5062A)* was used to measure the electrode frequency and damping. Above figure 3.6

demonstrates the network analyzer set up with the LCD showing damping spectra of a QCM electrode.

3.5 Cell Set up

QCM mass sensitive measurements were performed by preparing the QCMs, as explained above, with MIP on one electrode while the NIP on second electrode.

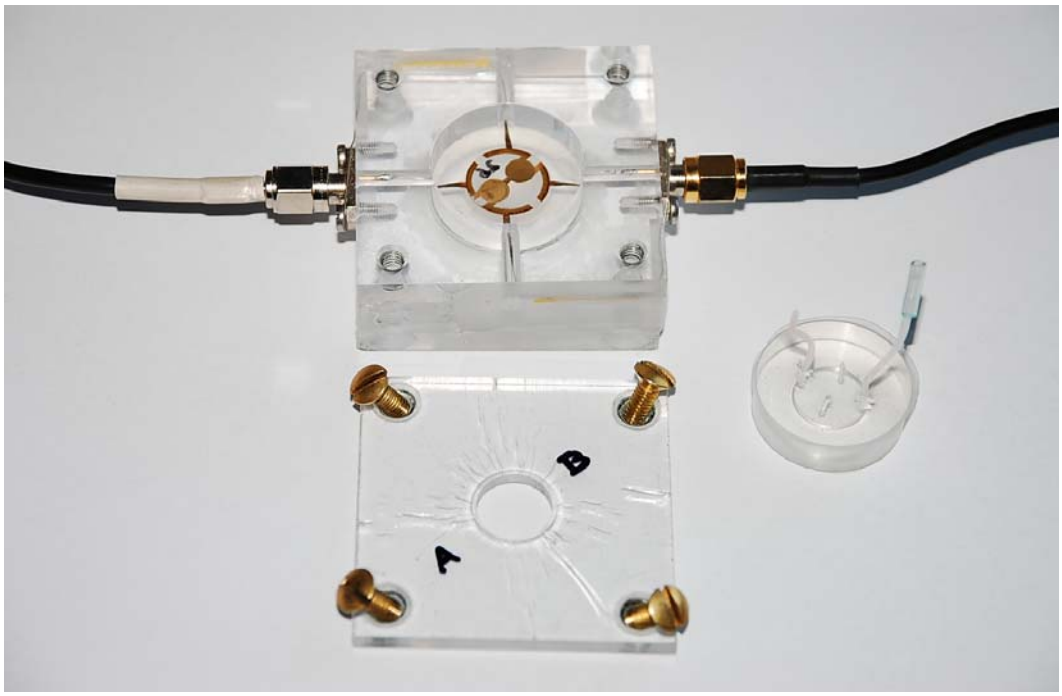

Figure 3.7 Measurement cell prior assembling the components

The designed QCM sensors were mounted in the cell by connecting the relevant wires with the QCM connections as shown in the figures 3.7 and 3.8. The cell provides suitable robust measurement conditions by protecting mounted QCM from external thermal and mechanical environmental effects. The cell contains an inlet for injecting the samples/solutions and an outlet for flowing out or passing solution through the QCM sensitive layer. The QCM is kept tightly sealed between two halves of PDMS cell during measurements to ensure stability and protection. They were polymerized by mixing silicone

elastomer base and silicone elastomer curing agent (9: 1) and hardened overnight at room temperature in the relevant size molds for the cell.

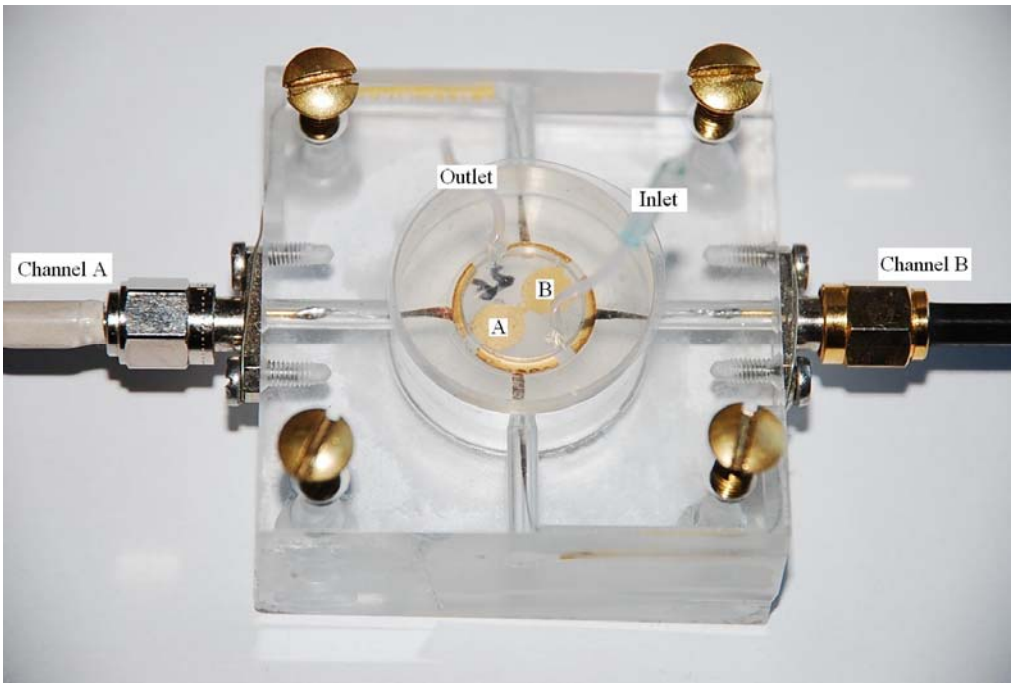

Figure 3.8 Measurement cell after assembling the components (outer case PMMA i.e. Poly (methyl methacrylate) and inner case PDMS i.e. Poly dimethylsiloxane)

The stabilized base line can be obtained after few minutes running the blank solution through the cell which can be monitored on line on Agilent GPIB bus adapter and processed via software LabView routine adapted in our laboratory.

Chapter 4
Folic Acid & Metabolites Imprinting Results and Discussion

4.1 Folic Acid Imprinting

Targeting bulk imprinting, rather than surface or substructure approaches, can be interesting by applying the entire molecule in bulk during polymerization. Bulk imprinting based on one of the largest molecule leaving its imprints in the matrix is advantageous to achieve highly selectivity as compared to that of its structural analogs or metabolites. Folic acid bulk imprinting remained successful by using methacrylic acid and vinyl pyrrolidone as monomers and EGDMA as cross linking monomer under UV light. In the first step, monomer to cross linker ratio, AIBN concentration were optimized for methacrylic acid-EGDMA MIP system.

4.1.1 Poly Methacrylate MIP Thin Films

For poly methacrylate MIP synthesis, increase and decrease of 1 cm distance between reaction tube and source with respect to optimum distance increases or decreases polymerization time by two hours, respectively with respect to optimum time. Figure 4.1 demonstrates the sensitivity of folic acid on optimized poly methacrylate bulk imprinted MIP thin film. 8.5 kHz (340 nm as 1 kHz equals 40 nm) layer height, measured on network analyzer, was achieved by MIP spin coating, drying hardening and after template washing. Three times larger sensor response of MIP as compared to that of NIP explains better incorporation of folic acid molecules into bulk imprinted thin film.

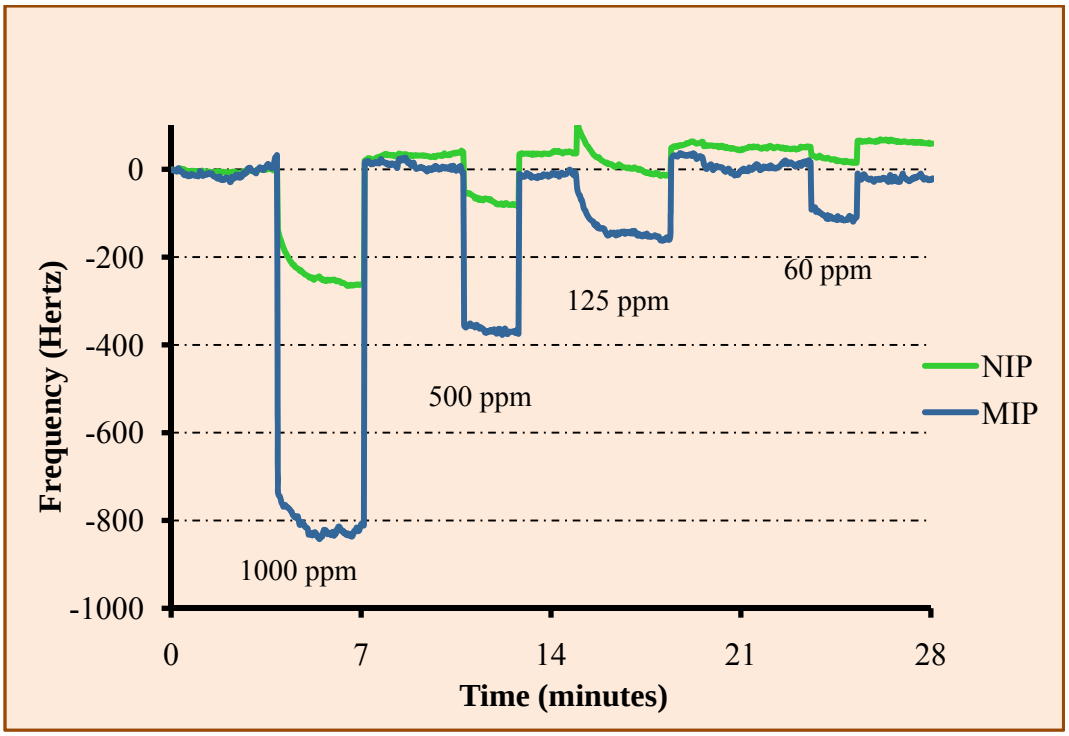

Figure 4.1 Sensor response of folic acid imprinted in poly methacrylate MIP and respective NIP, 8.5 kHz MIP layer height achieved by spin coating after template washing

The sensor response is reversible generating sensitivity at parts per million levels with 60 ppm LoD at S/N ratio ≥ 3. The better incorporation on MIP layer indicates a robust and sensitive recognition system is possible for folic acid by using bulk imprinting approach. Thus, the study of MIP morphology should yield interesting information regarding the layer roughness.

MIP Morphology

The AFM image in Figure 4.2 depicts the surface of methacrylate MIP showing surface roughness in the range of only few nanometers. The MIP surface layout is homogenous that indicates high suitability for using it as QCM sensor layer, because only minor viscous influence can be expected. Furthermore, low roughness leads to lower noise and thus better analytical performance in the terms of base line noise. To assess the extent of imprinting the selectivity pattern can be interesting information (i.e. shown in figure 4.3).

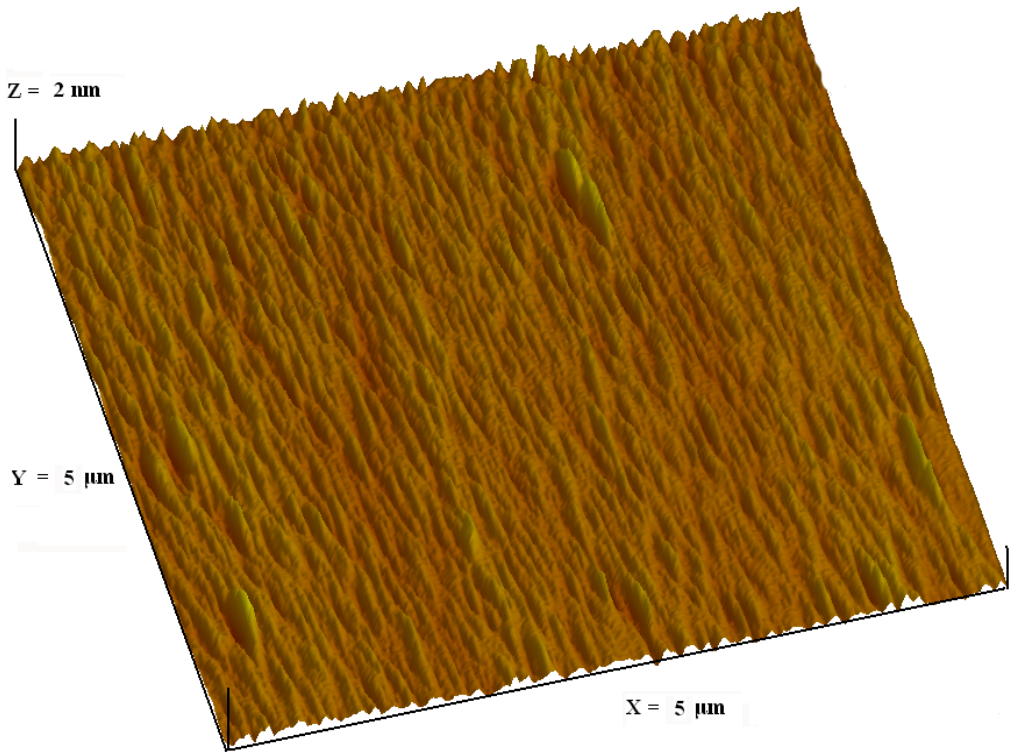

Figure 4.2 *AFM image of poly methacrylate MIP*

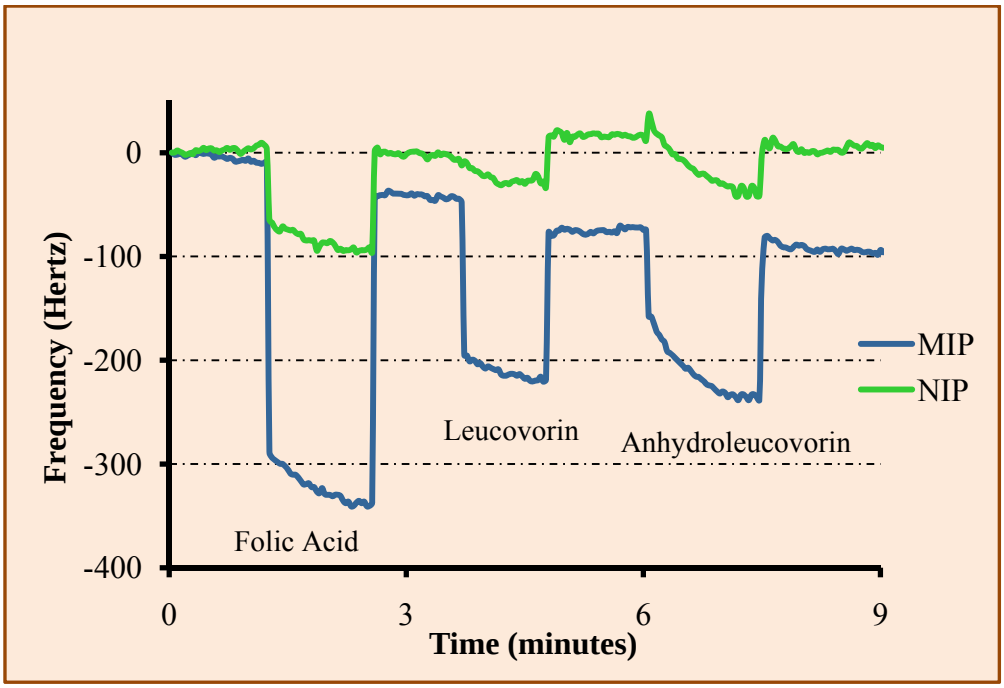

Figure 4.3 *Selectivity pattern at 500 ppm for folic acid imprinted poly methacrylate MIP and respective NIP, 9 kHz MIP layer height achieved by spin coating and after template washing*

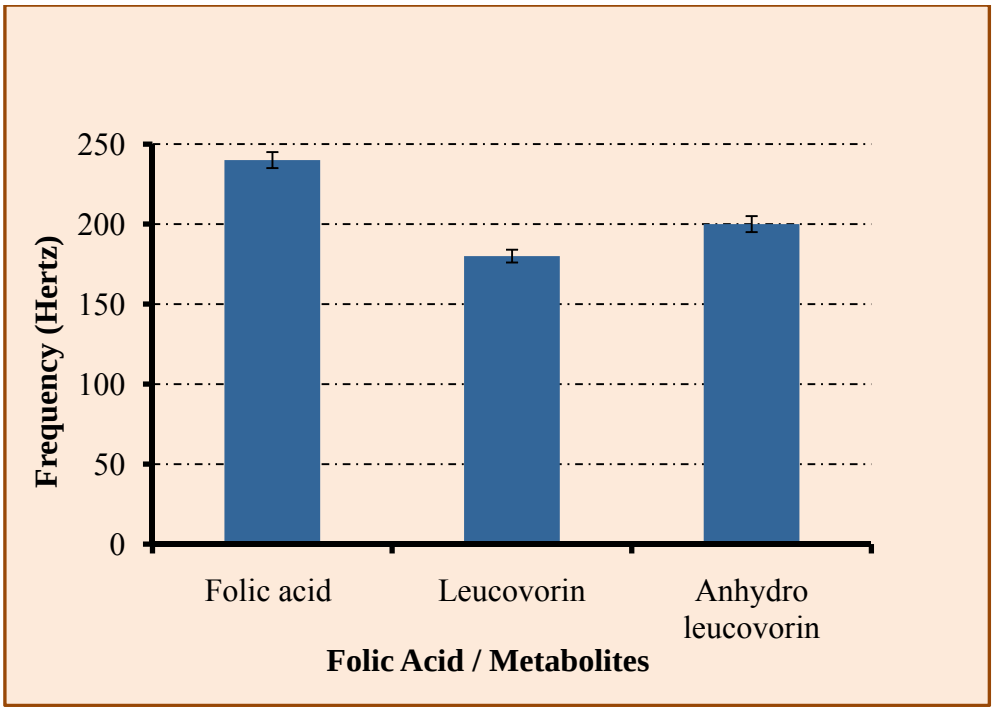

Figure 4.4 Selectivity pattern at 500 ppm for folic acid imprinted poly methacrylate MIP, 9 kHz MIP layer height achieved by spin coating and after template washing

To the above figure 4.4, folic acid and metabolites selectivity was measured at the same concentration level (500 ppm) in the same solution media (1 mM ammonium phosphate buffer pH 10). The figure demonstrates rather broad-band folic acid selectivity on comparing with its metabolites (leucovorin and anhydroleucovorin). This first attempt, in principle, indicates that selectivity can be achieved as metabolites leucovorin and anhydroleucovorin yielded comparatively lower sensor effects. The data suggests the possibility of further improvements in sensitivity and selectivity e.g. via NPs approach by applying effective template removal strategies. Furthermore poly vinyl pyrrolidone MIP could be better choice for these improvements because of it could interact more with N-H groups in the folic acid molecule. The MIP characterization can be interesting information to investigate into the possibility of improvement in sensitivity. Figures 4.5, 4.6 and 4.7 show MIP sensitivity on 5, 13 and 17 kHz layer heights respectively.

MIP Characterization

5 kHz MIP Layer Height

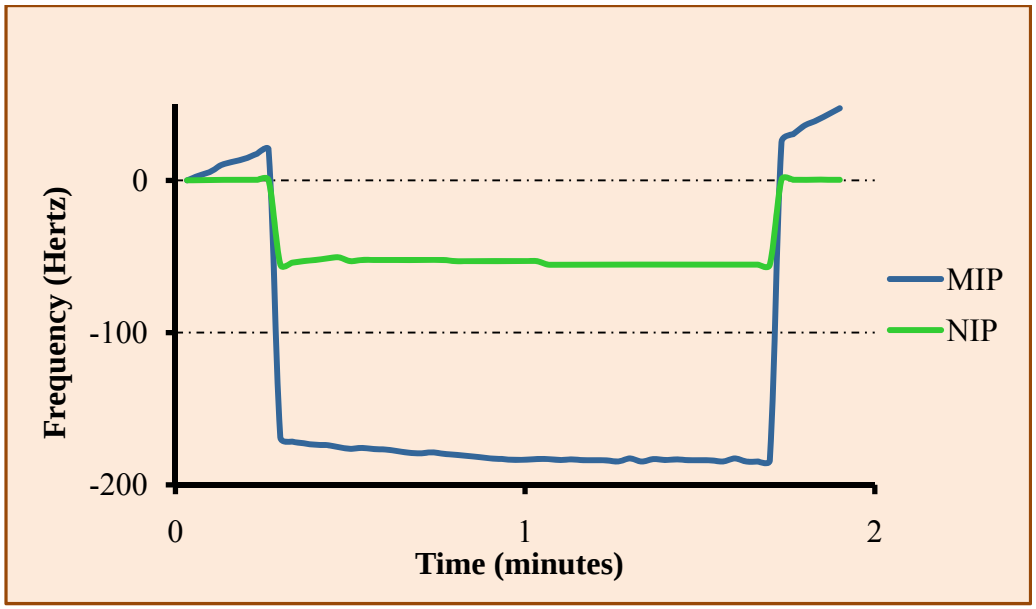

Figure 4.5 Sensitivity at 500 ppm, sensor response of folic acid imprinted in poly methacrylate MIP and respective NIP, 5 kHz MIP layer height achieved by spin coating at 4500 rpm after overnight drying and template washing

13 kHz MIP Layer Height

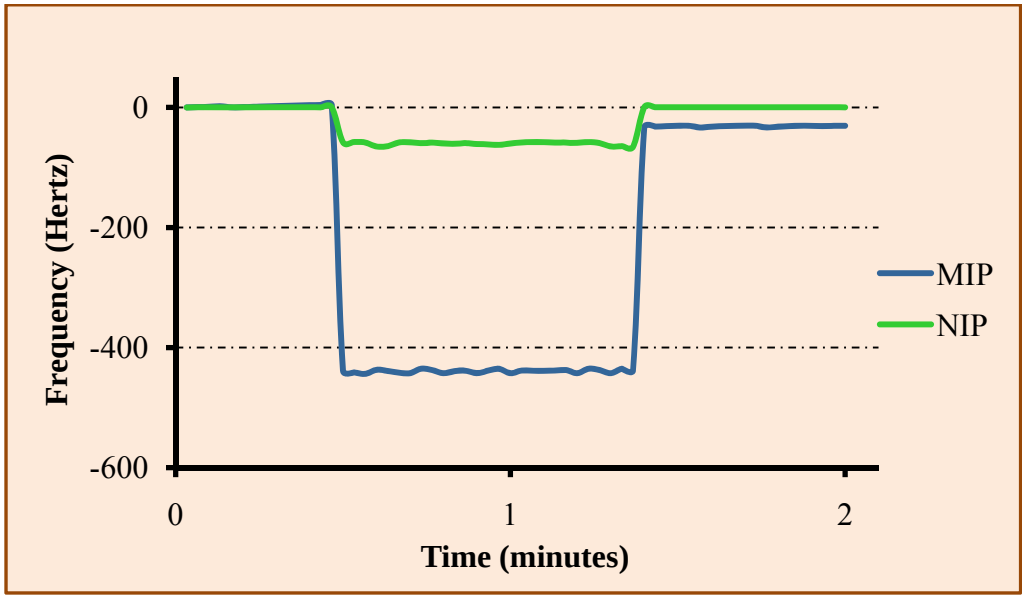

Figure 4.6 Sensitivity at 500 ppm, sensor response of folic acid imprinted in poly methacrylate MIP and respective NIP, 13 kHz MIP layer height achieved by spin coating at 2500 rpm after overnight drying and template washing

17 kHz MIP Layer Height

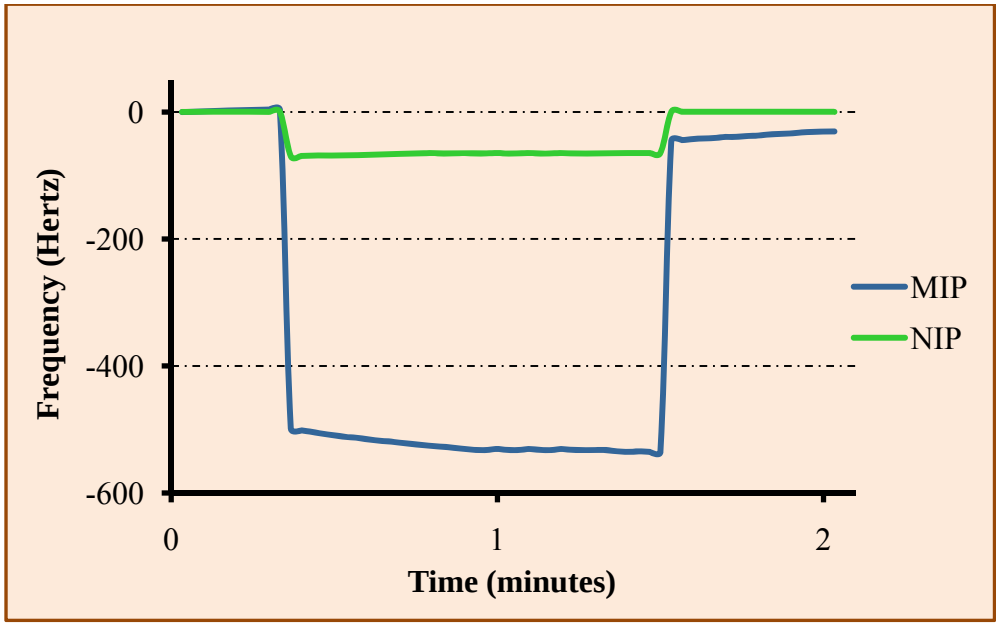

Figure 4.7 Sensitivity at 500 ppm, sensor response of folic acid imprinted in poly methacrylate MIP and respective NIP, 17 kHz MIP layer height achieved by spin coating at 2000 rpm after overnight drying and template washing

MIP Layer Height Effect on Sensitivity

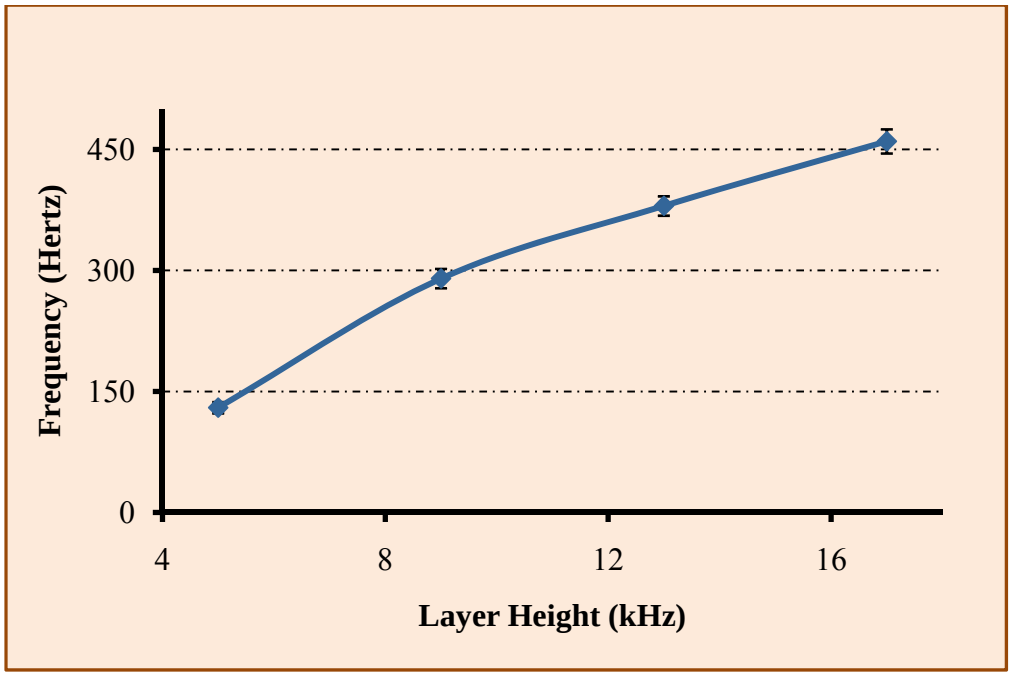

Figure 4.8 Layer height effect on MIP sensitivity at 500 ppm, sensor response of folic acid imprinted in poly methacrylate MIP

Figure 4.8 summarizes the folic acid sensitivity at 500 ppm on poly methacrylate MIP thin films having layer heights of 5, 9, 13 and 17 kHz respectively. The sensor response increases monotonously as a function of layer height and peaks at 17 kHz layer height. The layer height beyond 17 kHz for this MIP system is not achieve able for suitable sensor signals in mass sensitive measurements because it leads to higher damping of the respective electrode ultimately leading to decreased electronic quality and e.g. cross talk between the electrodes. The change of MIP system can be helpful to achieve better imprinting sites for folic acid. Vinyl pyrrolidone-EGDMA can be a better strategy to reach the goal of better sensitivity, detection limits and selectivity because possibility of better interaction with N-H group of folic acid. For this purpose, the optimized poly methacrylate MIP synthetic recipe has been applied to poly vinyl pyrrolidone system keeping all the parameters constant and same except the monomer replacement by N-vinyl 2-pyrrolidone.

4.1.2 Poly Vinyl Pyrrolidone MIP Thin Films

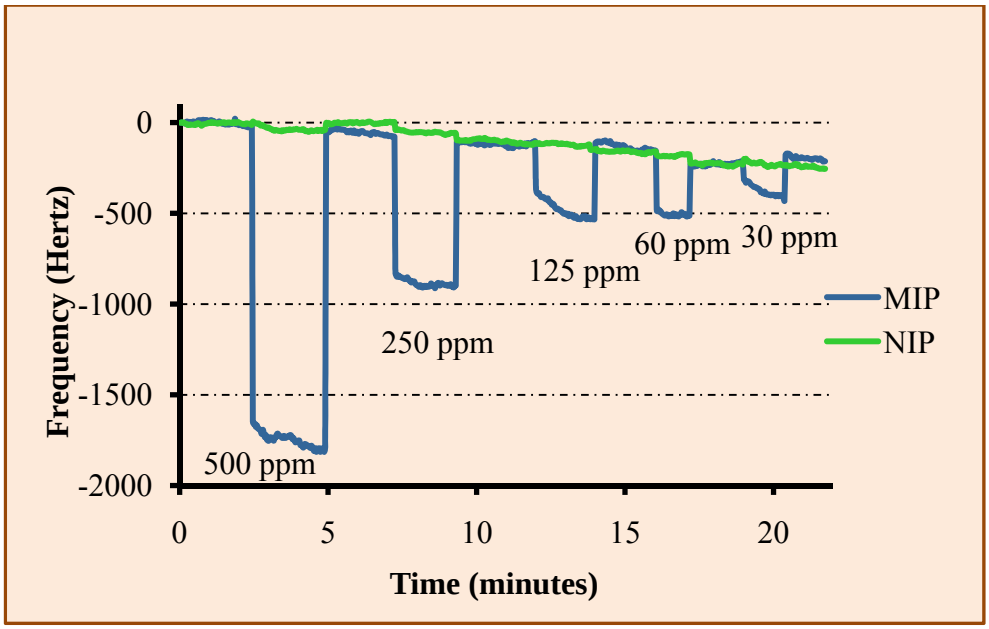

Figure 4.9 Sensor response of folic acid imprinted in poly vinyl pyrrolidone and respective NIP, 9 kHz layer height achieved by MIP spin coating and after template washing

For poly vinyl pyrrolidone MIP synthesis, increase and decrease of 1 cm distance between reaction tube and source with respect to optimum distance increases or decreases polymerization time by three hours, respectively with respect to optimum time. Figure 4.9 demonstrates the sensitivity of folic acid on optimized poly vinyl pyrrolidone bulk imprinted MIP thin film. 9 kHz layer height, measured on network analyzer, was achieved by MIP spin coating, drying hardening and after template washing. Outstanding sensor response of MIP as compared to that of NIP explains remarkable diffusion of folic acid molecules into bulk imprinted thin film demonstrating the success of bulk imprinting. In contrast to this, the poly vinyl pyrrolidone reference electrode containing NIP did not interact with folic acid molecules. The sensor response is highly reversible and robust showing sensitivity at parts per million levels with 30 ppm LoD at S/N ratio ≥ 3. The measurement with poly vinyl pyrrolidone MIP has the advantage of low NIP response on reference electrode as compared to that of measurement with poly methacrylate NIP. The reason behind this factor is the fundamental change of monomer i.e. vinyl pyrrolidone behaved obviously different as compared to methacrylate. This may be due to better interaction of the tertiary Nitrogen atom of vinyl pyrrolidone system with the N-H and O-H bonds of folic acid.

Figure 4.10 demonstrates the sensor characteristics for optimized imprinted poly vinyl pyrrolidone MIP thin film at 9 kHz layer height. One can see the improved sensitivity and LoD from vinyl pyrrolidone MIP thin film on comparing to that of poly methacrylate MIP thin film. The improvement led to the 7 times enhanced sensitivity at 500 ppm and 2 times improved LoD demonstrating that vinyl pyrrolidone system leads to superior recognition. The comparatively better incorporation on vinyl pyrrolidone MIP layer indicates a robust and appreciable sensitive recognition system is possible for folic acid by using bulk imprinting approach. This may be due to better

interaction of the tertiary Nitrogen atom with the N-H and O-H bonds of folic acid. The study of vinyl pyrrolidone MIP morphology could be interesting regarding the layer roughness and MIP layout.

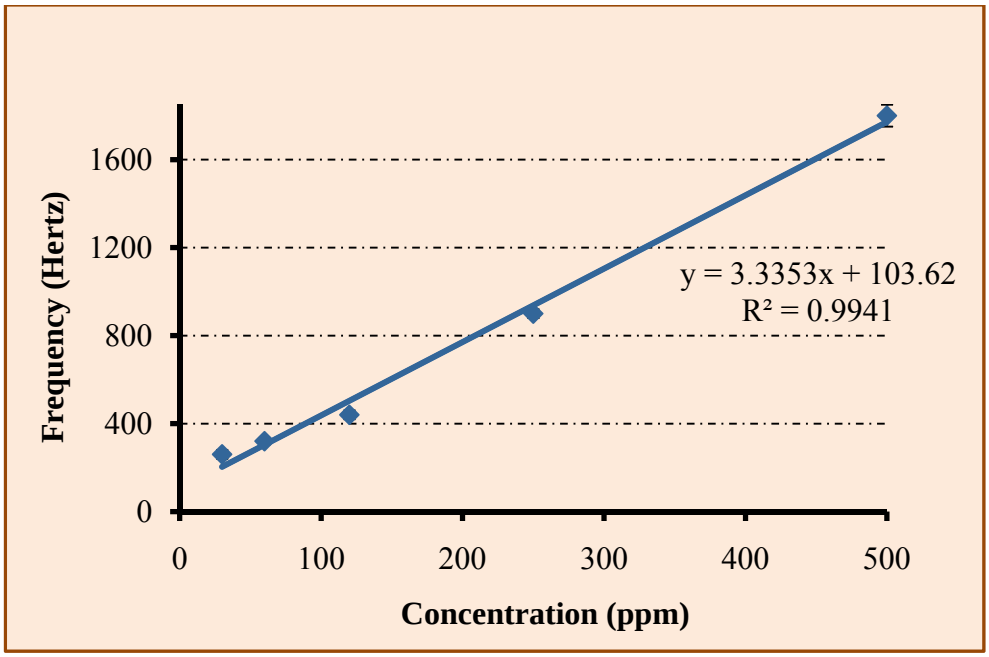

Figure 4.10 Sensor characteristics of folic acid imprinted in poly vinyl pyrrolidone, 9 kHz layer height achieved by MIP spin coating and after template washing

MIP Morphology

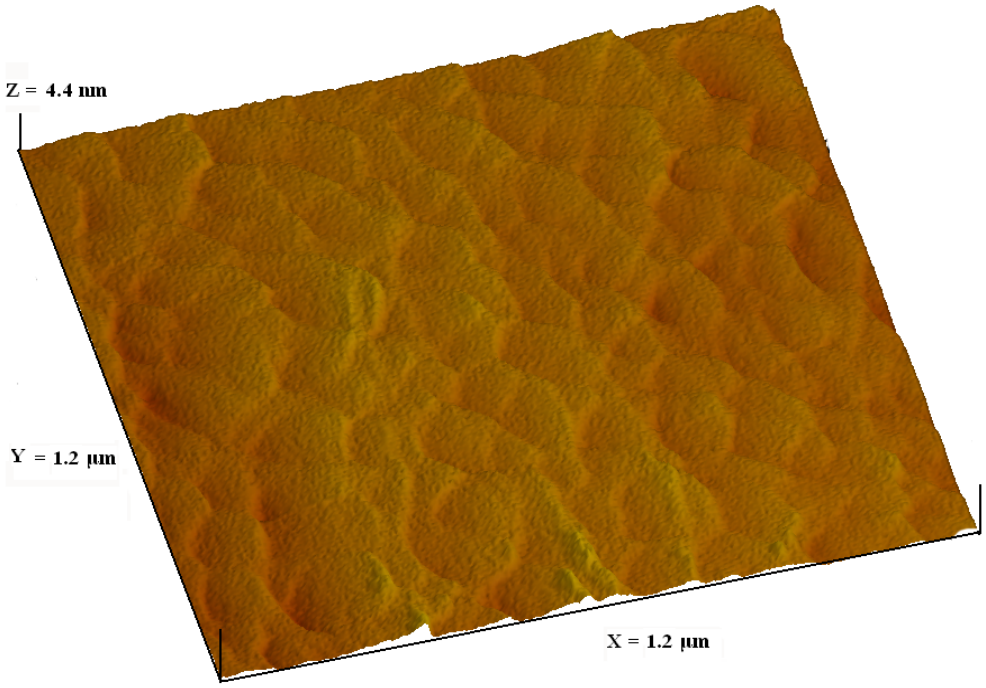

Figure 4.11 3D AFM image of poly vinyl pyrrolidone MIP thin film

The AFM image in Figure 4.11 displays the surface layout for vinyl pyrrolidone MIP thin film demonstrating surface roughness in the range of only a few nanometers to several hundred nanometers. The MIP surface layout is homogenous indicating high suitability for using it as QCM sensor thin film, as only negligible viscous influence can be expected. Furthermore, a better analytical performance in the terms of low base line noise can be expected. The study of selectivity pattern can be exciting to investigate into the extent of imprinting for this MIP thin film.

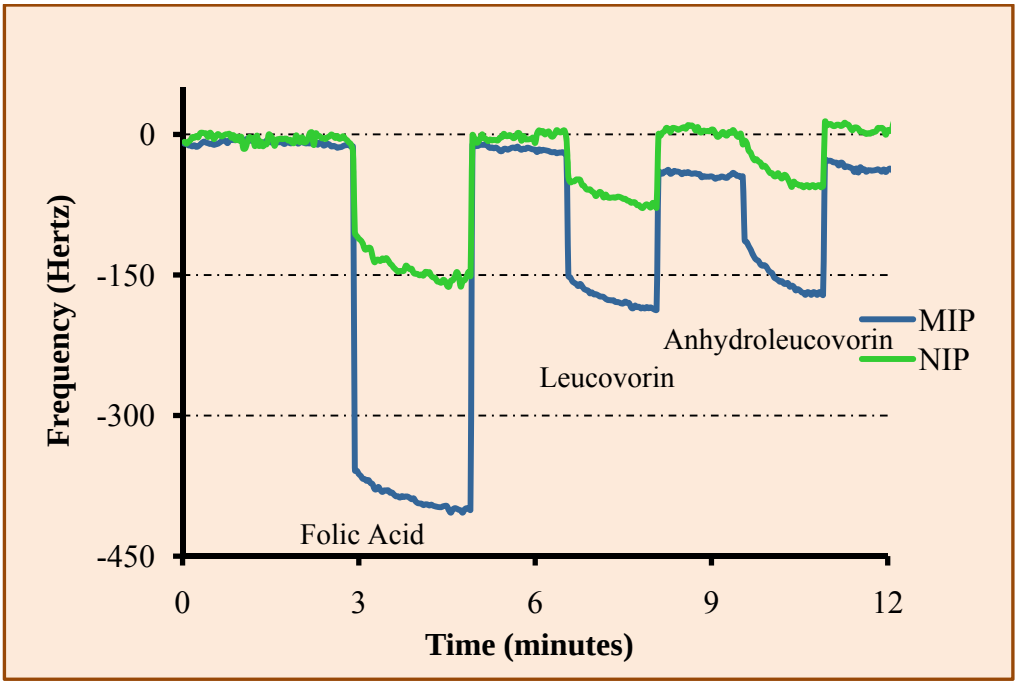

Figure 4.12 Selectivity pattern at 100 ppm for folic acid imprinted poly vinyl pyrrolidone MIP, 9 kHz layer height achieved by spin coating and after template washing

Figure 4.13 depicts 2.5 folds selectivity for folic acid as compared to that of its metabolites i.e. leucovorin and anhydroleucovorin at 100 ppm demonstrating remarkable outcome of the MIP. For this study, 9 kHz (i.e. 360 nm) layer height, measured on network analyzer, was achieved after the template washing. Folic acid imprinting in poly vinyl pyrrolidone gave better

selectivity pattern if we compare to that of poly methacrylate MIP system giving insight into the suitability of vinyl pyrrolidone for generating compactness in MIP. Further improvements in sensitivity and selectivity are possible by using MIP-NPs approach applying effective template removal strategies. The MIP characterization based on different layer heights can be interesting to look into the possibility of improvement in sensitivity.

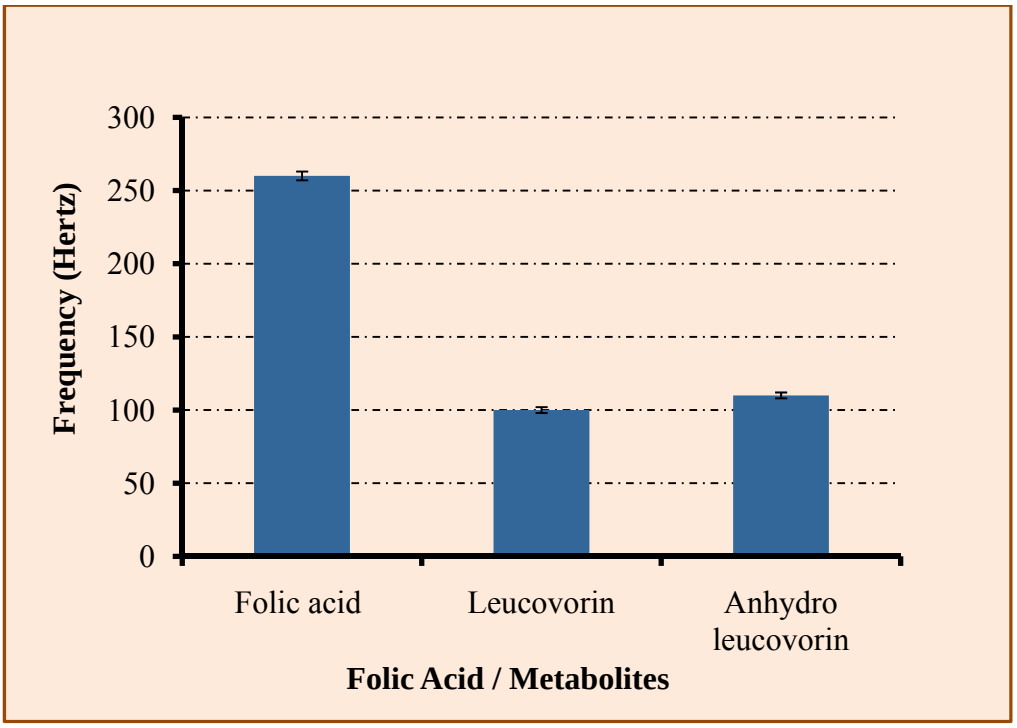

Figure 4.13 *Selectivity pattern at 100 ppm for folic acid imprinted poly vinyl pyrrolidone MIP, 9 kHz layer height achieved by spin coating and after template washing*

MIP Characterization

Figures 4.14 and 4.15 show the sensor response of folic acid at 100 ppm on layer heights of 6 and 15 kHz respectively for vinyl pyrrolidone MIP thin films. The sensor responses are reversible and robust demonstrating suitability of MIP for QCM transducer on using different heights of vinyl pyrrolidone MIP system.

6 kHz MIP Layer Height

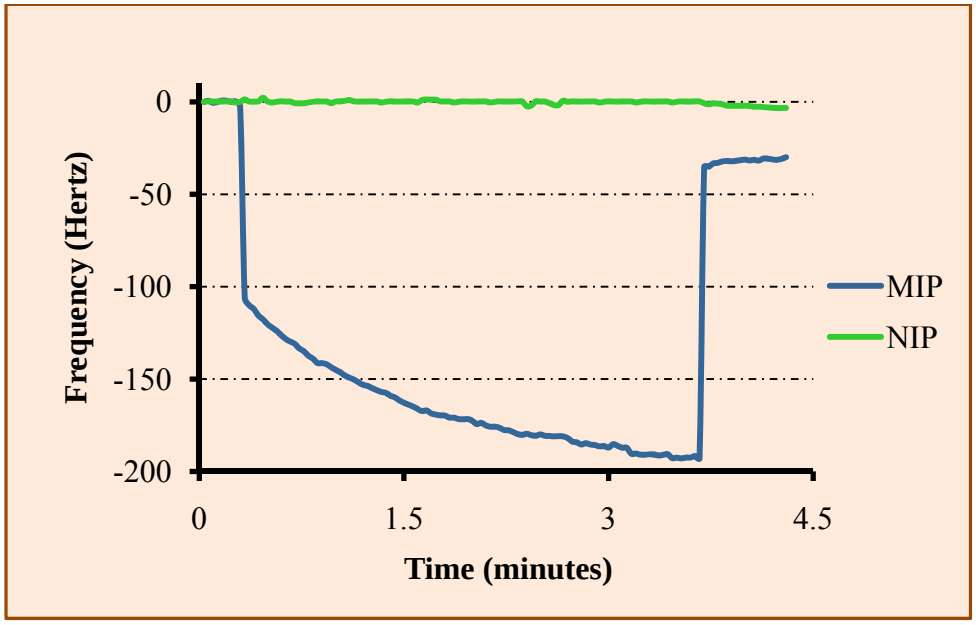

Figure 4.14 Sensitivity at 100 ppm, sensor response of folic acid imprinted in poly vinyl pyrrolidone, 6 kHz MIP layer height achieved by spin coating at 4500 rpm after overnight drying and template washing

15 kHz MIP Layer Height

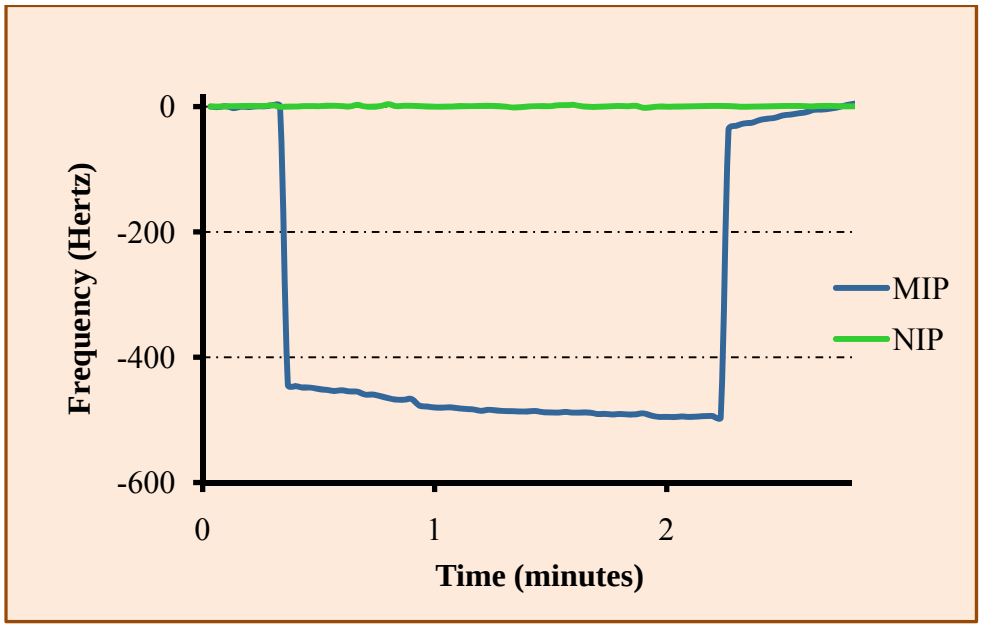

Figure 4.15 Sensitivity at 100 ppm, sensor response of folic acid imprinted in poly vinyl pyrrolidone, 15 kHz MIP layer height achieved by spin coating at 2000 rpm and after template washing

MIP Layer Height Effect on Sensitivity

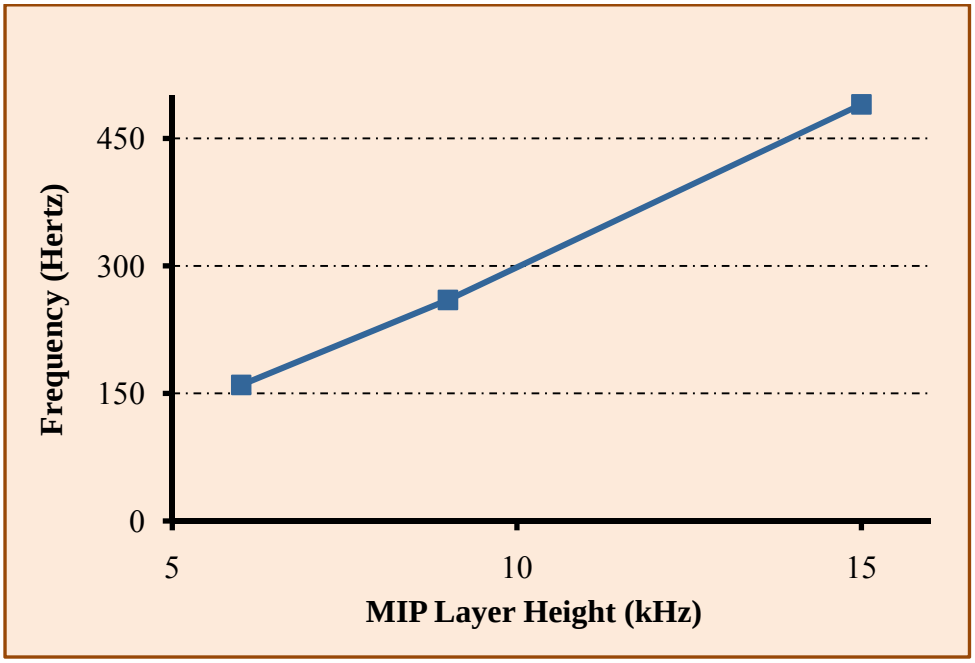

Figure 4.16 Layer height effect on MIP sensitivity at 100 ppm, sensor response of folic acid imprinted in poly vinyl pyrrolidone

The above Figure 4.16 sketches folic acid sensitivity on 6, 9 and 15 kHz layer heights of poly vinyl pyrrolidone MIP thin films on QCM electrodes. The sensor response is directly proportional to the layer height on the spin coated electrode and peaks until 15 kHz layer height. Thicker layer heights beyond 15 kHz for suitable electronic measurements cannot be achieved because it leads to higher damping ultimately giving cross talk in the mass sensitive measurements. Further improvement is possible by applying NPs approach to both methacrylate and vinyl pyrrolidone MIP systems. Obviously, NPs generated from MIP can offer enhanced surface area for better inclusion of folic acid molecules.

Nanoparticle Approach

Aiming the further improvements in sensitivity, the feasibility of NPs for poly methacrylate MIP system was tested by using acetonitrile for NPs

precipitation. NPs were precipitated by pouring MIP oligomer solution into vigorously stirring acetonitrile and subjected to AFM studies.

4.1.3 Poly Methacrylate MIP NPs

NPs Morphology

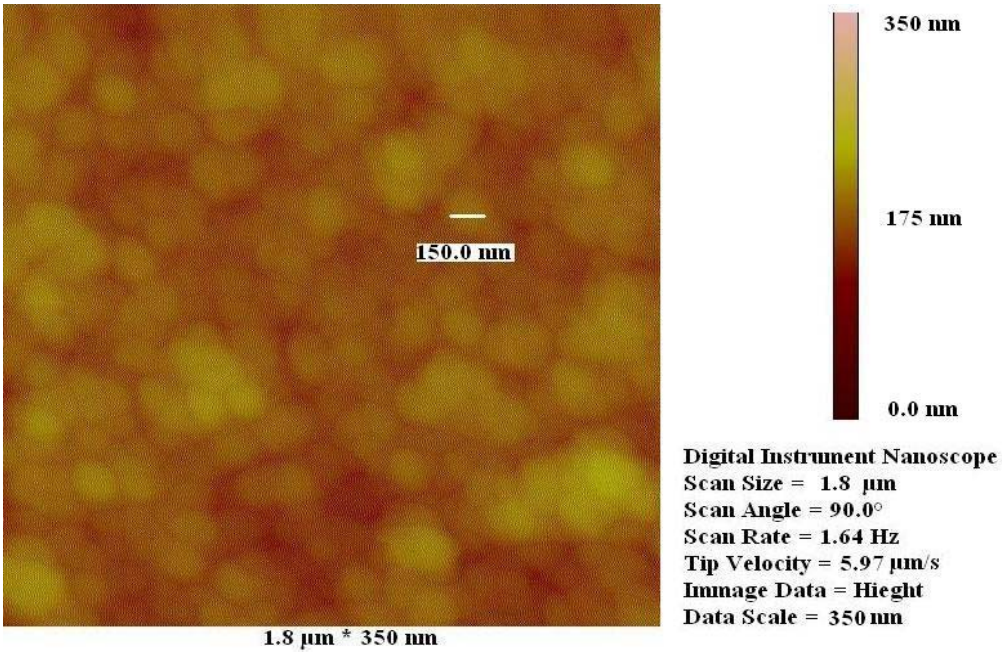

Figure 4.17 AFM image of poly methacrylate NPs

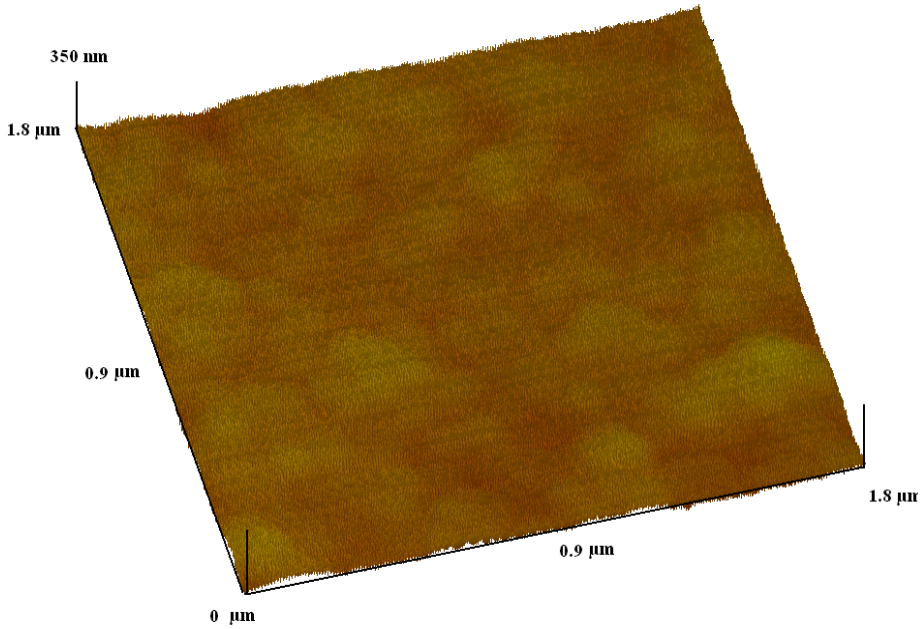

Figure 4.18 3D AFM image of poly methacrylate NPs

Figures 4.17 and 4.18 show 2D and 3D AFM images of NPs generated from poly methacrylate MIP, respectively. The NPs surface layout keeps homogeneity and low roughness in the range of few nanometers while NPs average diameter ranges 150 nm. The NPs surface studies indicate enhanced surface area as compared to that of MIP. Therefore, the AFM images imply increase in the accessibility of interacting sites for better diffusion of template molecules into the NPs.

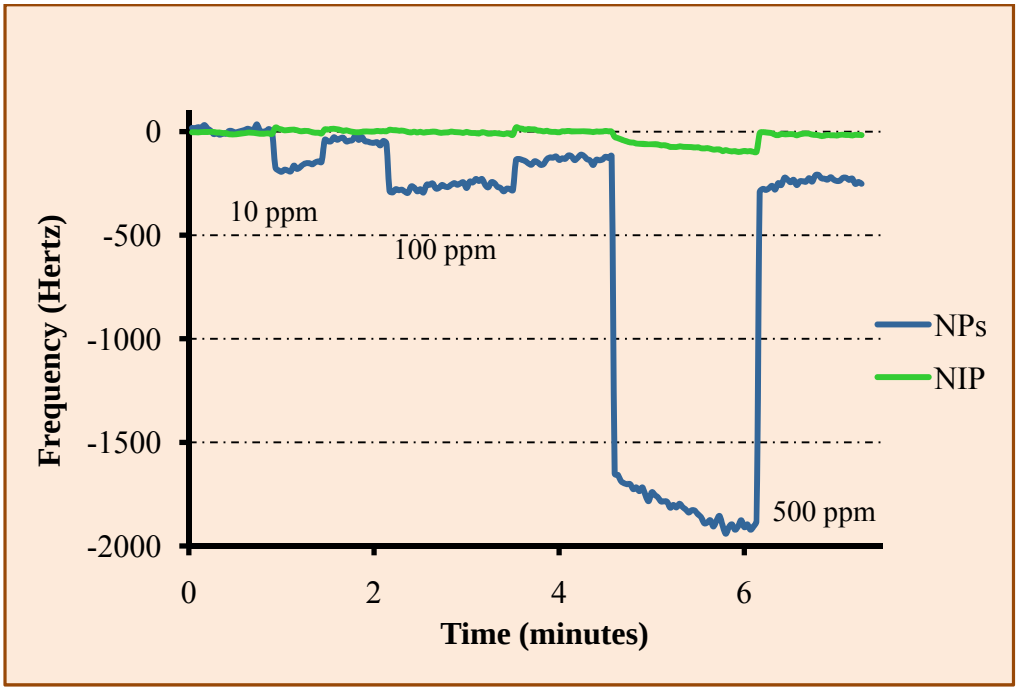

Figure 4.19 Sensor response of folic acid imprinted poly methacrylate NPs. 9 kHz layer height achieved for NPs spin coated on one electrode while the second electrode was spin coated with NIP beads

To test that claim, figure 4.19 demonstrates the sensor response of NPs generated from poly methacrylate MIP. 9 kHz layer height was achieved by spin coating of NPs on the oligomer layer of acrylic acid and EGDMA while the second electrode (reference) was spin coated with NIP beads. MIP-NPs gave sensitivity at parts per million levels with 10 ppm LoD at S/N ratio ≥ 3. The NPs sensitivity is 6 times as compared to that of MIP at 500 ppm analyte

concentration demonstrating appreciable outcome of the NPs approach. The enhanced sensitivity for NPs can be attributed due to the enhancement of NPs surface area as compared to that of MIP. Sensitivity enhancement can also be assigned due to larger accessible internal surface and substantially reduced average diffusion pathways within the NPs material. Furthermore the template removal via washing strategies remained effective in NPs approach as compared to that of MIP. Table 4.1 explains the different individual washing strategies for template removal from MIP while combination of these strategies remained successful for NPs approach in mass sensitive measurements. The reason in breakthrough in sensitivity is contributed by the factor that combination of these washing strategies was applied for NPs washing. While in the case of MIP, only methanol was applied for template washing.

Table 4.1 Different washing strategies for template removal from poly methacrylate MIP spin coated on QCM electrode

Solvent	Washing duration (hours)	MIP layer height (kHz)	MIP- layer height (% decreased)	NIP layer height (kHz)	NIP layer height (% decreased)
Water	2	12	2	11	1
Water (60°)	2	13	3	10	2
Methanol	2	11	10	10	3
Water (pH10 with NH_3)	2	13	3	11	2
10 mM Ammonium phosphate (pH 10)	1/2	13	50	11	45

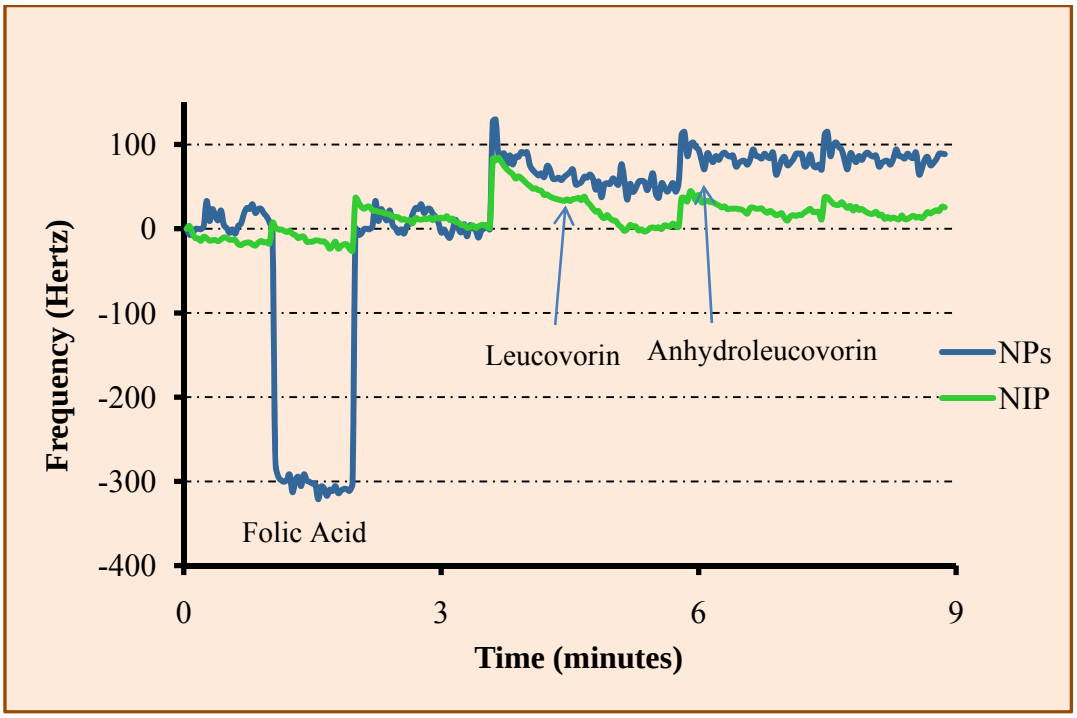

Figure 4.20 Selectivity pattern at 100 ppm for folic acid imprinted poly methacrylate NPs, 9 kHz layer height achieved by NPs spin coating on measuring electrode of QCM while the second electrode was spin coated with NIP beads

The above Figure 4.20 depicts the selectivity pattern for folic acid and its metabolites on poly methacrylate NPs having layer height of 9 kHz. Outstanding selectivity for folic acid as compared that of its metabolites (i.e. leucovorin and anhydroleucovorin) has been achieved for poly methacrylate NPs. This demonstrates astonishing selectivity for folic acid giving the complete picture of imprinting of different groups of folic acid molecule in the NPs. The metabolites, at the same concentration level (100 ppm) in the same solution media (1 mM ammonium phosphate buffer pH 10), did not yield any frequency change on electrode containing the NPs. The reason in breakthrough in selectivity is contributed by the factor that combination of different washing strategies was applied for NPs washing. These washing methodologies effectively removed the template along with un-reacted constituents from the matrix of NPs. In the case of MIP, only methanol was

applied for template washing (as explained above). The data demonstrates sensitivity and LoD improvements along with the astonishing effect on the selectivity pattern on comparing the response of the NPs to that of the MIP. The positive effects are contributed due to effective template removal from the NPs by different washing strategies (i.e. with water containing pH 10 with few drops of NH_3) along with increased surface area of NPs. Finally the washing process, repeated by distilled water and methanol separately, remained positive effective to achieve imprinted template free NPs. The NPs characterization based on layer heights can be interesting to look into the behavior of NPs regarding sensitivity and detection limits.

NPs Characterization

Figures 4.21, 4.22, 4.23, 4.24 and 4.25 show the sensor response of folic acid on poly methacrylate NPs on layer heights of 5, 6.5, 9, 12 and 15 kHz respectively.

5 kHz Layer Height

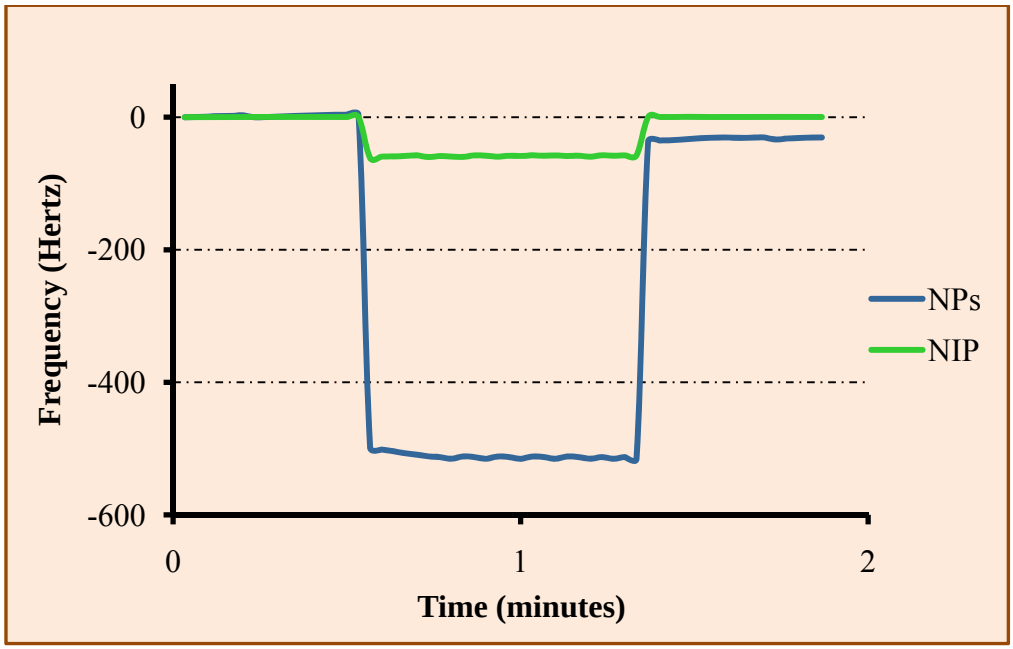

Figure 4.21 Sensor response of folic acid imprinted poly methacrylate NPs at 500 ppm, 5 kHz layer height achieved by NPs spin coating while the reference electrode was spin coated with NIP beads

6.5 kHz Layer Height

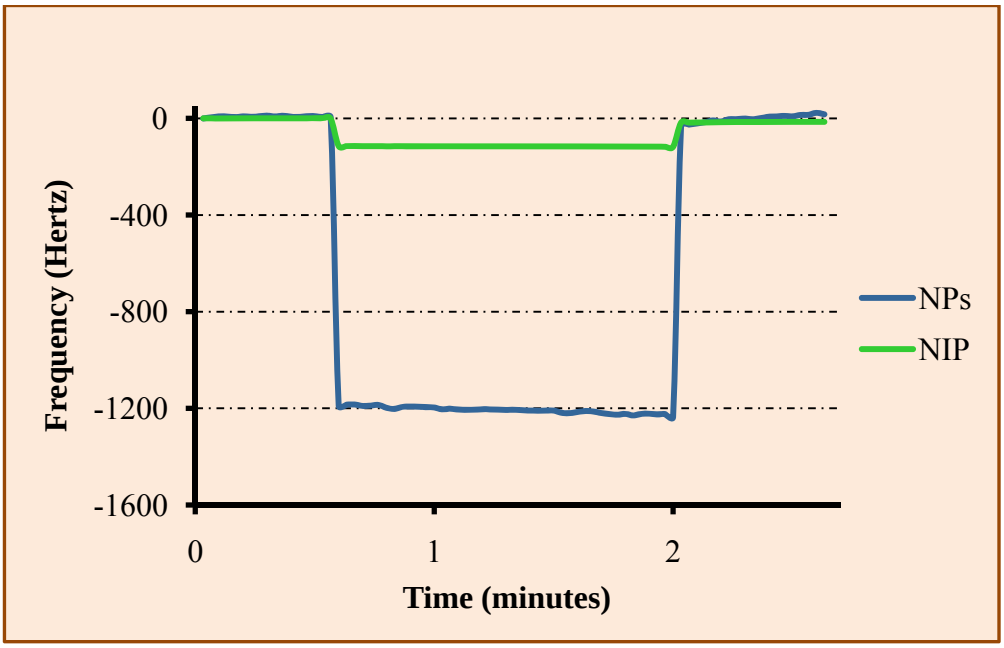

Figure 4.22 Sensor response of folic acid imprinted poly methacrylate NPs at 500 ppm, 6.5 kHz layer height achieved by NPs spin coating while the reference electrode was spin coated with NIP beads

9 kHz Layer Height

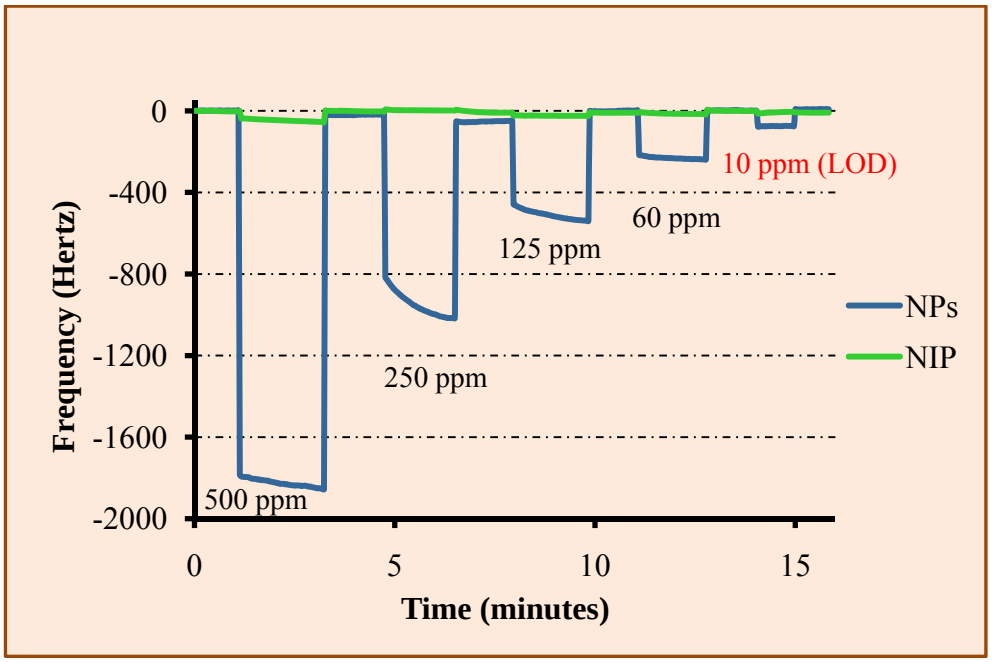

Figure 4.23 Sensor response of folic acid imprinted poly methacrylate NPs, 9 kHz layer height achieved by NPs spin coating while the reference electrode was spin coated with NIP beads

12 kHz Layer Height

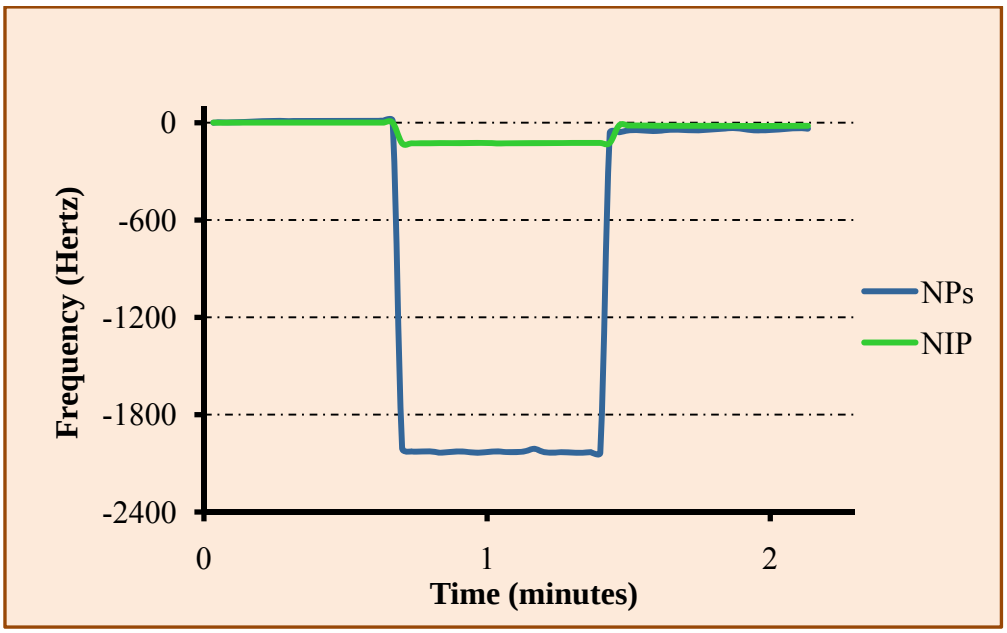

Figure 4.24 *Sensor response of folic acid imprinted poly methacrylate NPs at 500 ppm, 12 kHz layer height achieved by NPs spin coating while the reference electrode was spin coated with NIP beads*

15 kHz Layer Height

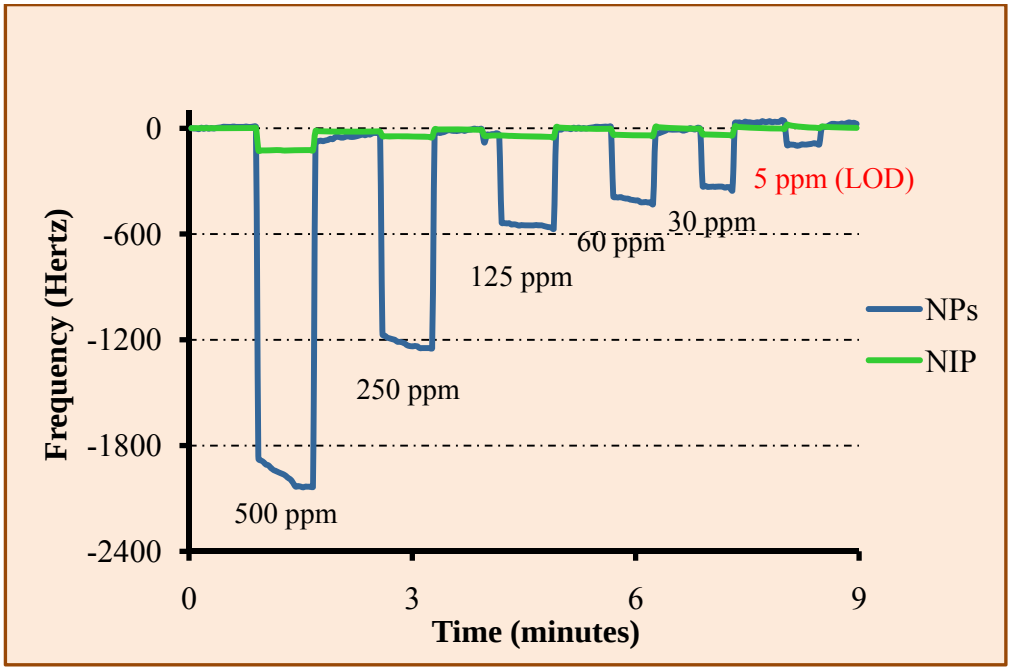

Figure 4.25 *Sensor response of folic acid imprinted poly methacrylate NPs at 500 ppm, 15 kHz layer height achieved by NPs spin coating while the reference electrode was spin coated with NIP beads*

The above Figures 4.21, 4.22, 4.23, 4.24 and 4.25 demonstrate the NPs sensor response at layer heights of 5, 6.5, 9, 12 and 15 kHz respectively. The improvements in NPs sensitivity and detection limits with the increase of NPs layer heights on the measuring electrode are demonstrated from the data. Obviously the increase in layer height provides enhanced surface area for better diffusion of folic acid into the cavities. The improvement in detection limits led to10 ppm LoD at S/N ratio ≥ 3 on 9 kHz layer height. Which is further improved by a factor of two on layer height 15 kHz ultimately leading to 5 ppm at S/N ratio ≥ 3 (above figure 4.25). The sensor responses achieved from NPs approach are robust, faster and more reversible as compared to that of MIPs. The S/N ratio improvements can be assigned to better diffusion pathways due to affective template washing along with removal of un-reacted constituents in NPs approach. Furthermore LoD and sensitivity improvements in the case of NPs are advantageous over the conventional molecular imprinted polymers.

MIP NPs Layer Height Effect on Sensitivity

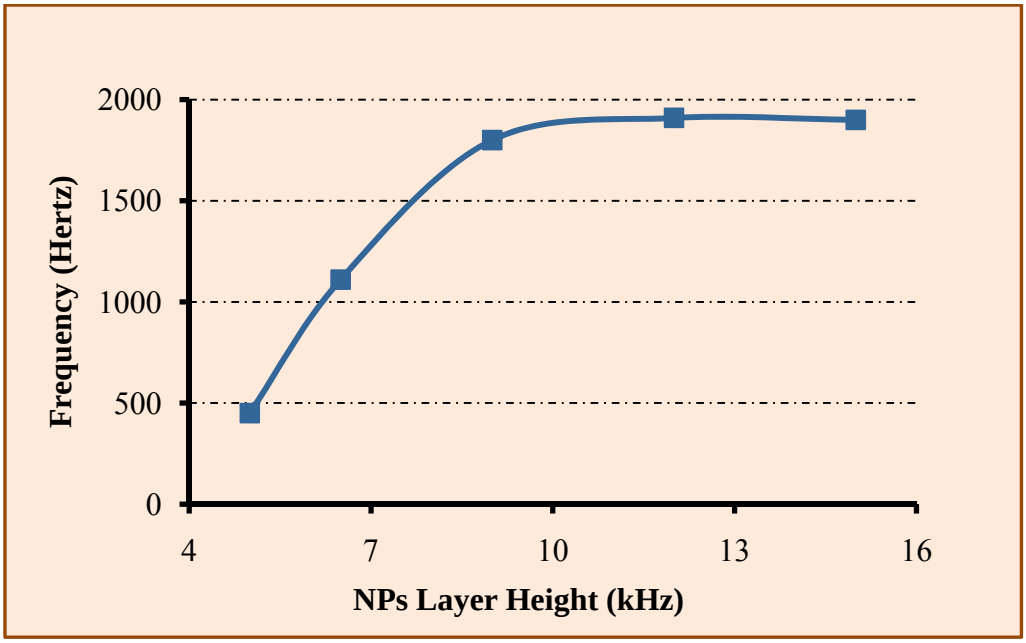

Figure 4.26 Layer height effect on poly methacrylate NPs sensitivity at 500 ppm

The Figure 4.26 summarizes the NPs sensitivity at 500 ppm on 5, 6.5, 9, 12 and 15 kHz layer heights. The sensor response increases linearly as a function of layer height from 5 kHz to 9 kHz while the saturation state is reached after 9 kHz layer height. The saturation state can be explained on the basis of diffusion on NPs layer i.e. for such a large molecule the diffusion phenomena can be too slow to access the lower parts of NPs layer. The layer height beyond 15 kHz for NPs are not suitable for mass sensitive measurements because it leads to higher damping on the QCM electrode generating low electronic quality or cross talks in the mass sensitive measurements. A comparison of layer height effect for MIP and NPs can give the complete picture of bulk imprinting for both approaches.

MIP and NPs Layer Height Effect on Sensitivity (Comparison)

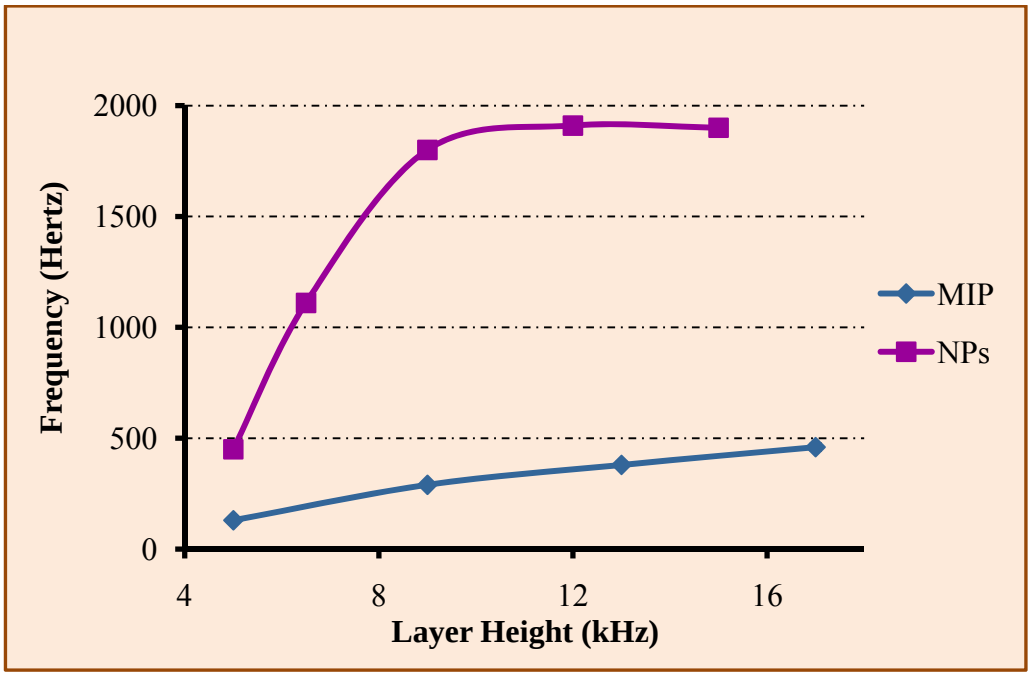

Figure 4.27 Layer height effect on poly methacrylate MIP and NPs sensitivity at 500 ppm

Figure 33 compares the sensor sensitivity on both thin films at 500 ppm. For NPs the saturation state is reached after rapid proportional increase of sensor response from 5 kHz to 9 kHz. The reason behind the saturation

state demonstrates that the cavities become inaccessible on increasing the layer height of NPs. Behaving differently the MIP thin film demonstrates linear increase in sensor response throughout dynamic range of layer height. Generally the MIP sensitivity is substantially lower than that of NPs. The difference in sensitivity for both cases can be assigned to the better accessible interaction sites in NPs for shorter diffusion pathways providing large number of entrances i.e. diffusion cavities. Diffusion also may explain saturation on NPs layer: for such a large molecule, it may be too slow to reach the "lower" parts of the layer. A further comparative study regarding sensor characteristics for both thin films can explain better about diffusion phenomena.

MIP and NPs Sensor Characteristics (Comparison)

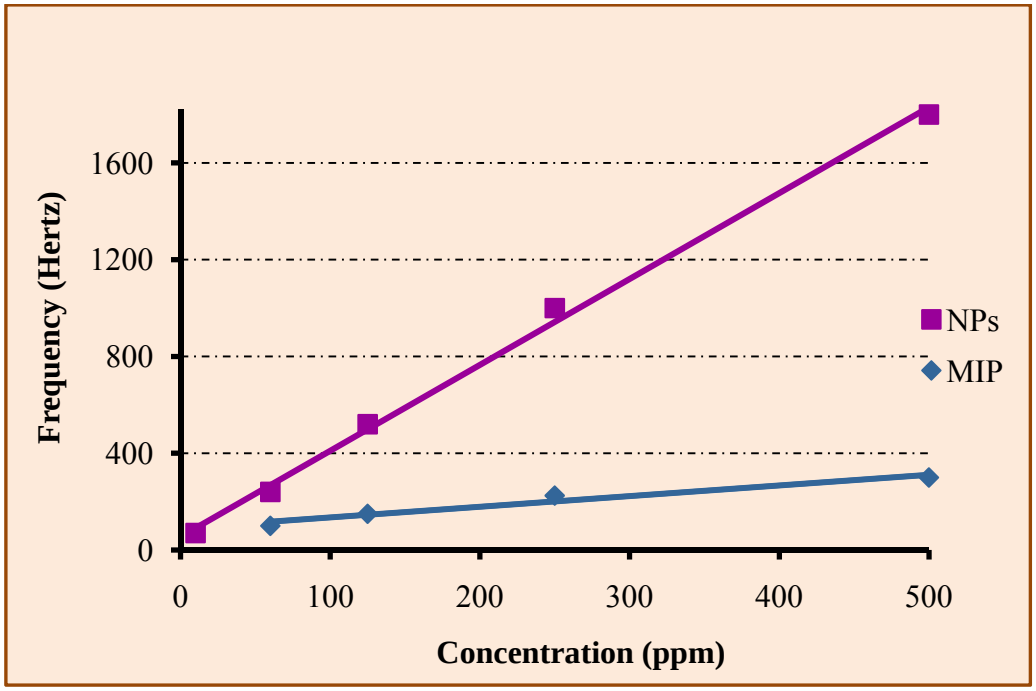

Figure 4.28 Sensor characteristics of poly methacrylate MIP and NPs respectively at 9 kHz layer height

Figure 4.28 compares the sensor characteristics of MIP and NPs respectively. NPs approach worked well with the sensitivity and LoD improvements. The sensitivity difference increases linearly as a function of

increase in folic acid concentration reaching 6 times at 500 ppm. On the other hand the minimum difference is found at MIP LoD (i.e. at 60 ppm) reaching 2.5 times. The reason behind this factor is that the cavities are better accessible on NPs at higher concentrations as compared to lower concentrations. This means the NPs and MIP morphology behaves differently with the variation of folic acid concentrations which is superior in NPs approach. A study of selectivity pattern on different layer heights can be interesting regarding the extant of imprinting for NPs approach.

15 kHz NPs Layer Height (Selectivity)

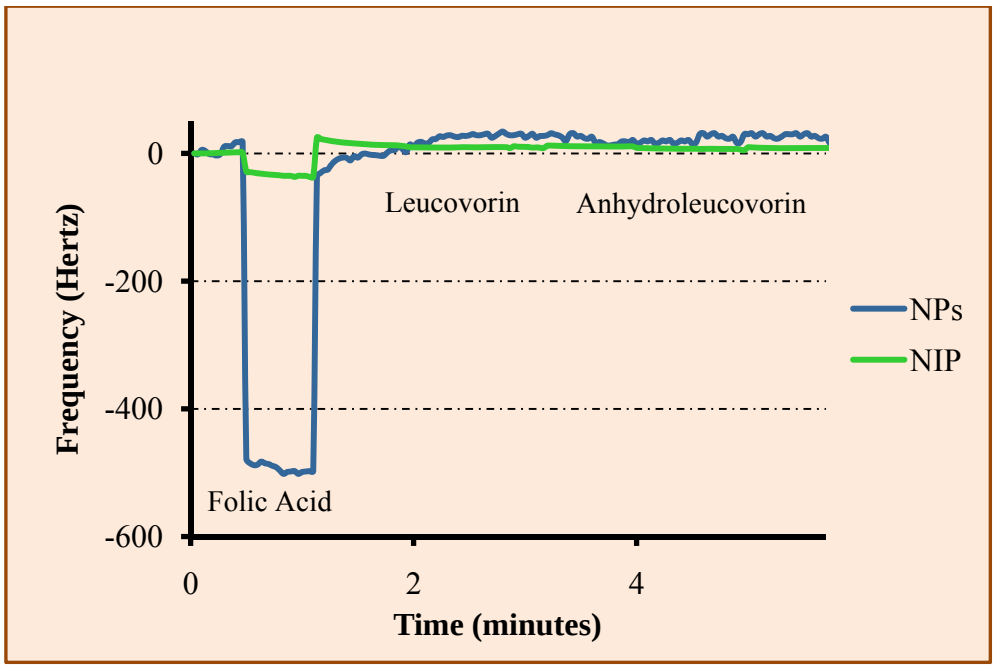

Figure 4.29 Selectivity pattern at 100 ppm, 15 kHz layer height achieved by NPs spin coating on measuring electrode while the second electrode was spin coated with NIP beads

Figure 4.29 compares the cross sensitivity of folic acid and its metabolites at 100 ppm on 15 kHz layer height for poly methacrylate NPs. The metabolites did not show any sensor response demonstrating a good picture of folic acid imprinting for NPs approach.

NPs Layer Height Effect on Selectivity

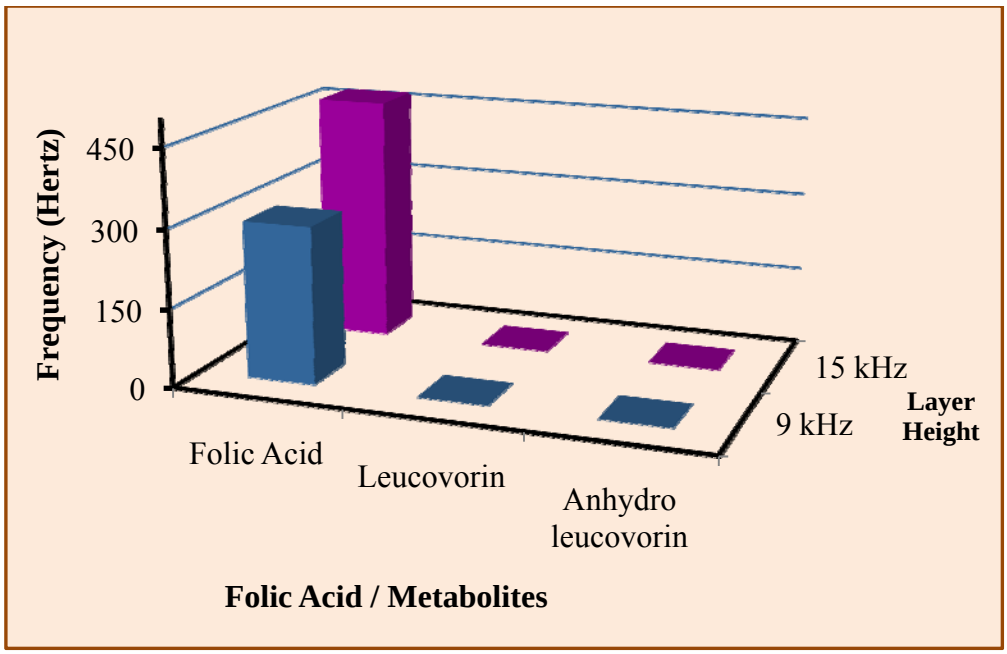

Figure 4.30 Selectivity pattern at 100 ppm, 15 kHz layer height achieved by NPs spin coating on measuring electrode while the second electrode was spin coated with NIP beads

Figure 4.30 compares the selectivity pattern at 100 ppm achieved on 9 and 15 kHz layer heights of poly methacrylate NPs. The pattern follows outclass selectivity for folic acid as compared to that of metabolites as metabolites did not show any signal in cross sensitivity measurements. The folic acid signal increases with the increase of layer height and peaks at 470 hertz (at 100 ppm) with layer height 15 kHz. On the other hand leucovorin and anhydroleucovorin signals move like stable base line in the measurements without showing any sorts of mass deposition effect on QCM electrode using diffusion tracks. The reason in breakthrough in selectivity is contributed by the factor that combination of different washing strategies was applied for NPs washing. While in the case of MIP, only methanol was applied for template washing (as explained above).

4.1.4 Poly Vinyl Pyrrolidone MIP NPs

Targeting the further improvements in sensitivity and detection limits, the feasibility of NPs for poly vinyl pyrrolidone MIP system was examined by using acetonitrile for NPs precipitation. NPs precipitation was achieved by pouring MIP oligomer solution into vigorously stirring acetonitrile and confronted to AFM measurements.

NPs Morphology

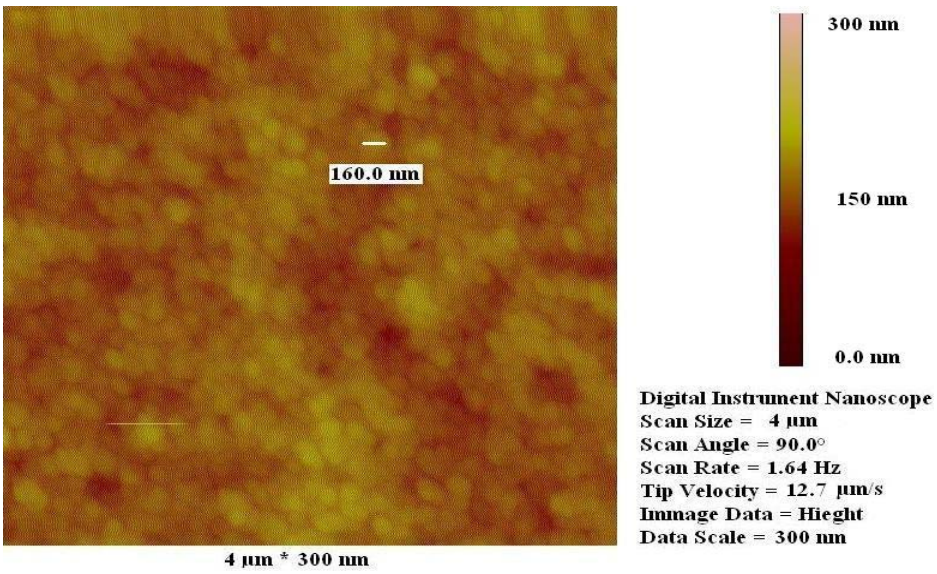

Figure 4.31 *2D AFM image of poly vinyl pyrrolidone NPs*

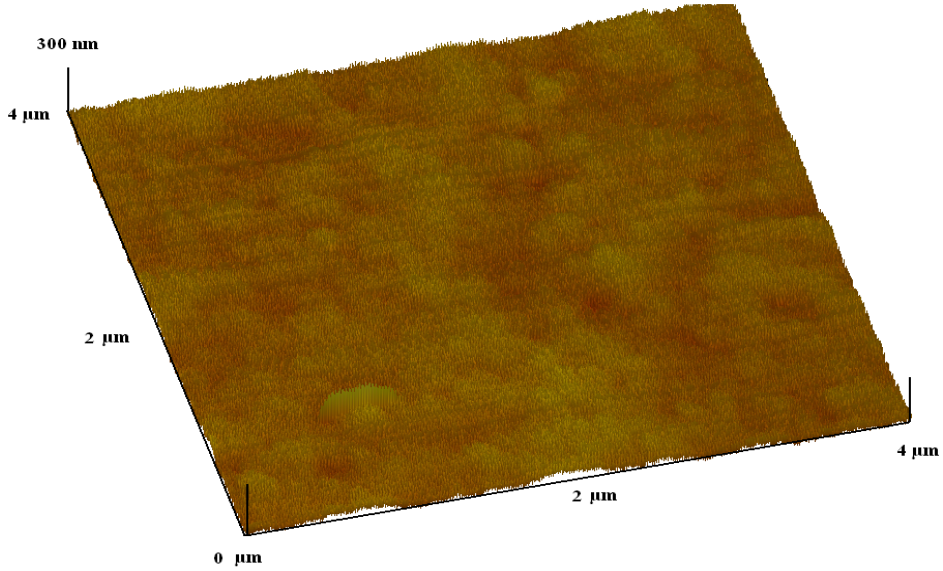

Figure 4.32 *3D image of poly vinyl pyrrolidone NPs*

Figures 4.31 and 4.32 comprise 2D and 3D AFM images of NPs, respectively, generated from poly vinyl pyrrolidone MIP using acetonitrile for precipitation. The NPs surface layout possesses homogeneity and low roughness in the range of few nanometers while NPs average diameter ranges 150 nm. Apparently the NPs surface indicates enhanced surface area as compared to that of MIP. AFM images imply increase in the accessibility of better diffusion pathways for better inclusion of template molecules into the NPs. NPs characterization based on layer height for sensitivity, detection limits and selectivity measurements can help investigating into further improvements in recognition system.

NPs Characterization

Figures 4.33, 4.34 and 4.35 show the sensor response of folic acid on vinyl pyrrolidone NPs on layer heights of 13, 17and 21 kHz respectively.

13 kHz Layer Height

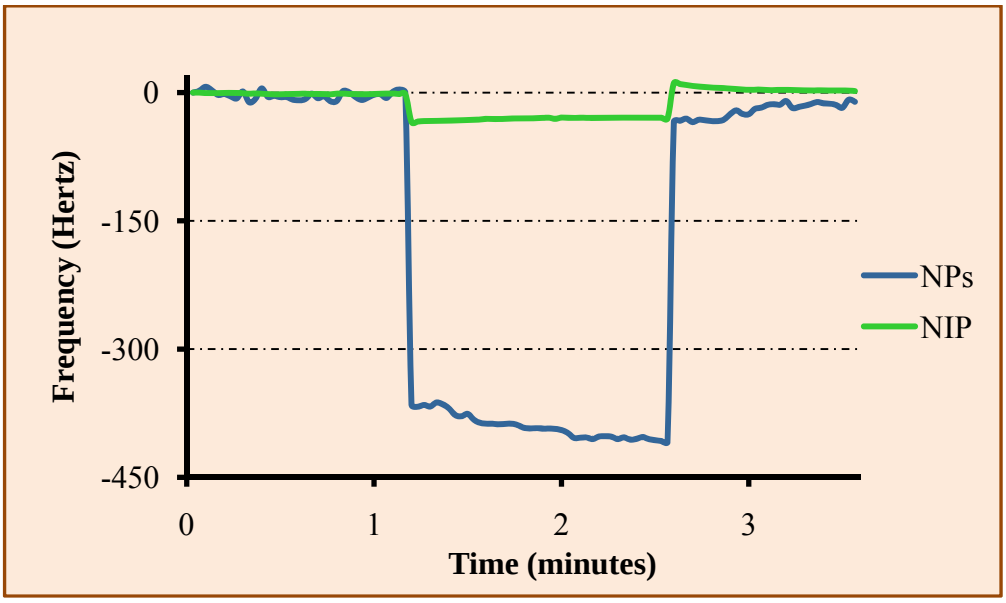

Figure 4.33 Sensor response of folic acid imprinted poly vinyl pyrrolidone NPs at 100 ppm, 13 kHz layer height achieved by NPs spin coated electrode while the reference was spin coated with NIP beads

17 kHz Layer Height

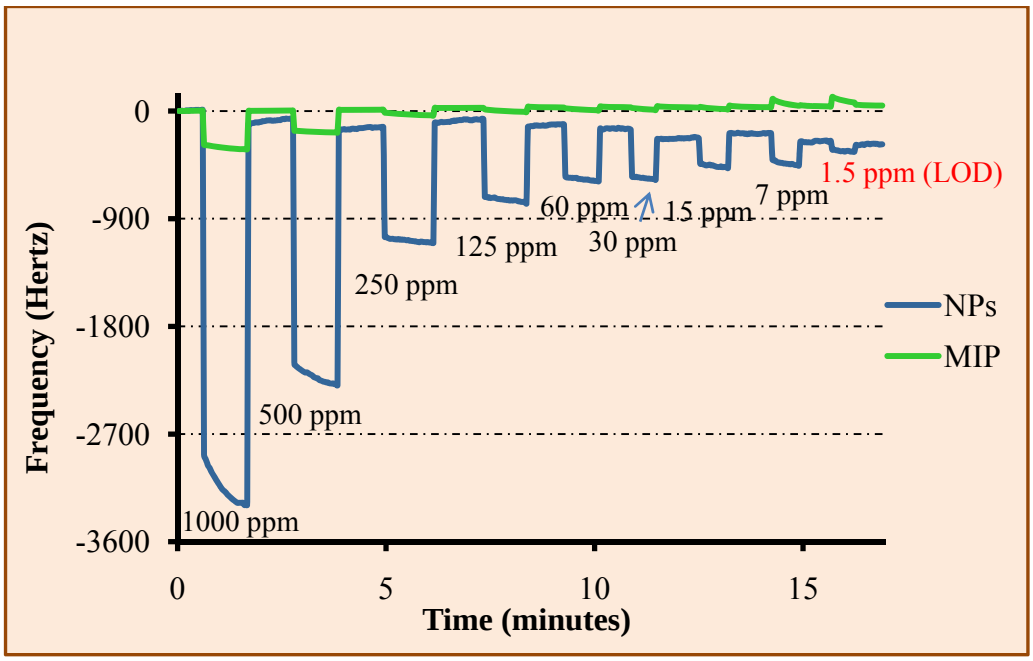

Figure 4.34 Sensor response of folic acid imprinted poly vinyl pyrrolidone NPs at 100 ppm, 17 kHz layer height achieved by NPs spin coated electrode while the reference electrode was spin coated with NIP beads

21 kHz NPs Layer Height

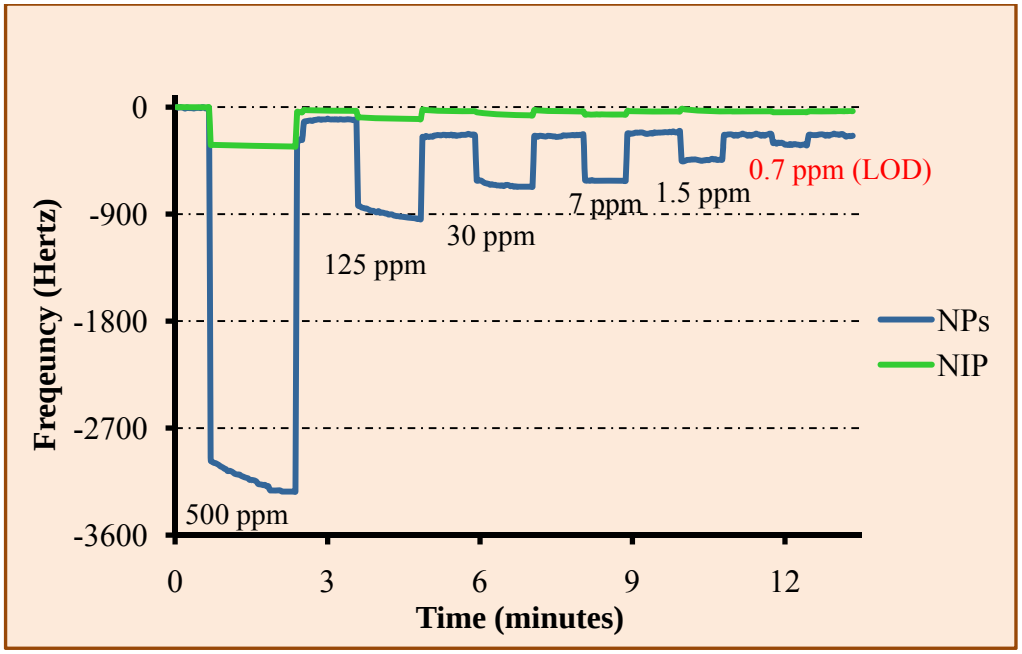

Figure 4.35 Sensor response of folic acid imprinted poly vinyl pyrrolidone NPs at 100 ppm, 21 kHz layer height achieved by NPs spin coated electrode while the reference electrode was spin coated with NIP beads

The above Figures 4.33, 4.34 and 4.35 depict the NPs sensor response at layer heights of 13, 17 and 21 kHz respectively. Data demonstrates improvements in NPs sensitivity and detection limits with the increase of NPs layer heights explaining better diffusion. Apparently the increase in layer height provides enhanced surface area for better diffusion of folic acid into NPs diffusion pathways. The detection limits improvement led to 1.5 ppm LoD at S/N ratio ≥ 3 at 17 kHz layer height. On further increasing the NPs layer height to 21 kHz LoD has been improved to 0.7 ppm at S/N ratio ≥ 3 that is two folds improvement as compared to that of 17 kHz (above figure 4.35). The improvements explain increase in accessible diffusion pathways for gigantic molecules of folic acid for better inclusion on higher NPs layers. The improved accessible diffusion pathways are further supported by the facts that sensor signals of NPs are robust, faster, better in shape and more reversible as compared to that of MIPs. The comparatively better S/N ratio can be attributed to better diffusion pathways achieved from affective template washing along with removal of un-reacted constituents from matrix using NPs approach.

NPs Layer Height Effect on Sensitivity

The plot 4.36 summarizes the NPs sensitivity at 100 ppm on 9, 13, 17 and 21 kHz layer heights. A linear relationship exists between sensor response and layer height demonstrating increase in sensitivity with the increase of NPs mass on the QCM electrode. Diffusion of folic acid molecules becomes more efficient with the increase in NPs on the electrode leading to better sensitivity. The layer heights exceeding 21 kHz for NPs are not suitable for proper mass sensitive measurements leading to higher damping on the QCM electrode ultimately generating low electronic quality or cross talks. A comparison of layer height effect for MIP and NPs can give the complete picture of bulk imprinting for both approaches.

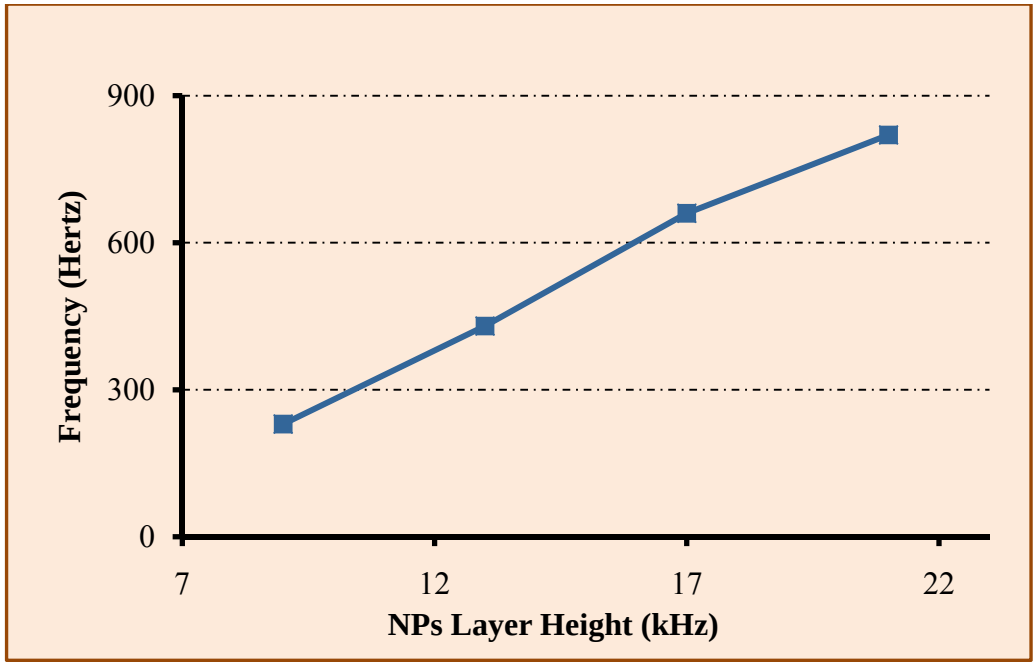

Figure 4.36 Layer height effect on poly vinyl pyrrolidone NPs' sensitivity at 100 ppm

MIP and NPs Layer Height Effect on Sensitivity (Comparison)

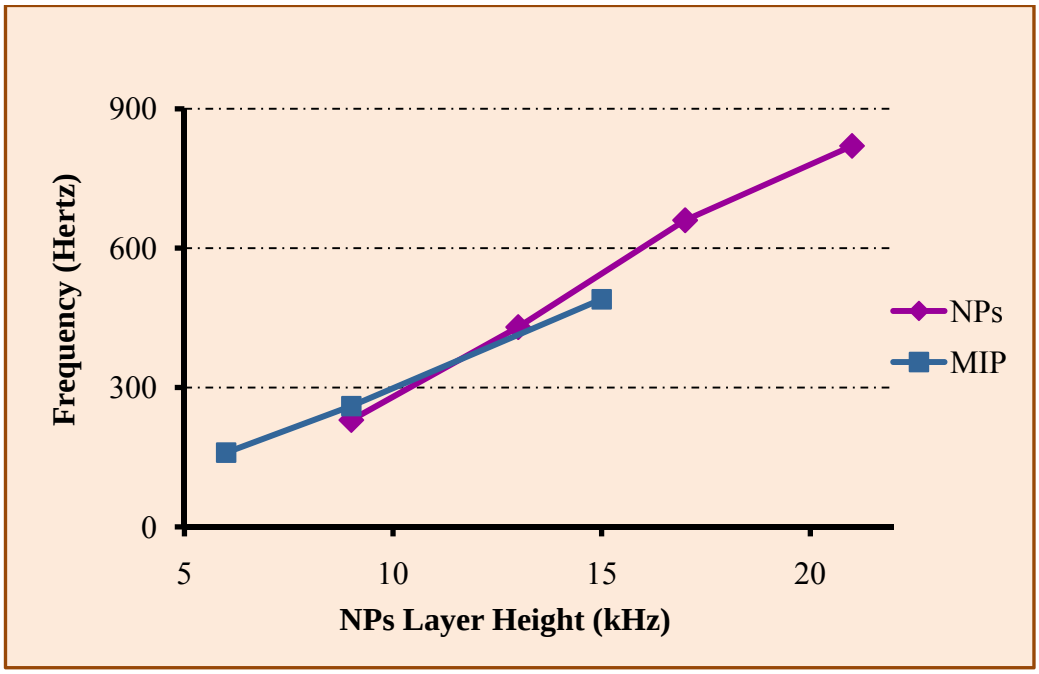

Figure 4.37 Layer height effect on poly vinyl pyrrolidone MIP and NPs' sensitivity at 100 ppm

Figure 4.37 compares the MIP and NPs sensitivity at 100 ppm for poly vinyl pyrrolidone system. The sensor response is directly related to layer height in both cases but the range of NPs layer height and sensitivity exceeds over that of MIP. Within the overlapped layer heights both thin films demonstrate more or less the same sensor responses. While behaving slightly differently after that, NPs ranges higher layer heights with enhanced sensitivity. This difference in sensitivity for both cases can be assigned to the better NPs matrix possessing better accessible interaction sites providing large number of entrances over wide range of layer heights. While comparing with poly methacrylate, the difference of MIP and NPs is not substantially dominant in NPs. The main reason is that template washing remained effective for poly vinyl pyrrolidone MIP as compared to that of poly methacrylate MIP that ultimately led to enhanced sensor response for the first case. A further study regarding sensor characteristics on different layer heights for NPs can explain better about diffusion phenomena.

NPs Layer Height Effect on Sensor Characteristics and Linearity

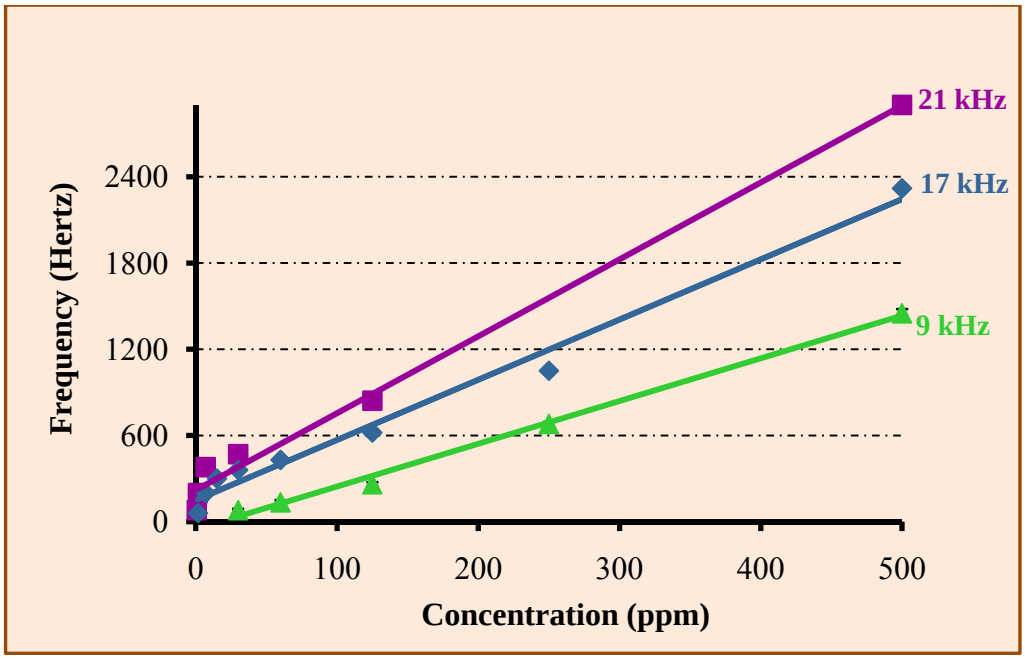

Figure 4.38 Layer height effect on sensor characteristics for poly vinyl pyrrolidone NPs

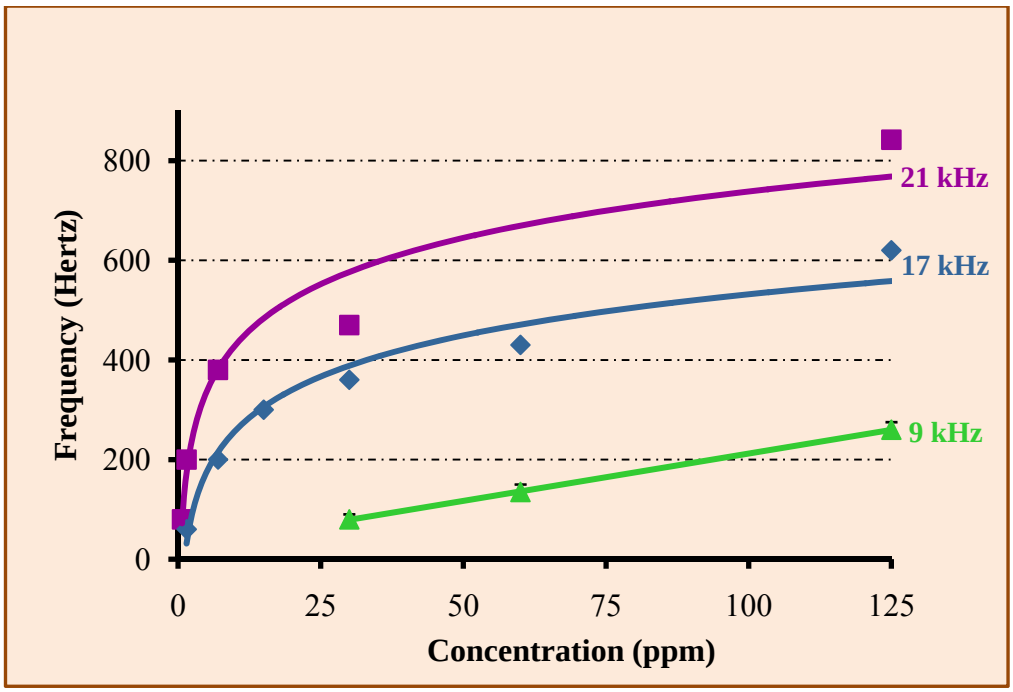

Figure 4.39 Layer height effect on sensor characteristics near LODs for poly vinyl pyrrolidone NPs

The above Figures 4.38 and 4.39 compare the sensor characteristics of poly vinyl pyrrolidone NPs on different layer heights. The sensor response increases with the increase of layer height on every layer height. The plots are directly proportional to sensor response to the concentration on every layer height representing excellent sensitivity relationship with different concentrations. The sensor characteristics for 17 and 21 kHz layer heights are parabolic shaped in the junction of LoDs and 30 ppm range. The S/N ratio on every layer explains improved accessible diffusion pathways in the NPs matrix. A comparative study of selectivity pattern on different layer heights of NPs can be important to investigate into the depth of imprinting.

NPs Layer Height Effect on Selectivity Pattern

Figures 4.40, 441 and 442 demonstrate the selectivity pattern on layer heights of 9, 17 and 21 kHz for poly vinyl pyrrolidone NPs.

9 kHz NPs Layer Height

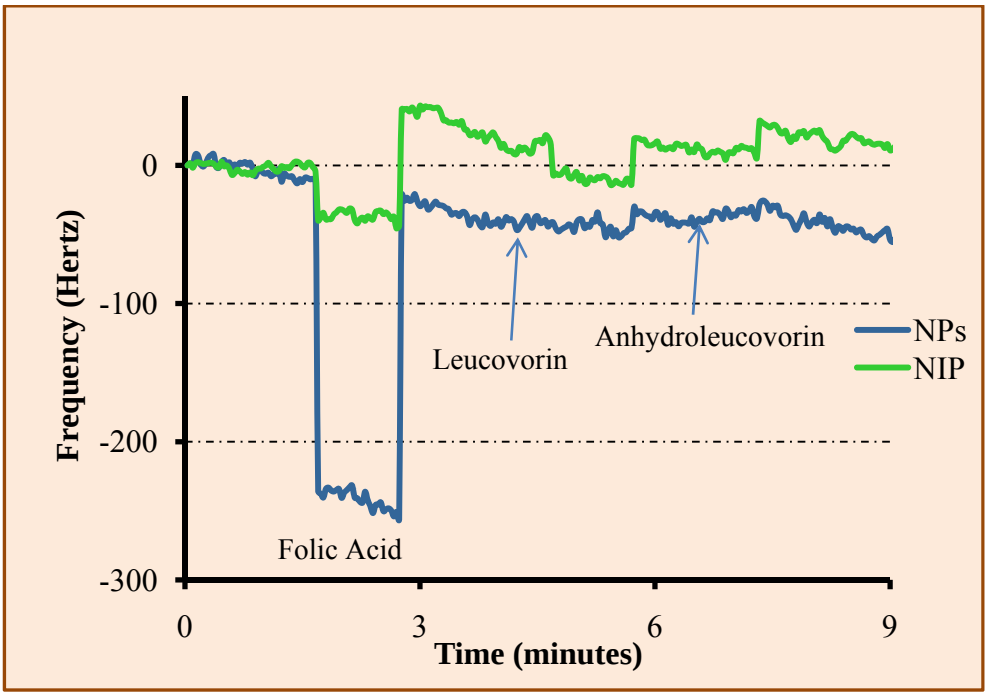

Figure 4.40 Selectivity pattern at 100 ppm on poly vinyl pyrrolidone NPs at 9 kHz layer height

17 kHz NPs Layer Height

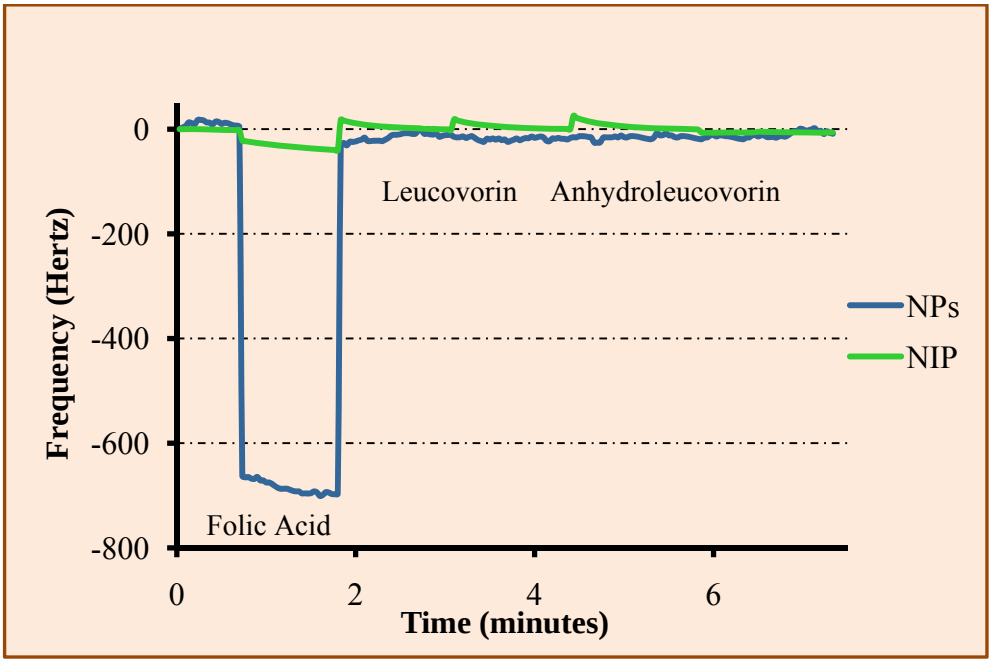

Figure 4.41 Selectivity pattern at 100 ppm on poly vinyl pyrrolidone NPs at 17 kHz layer height

21 kHz NPs Layer Height

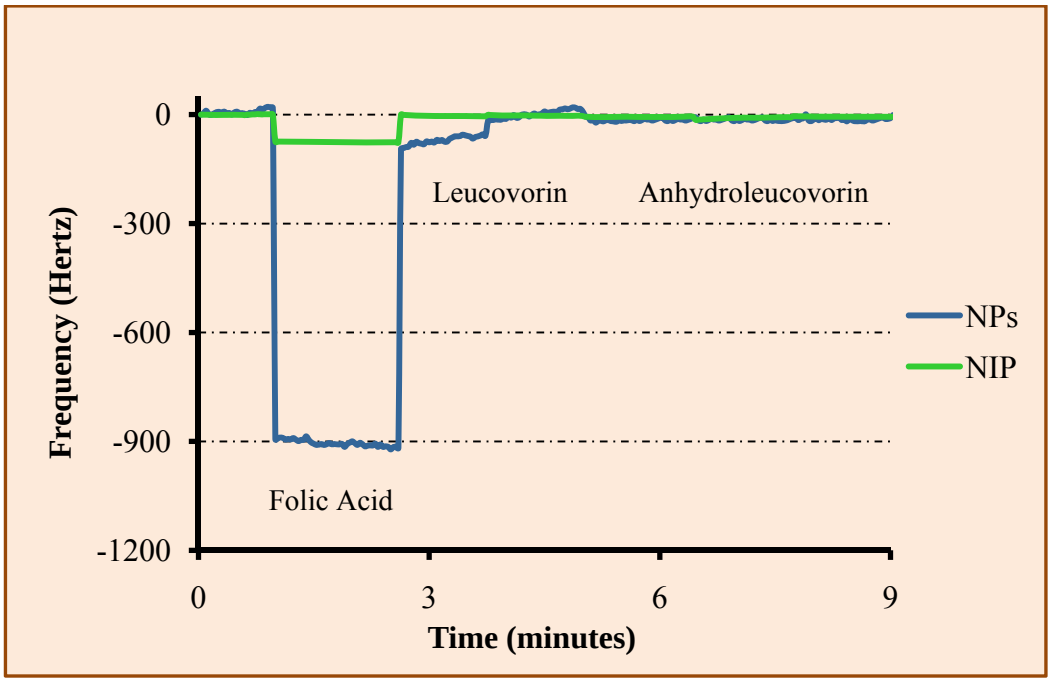

Figure 4.42 Selectivity pattern at 100 ppm on poly vinyl pyrrolidone NPs at 21 kHz layer height

NPs Layer Height Effect on Selectivity

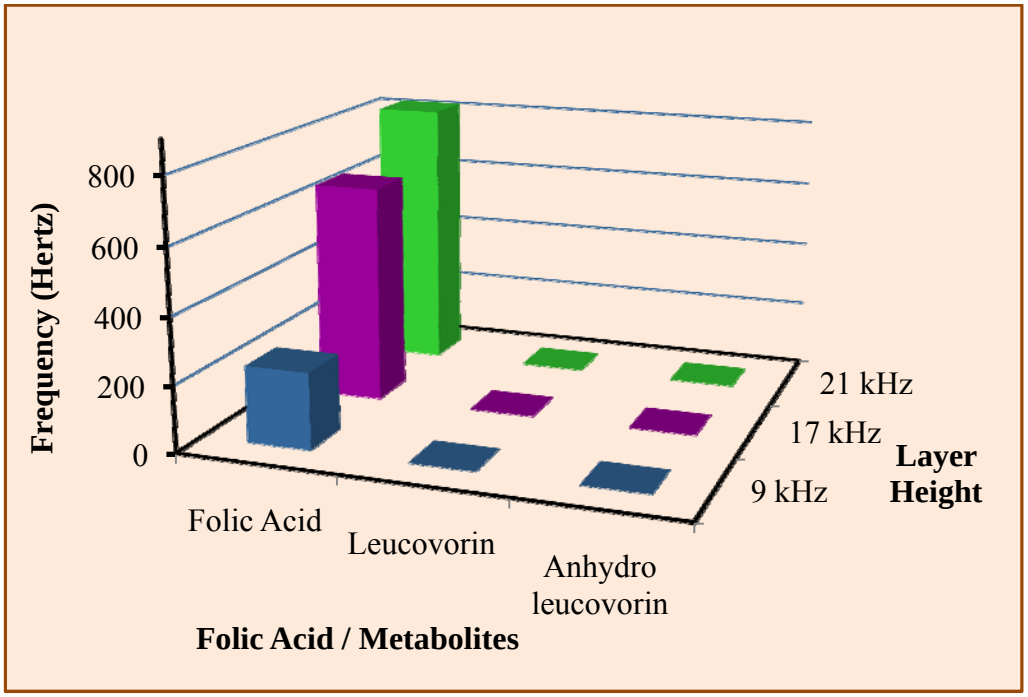

Figure 4.43 Layer height effect on selectivity pattern at 100 ppm on poly vinyl pyrrolidone NPs

Figure 4.43 compares the selectivity pattern at 100 ppm achieved on 9, 17 and 21 kHz layer heights of poly vinyl pyrrolidone NPs. NPs follows outclass selectivity for folic acid defeating the metabolites signals to zero in mass sensitive measurements. The folic acid signal increases linearly with the increase of layer height and peaks at 820 hertz (at 100 ppm) with layer height 21 kHz. On the other hand leucovorin and anhydroleucovorin signals move like stable base line in the measurement curves without showing the mass effect deposition on the electrode via diffusion. The contributing reason in breakthrough in selectivity is that combination of different washing strategies was applied for NPs washing. These combined washing methodologies effectively removed the template along with un-reacted constituents from the matrix of NPs. While in the case of MIP, only methanol was applied for template washing. The details of different washing strategies are presented in table 4.2 below.

Table 4.2 Different washing strategies for template removal from poly vinyl pyrrolidone MIP spin coated on QCM electrode

Solvent	Washing duration (hours)	MIP layer height (kHz)	MIP- layer height (% decreased)	NIP layer height (kHz)	NIP layer height (% decreased)
Water	2	13	2	11	1
Water (60°)	2	12	4	11	2
Methanol	2	12	14	12	3
Water (pH10 with NH_3)	2	13	4	10	2
10 mM Ammonium phosphate (pH 10)	1/2	13	60	10	50

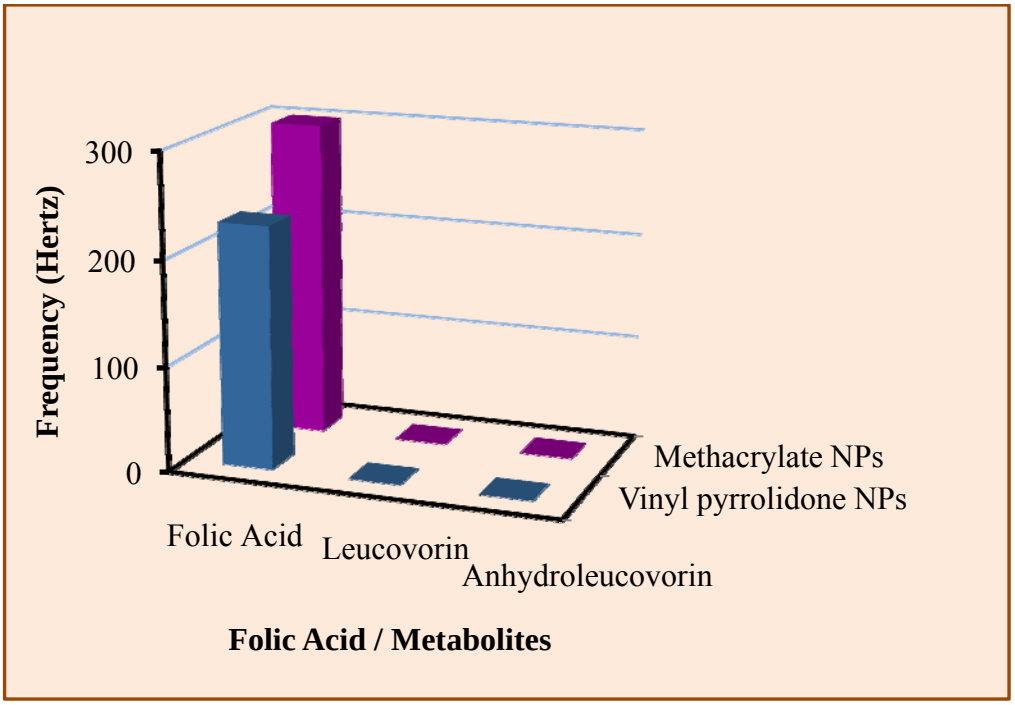

Figure 4.44 Selectivity pattern (at 100 ppm), folic acid imprinted NPs generated from poly vinyl pyrrolidone and methacrylate MIPs

Figure 4.44 compares the selectivity patterns of NPs achieved from poly methacrylate and vinyl pyrrolidone respectively at 9 kHz layer height. Outclass selectivity for folic acid as compared that of its metabolites has been achieved in each case supporting the successful bulk imprinting NPs approach.

4.1.5 Summary

Figure 4.45, compares the selectivity pattern on MIPs and NPs thin films for poly methacrylate and vinyl pyrrolidone. NPs approach remained successful in the terms of sensitivity and selectivity in the case of poly methacrylate MIP. The same effect was observed in the case of poly vinyl pyrrolidone NPs. The selectivity pattern of the bulk imprinted MIP / MIP-NPs is affected by the washing strategies to remove the template from matrix[116] further more NPs size also contributes to the selectivity patterns[117]. The contributing reason in breakthrough in selectivity is that combination of

different washing strategies was applied for NPs washing. These combined washing methodologies effectively removed the template along with un-reacted constituents from the matrix of NPs. While in the case of MIP, only methanol was applied for template washing.

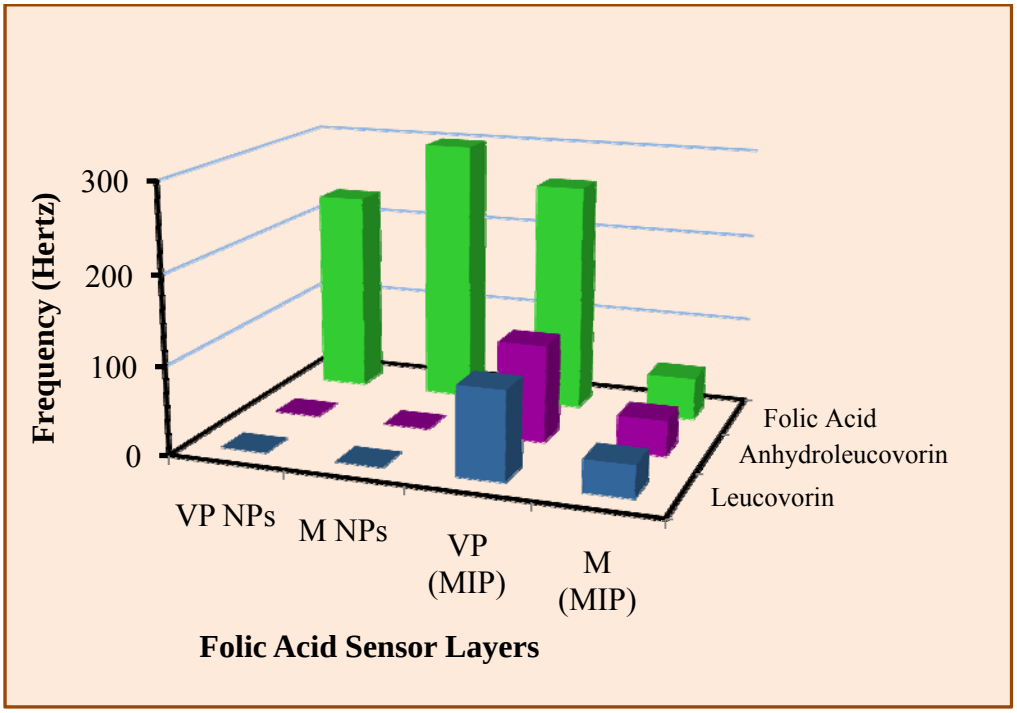

Figure 4.45 Selectivity pattern (at 100 ppm), folic acid imprinting on different sensor layers, VP NPs (poly vinyl pyrrolidone NPs), M NPs (poly methacrylate NPs), VP (MIP) (vinyl pyrrolidone MIP), layer height 9 kHz

In summary, over all, the data demonstrates sensitivity and LoD improvements along with the positive effect on the selectivity pattern on comparing the response of the NPs to that of the MIP. While comparatively poly vinyl pyrrolidone recognition systems (i.e. both MIP and NPs) provide better sensitivity and detection limits as compared to that of relative poly methacrylate. Regarding detection limits, 5 ppm LoD at S/N ratio ≥ 3 was achieved by using poly methacrylate NPs (at layer height of 15 kHz) which is further 7 folds improved (i.e. 0.7 ppm at S/N ratio ≥ 3) by using poly vinyl pyrrolidone NPs at layer height of 21 kHz. The present study has opened the

doors of using MIP bulk imprinting technology and NPs approach using QCM for so called elephant molecules (e.g. folic acid) imprinting and sensing. Before this, very little work has been reported on bulk imprinting of larger molecules in literature. The future applications can be extended to other larger molecules from different classes of organic compounds. The scope of applications can also be extended to other transducers like SAW, electrochemical or other means of sensor technology.

4.2 Leucovorin Imprinting

Leucovorin molecule is different from folic acid structure because of one carbonyl group that is attached to tertiary amine in pteridine ring in leucovorin. While the further structural difference is the attachment of two hydrogen atoms converting two tertiary amines to secondary amines in pteridine moiety in leucovorin making aromatic ring into aliphatic 6 carbon ring. The structural difference makes leucovorin hydrophobic nature. Leucovorin solubility was tested on different solvents but no organic solvent was found for complete solubility. Water was the only solvent found for leucovorin bulk imprinting polymerization after the solubility trials. Folic acid MIP recipes were tried for leucovorin imprinting using N, N' (1, 2-Dihydorxyethylene) bisacrylamide as cross linker and water as solvent but no signal was observed. The purpose of using N, N' (1, 2-Dihydorxyethylene) bisacrylamide as cross linking monomer is obviously advantageous for MIP synthesis in aqueous media over EGDMA. AIBN was replaced by sodium peroxidisulphate because it could not initiate the polymerization required for MIP synthesis. Finally poly methacrylate MIP was prepared and optimized using sodium peroxidisulphate as polymerization initiator.

4.2.1 Poly Methacrylate MIP

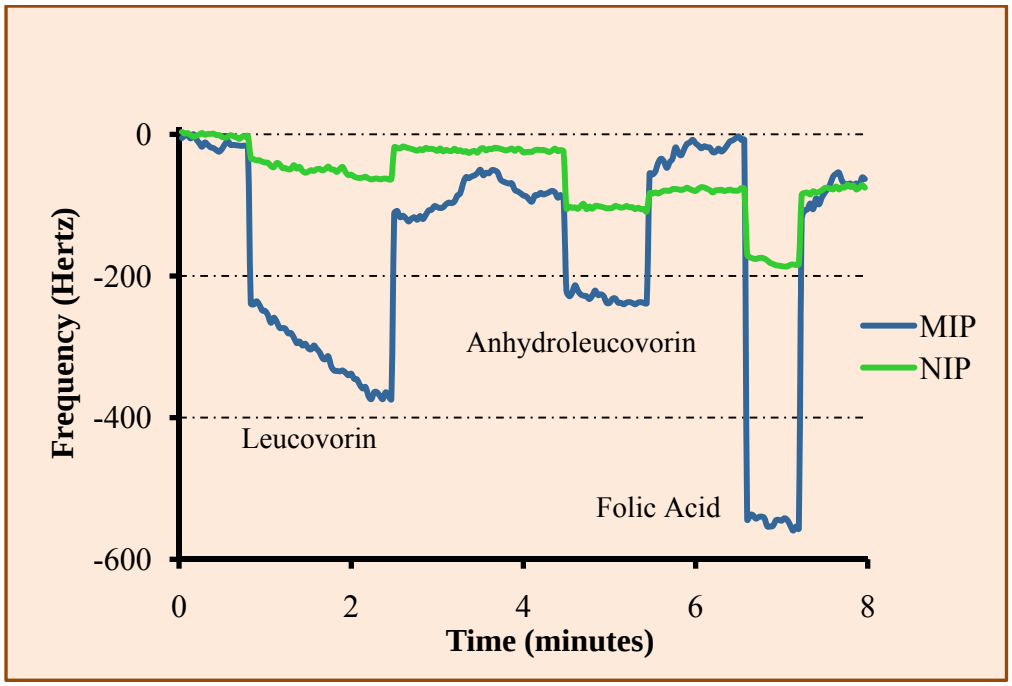

Figure 4.46 Selectivity pattern at 500 ppm, leucovorin imprinted in poly methacrylate generated from methacrylic acid: N, N' (1, 2-Dihydorxyethylene) bisacrylamide (3.5: 1.5 mg), 7 kHz layer height achieved by MIP was spin coating and after template washing

Figure 4.46, gives the first shot of leucovorin imprinting using sodium peroxidisulphate as radical initiator because the polymerization was unsuccessful using AIBN in water. 7 kHz (280 nm) MIP layer height generated from poly methacrylate after the template washing, was measured on network analyzer. Leucovorin selectivity was measured at the same concentration level (500 ppm) in the same solution media (1 mM ammonium phosphate buffer pH 10). The curve demonstrates broad band selectivity for leucovorin as compared to that of folic acid and anhydroleucovorin. Although the polymerization remained successful by using sodium peroxidisulphate as initiator in aqueous media, yet further optimization in monomer to cross liner monomer is required to achieve compactness in MIP. To target the carbonyl and amine groups in the moiety of pteridine in the leucovorin (that make the

molecule hydrophilic nature) further optimization of monomer to cross linker monomer can provide imprinting of these groups. The sensor response suggests a robust recognition system is possible based on poly methacrylate.

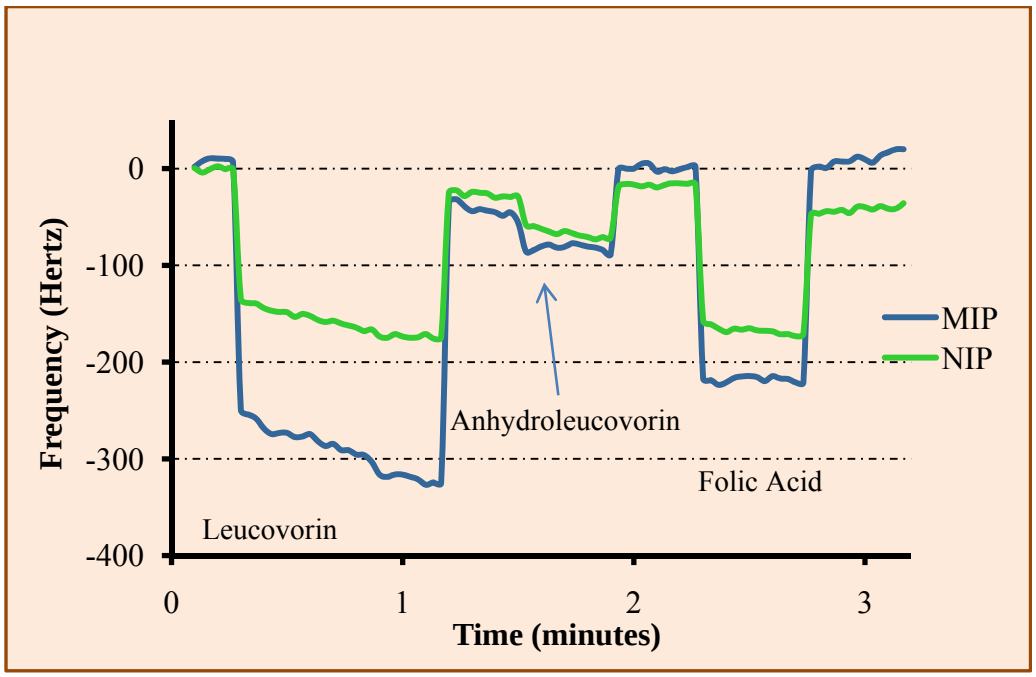

Figure 4.47 Selectivity pattern at 500 ppm, leucovorin imprinted in poly methacrylate generated from methacrylic acid: N, N' (1, 2-Dihydorxyethylene) bisacrylamide (4: 1 mg), 6 kHz layer height achieved by MIP was spin coating and after template washing

Figure 4.47 compares the selectivity pattern in modified poly methacrylate MIP at 6 kHz layer height achieved after template washing. The sensor response of leucovorin is three times larger as compared to that of folic acid while anhydroleucovorin response is basically zero. The proper template washing can further improve the response and help in reducing the non specific response of NIP. Comparatively three times more loss (than expected) in layer height was noted while templates washing in water at 50°C which reflects that the deposited thin films are not optimally stable. The modification in the template washing procedure or hardening the thin films can resolve the situation.

4.2.2 Optimized MIP

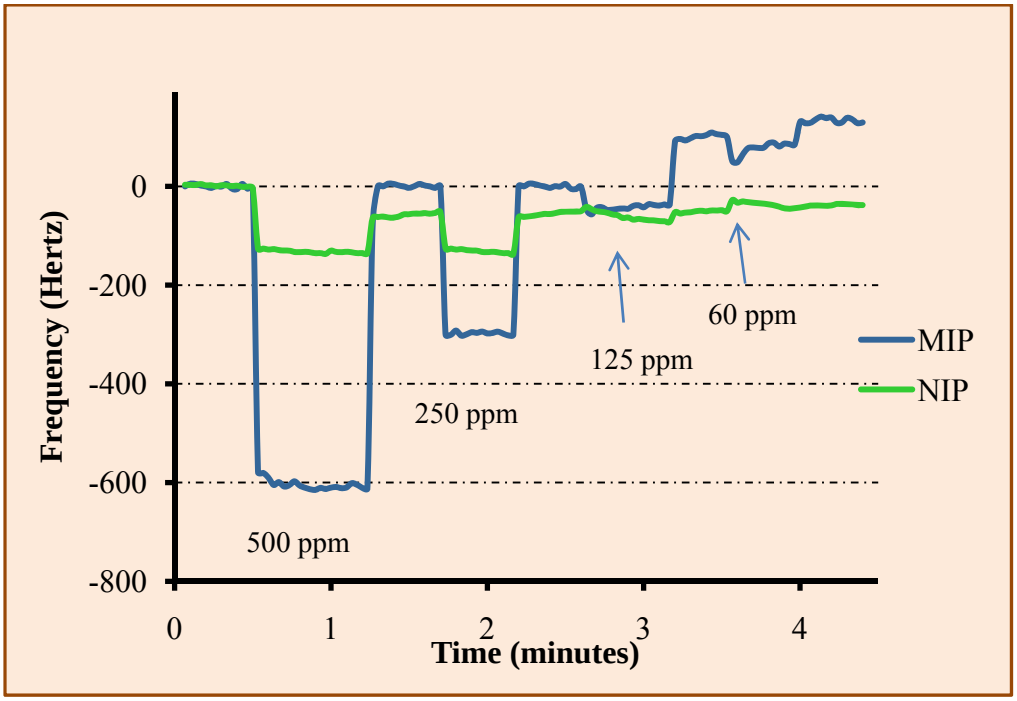

Figure 4.48 Sensor response of leucovorin imprinted in poly methacrylate at 8 kHz layer height, spin coated QCM heated at 100°C prior to washing

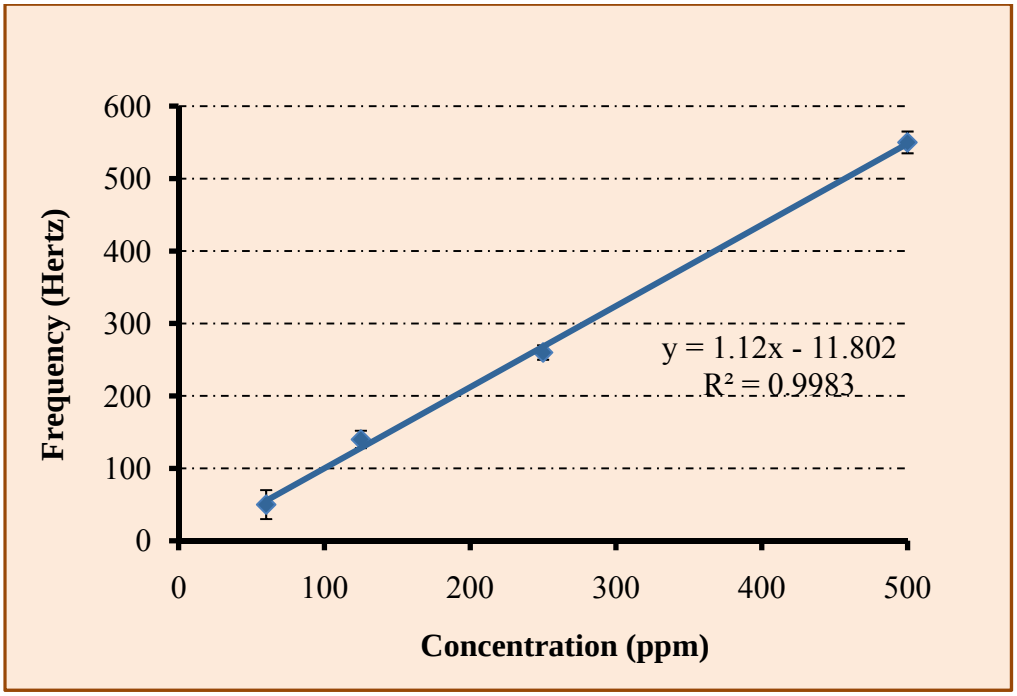

Figure 4.49 Sensor characteristics of leucovorin imprinted in poly methacrylate at 8 kHz layer height, spin coated QCM was heated at 100°C prior to washing

Figure 4.49 explains the sensor characteristics for poly methacrylate MIP thin film at 8 kHz layer height. In MIP synthesis, increase and decrease of 1 cm distance between reaction tube and source with respect to optimum distance increases or decreases polymerization by 0.5 hour, respectively with respect to optimum time. The breakthrough in the sensor response is due to heating the spin coated QCM at 100°C for drying the thin films on the electrodes. The MIP thin film was generated by spin coating and after heating QCM at 100°C for 2 hours prior to template washing. Heating of QCM at 100°C is obviously advantageous in this case for hardening and drying the thin films. On comparing the above both figures 4.47 and 4.49, we can see that sensitivity has been improved by a factor of four at 500 ppm after heating QCM at 100°C prior to template washing in later case. The sensitivity of imprinted leucovorin in poly methacrylate covers the ppm range with 60 ppm LoD at S/N ratio $\geq$ 3. The sensor response is directly proportional to the leucovorin concentration. While base line noise is low representing suitability of MIP thin film for mass sensitive measurements. A minor drift in the parent frequency of measuring electrode may be due to loss of some mass from the electrode. The study of MIP morphology using AFM can be interesting to investigate into the thin film roughness.

MIP Morphology

The 3D AFM image in Figure 4.49 depicts the surface morphology of leucovorin imprinted methacrylate MIP thin film demonstrating surface roughness in the range of only few tens to hundreds nanometers. Owing to homogenous layout, a very minute noise can be expected from the thin film indicating its suitability for QCM based mass sensitive measurements. The imprinting evaluation based on the selectivity pattern can be interesting information at this stage.

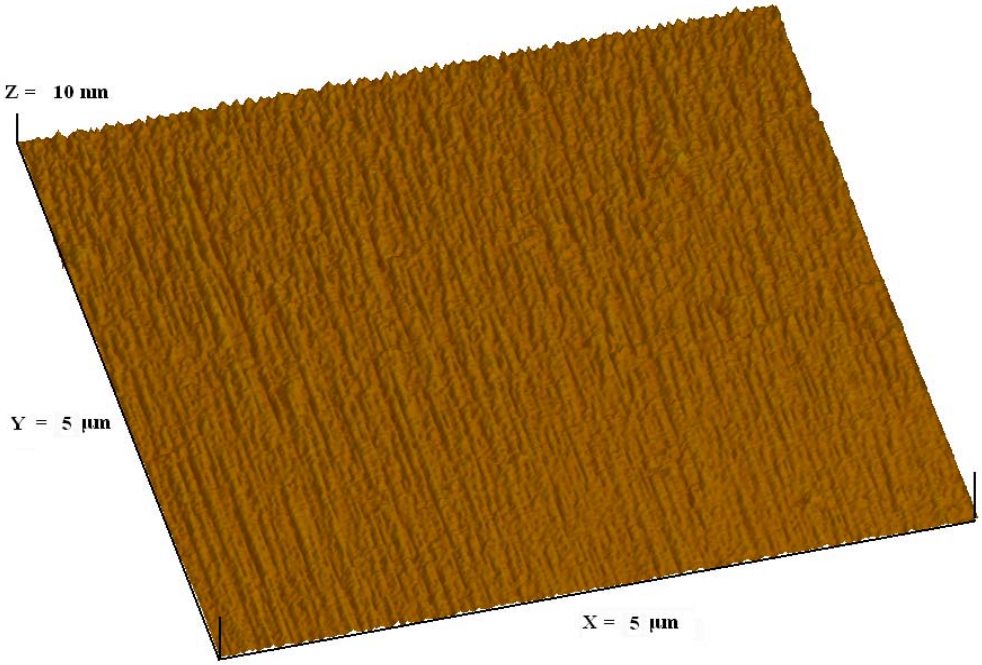

Figure 4.50 *3D AFM image for leucovorin imprinted poly methacrylate thin film*

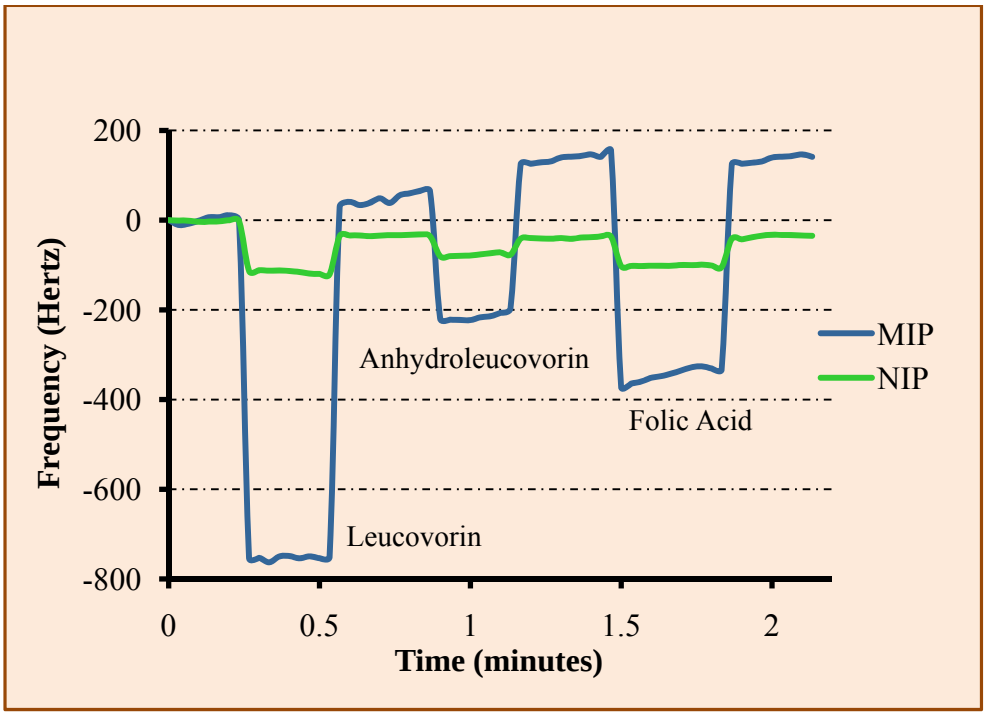

Figure 4.51 *Selectivity pattern at 500 ppm for leucovorin imprinting in optimized poly methacrylate MIP at 8 kHz layer height*

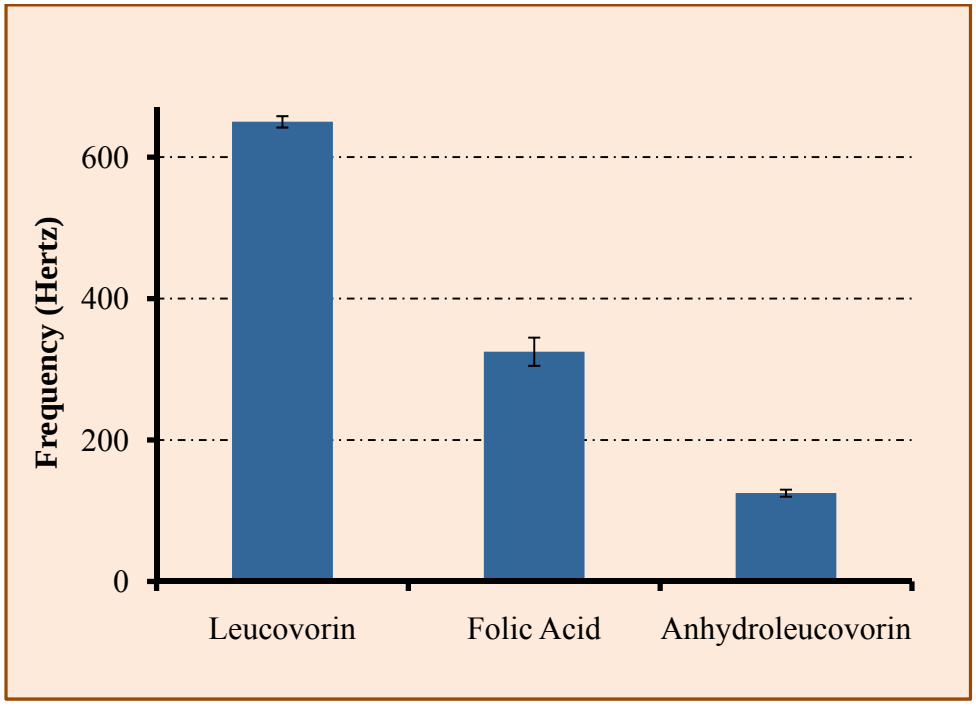

Figure 4.52 Selectivity pattern at 500 ppm for leucovorin imprinting in optimized poly methacrylate MIP at 8 kHz layer height

Figure 4.52 demonstrates the selectivity pattern at 500 ppm for leucovorin imprinted optimized MIP at 8 kHz layer height. Leucovorin cross sensitivity is five times and two times as compared to that of anhydroleucovorin and folic acid respectively. The designed molecular imprints of leucovorin in the MIP are unsuitable penetrating structural analogs anhydroleucovorin or folic acid into the MIP cavities. The sensor responses of anhydroleucovorin and folic acid decreased kinetically demonstrating improper fitting into the cavities due to additional carbonyl group and the difference between the aromatic and the aliphatic systems.

4.3 Anhydroleucovorin Imprinting

Removal of water molecule from the moiety of pteridine ring of leucovorin makes the anhydroleucovorin molecule. The structural difference affects the solubility of molecule that is different from leucovorin and folic acid. In the solubility tests methanol is found to be a good solvent for anhydroleucovorin while it is only slightly soluble (at below 0.3 % level) in DMF. For characterization of all metabolites imprinting could be interesting but monomers are insoluble in methanol. Therefore other solvent system is needed for anhydroleucovorin imprinting because polymerization for methacrylic acid or vinyl pyrrolidone based MIPs is impossible using methanol as solvent because of insolubility of monomers in methanol. Furthermore methanol and DMF can be explored for emulsion polymerization for anhydroleucovorin imprinting using methacrylic acid or vinyl pyrrolidone as monomers and EGDMA as cross linking monomer. In the initial trials folic acid MIP recipes can be interesting to look into anhydroleucovorin imprinting using anhydroleucovorin as template in DMF.

4.3.1 Poly Vinyl Pyrrolidone (EGDMA as Cross Linker)

Figure 4.52 depicts the selectivity pattern using poly vinyl pyrrolidone MIP (folic acid recipe but anhydroleucovorin as template) cross lined by EGDMA at 11 kHz (440 nm) layer height. The figure demonstrates that the MIP layer is two times more selective for anhydroleucovorin as compared to leucovorin and 25% more selective as compared to folic acid. The senor response is reversible and robust suggesting further improvement is possible in selectivity by achieving optimized MIP parameters. To improve the structural stability after template removal in MIP, the use of N, N' (1, 2-Dihydorxyethylene) bisacrylamide as cross liker monomer can be interesting to investigate into the selectivity pattern.

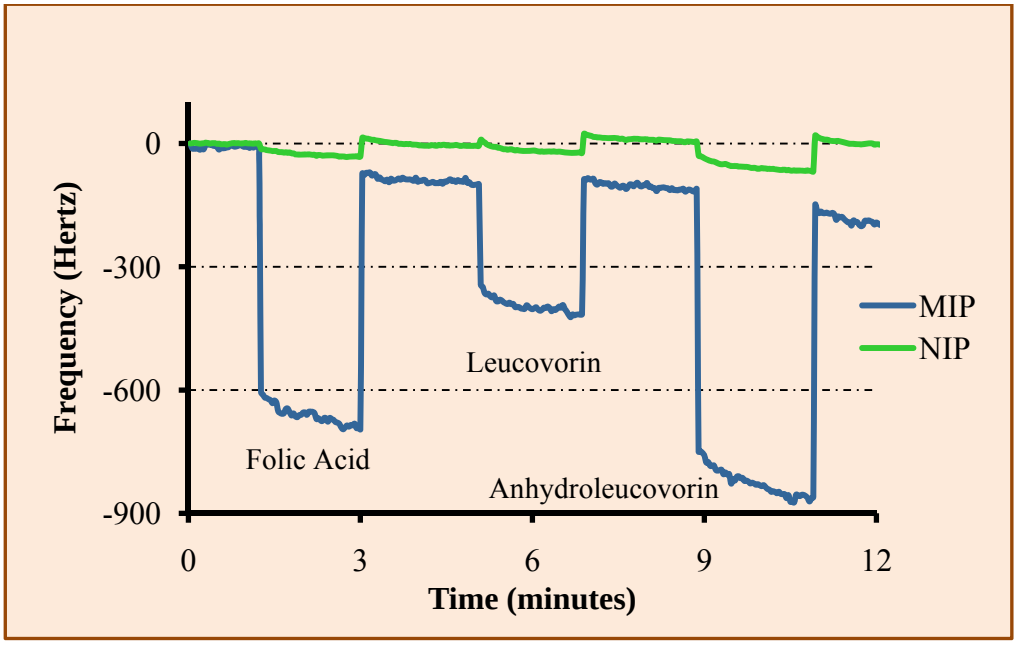

Figure 4.53 Selectivity pattern at 500 ppm, anhydroleucovorin imprinting in poly vinyl pyrrolidone in DMF, 11 kHz layer height achieved by MIP spin coating and after template washing

4.3.2 Poly Vinyl Pyrrolidone MIP (Acryl Amide as Cross Linker)

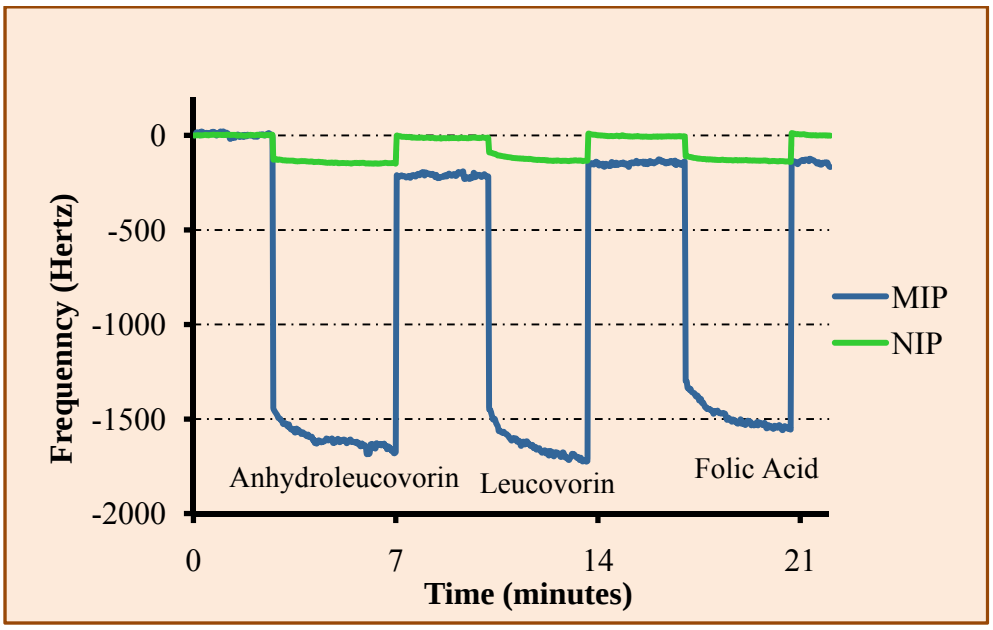

Figure 4.54 Selectivity pattern at 500 ppm, anhydroleucovorin imprinting in poly vinyl pyrrolidone using N, N' (1, 2-Dihydorxyethylene) bisacrylamide as cross linker, 18 kHz layer height achieved by MIP spin coating and after template washing

Figure 4.54 shows the selectivity pattern for poly vinyl pyrrolidone MIP using N, N' (1, 2-Dihydorxyethylene) bisacrylamide as cross linker at 18 kHz (720 nm) layer height. Broad band selectivity has been achieved exhibiting more or less the same sensor response for anhydroleucovorin on comparing with that of leucovorin and folic acid. The senor response is reversible, robust and attracting with two folds sensitivity at 500 ppm on comparing with that of EGDMA cross linked MIP. Although the sensitivity has been improved, yet further changes for structural stability after template removal in MIP can improve its selectivity. In this respect, the addition of methacrylic acid as co-monomer can be interesting for emulsion polymerization using small amount of methanol in DMF based MIP. Emulsion polymerization is a form of radical polymerization that usually takes place with an emulsion incorporating solvent (e.g. water, DMF etc), monomer, and surfactant solvent.

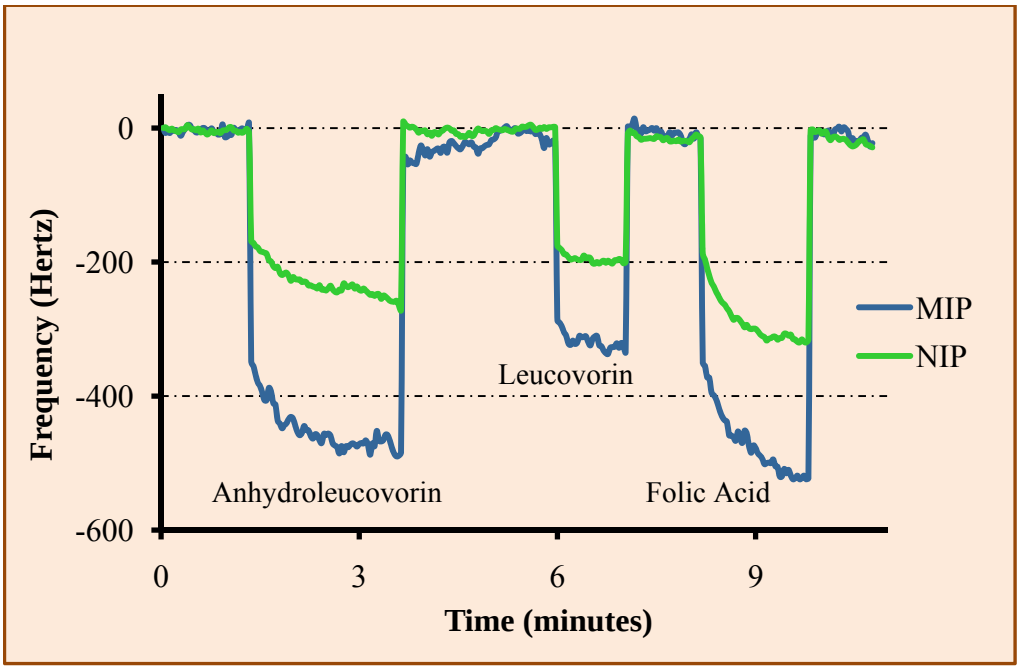

Figure 4.55 Selectivity pattern at 500 ppm, anhydroleucovorin imprinted in poly methacrylate-vinyl pyrrolidone (1:1) using methanol: DMF (1:9), 7 kHz layer height achieved after MIP spin coating, drying and template washing

The polymerization in 100% methnol remains unfruitful even keeping the mixture under UV for 24 hours. Although vinyl pyrrolidone and methacrylate (1:1 w/w) showed polymerization while using anhydroleucovorin as template in DMF, yet anhydroleucovorin precipation was observed as NIP did not show precipitation. The templete solubility decreased upon polymerization, ultinately led to the metabolite precipation. Figure 4.55 depicts the attempt for emulsion polymerization for anhydroleucovorin imprinting in methanol: DMF(1:9). The cross sensitivity was measured at 7 kHz MIP layer height at 500 ppm. Further increasing the methanol in solvent composition for emulsion polymerization can be intersting to look into sensitivity and selectivity improvements in mass sensitive measurements.

4.3.3 Optimized MIP

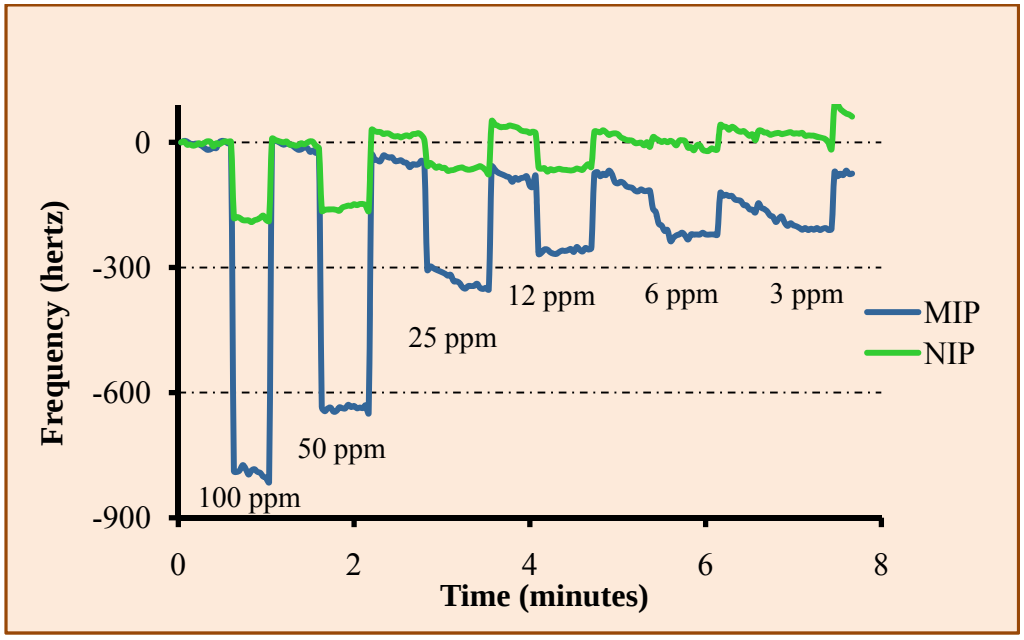

Figure 4.56 Sensor characteristics for anhydroleucovorin imprinted in poly methacrylate - vinyl pyrrolidone using methanol: DMF (2:3), 8.5 kHz MIP layer height achieved after drying and template removal

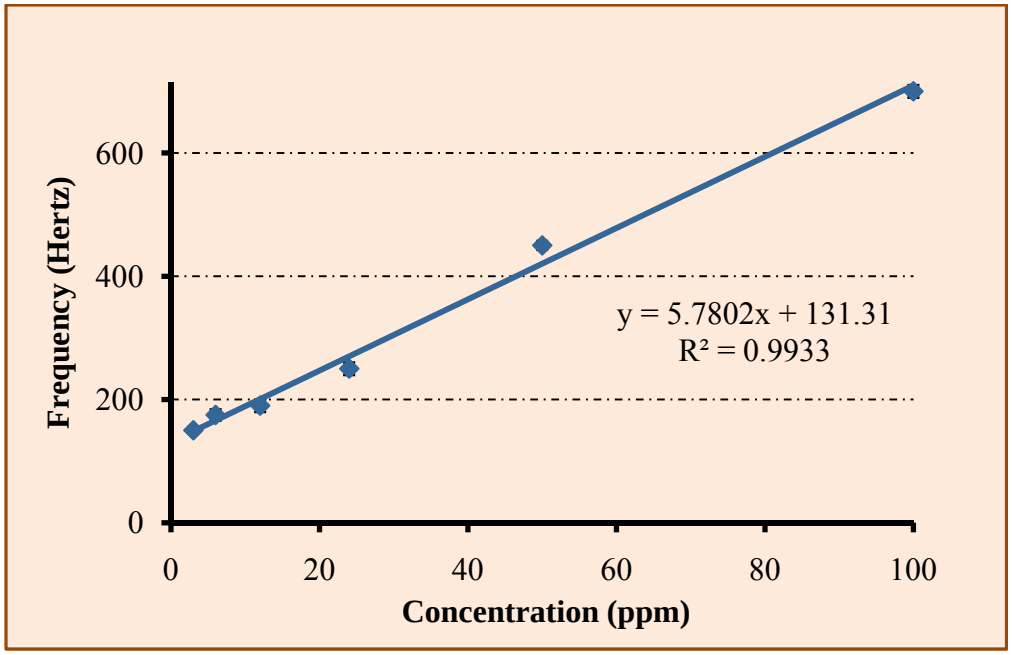

Figure 4.57 Sensor characteristics for anhydroleucovorin imprinted in poly methacrylate - vinyl pyrrolidone using methanol: DMF (2:3), 8.5 kHz MIP layer height achieved after drying and template removal

The above figure 4.57 explains the sensor characteristics for anhydroleucovorin imprinted in emulsion polymerized methacrylate-vinyl pyrrolidone in methanol: DMF (2:3). The emulsion polymerization in the present case has been generated from a surfactant (methanol) and solvent (DMF) generating particles in the range of hundreds of nanometers during polymerization. A specific ratio between surfactant and solvent (i.e. 2:3 in this case) is needed to generate such particles during polymerization. 8.5 kHz layer height was achieved for spin coated MIP electrode after template washing. In optimized MIP synthesis, increase and decrease of 1 cm distance between reaction tube and source with respect to optimum distance increases or decreases polymerization by 1.5 hour, respectively with respect to optimum time. The sensitivity of anhydrolucovorin covers the ppm range with 3 ppm LoD at S/N ratio $\geq$ 3. Obviously emulsion MIP provides enhanced surface area for better diffusion of anhydroleucovorin into MIP diffusion pathways ultimately leading to better sensitivity and detection limits. The improved

accessible diffusion pathways are further supported by the facts that sensor signals are robust, faster, better in shape and more reversible as compared to that of normal MIP (i.e. on comparing with that of figure 4.55). Moreover, comparatively better S/N ratio can be assigned to better diffusion pathways achieved. The sensitiviy of anhydroleucovorin (MIP) is 2 times as compared to that of folic acid imprinted in poly vinyl pyrrolidone (MIP) while five times as compared to that of leucovorin imprinted in polymethacrylate (MIP) at 100 ppm level. The enhanced sensitivity for anhydroleucovorin MIP can be assigned to emulsion polymerization factor which offers better surface enternaces as compared to that of normal MIP for sensing template. AFM studies for emulsion MIP morphology can be interesting here.

MIP Morphology

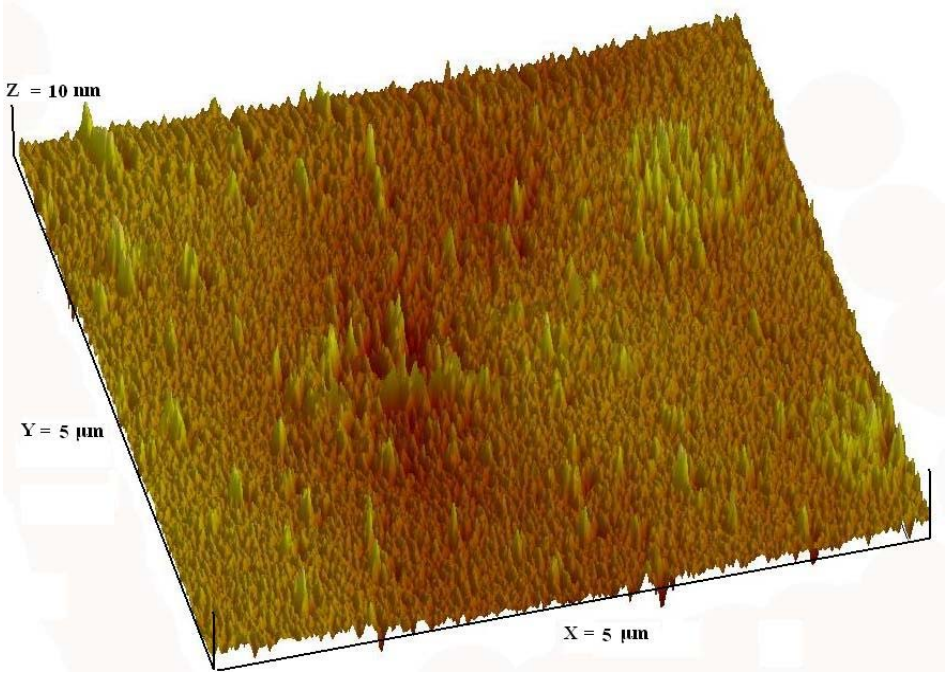

Figure 4.58 AFM image of anhydroleucovorin emulsion MIP

Figure 4.58 is a 3D AFM image of anhydroleucovorin imprinted poly methacrylate-vinyl pyrrolidone emulsion MIP thin film. The surface layout keeps roughness in the range of tens of nanometers to few hundred nanometers. The nanoparticles structures suggest that it may of course also be

possible that one of the solvents works as a porogen (i.e. surfactant). Obviously the surface indicates enhanced surface area implying increase in the accessibility of better diffusion pathways for better inclusion of template molecules into the MIP. The MIP surface layout is homogenous all together demonstrating its high suitability for application on QCM transducer, as only negligible noise can be expected.

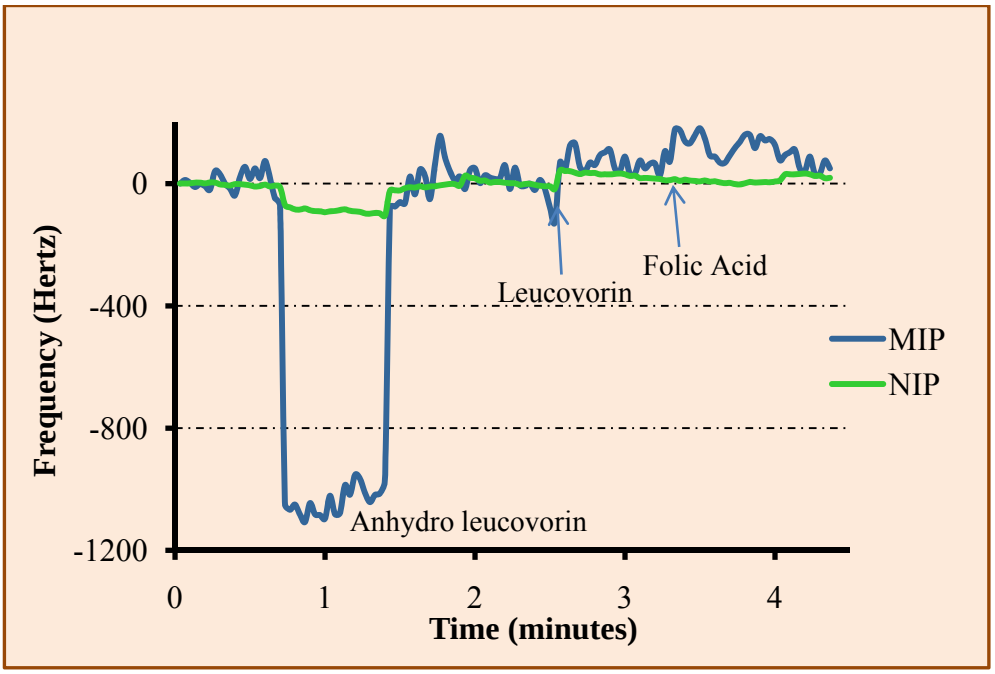

Figure 4.59 Selectivity pattern at 100 ppm at anhydroleucovorin imprinted optimized MIP; 9 kHz MIP layer height achieved after drying and template removal

Figure 4.60 depicts the selectivity pattern at 100 ppm for anhydroleucovorin imprinted optimized emulsion MIP at layer 9 kHz layer height. One can see a surprisingly high effect on anhydroleucovorin selectivity and sensitivity on comparing figures 4.60 and 4.57. Good sensitivity along with appreciable selectivity are indication of effective imprinting and generation of imprints of the different groups of anhydroleucovorin onto the MIP. Anhydroleucovorin emulsion MIP demonstrates outstanding selectivity as compred to that of folic acid and

leucovorin bulk MIPs. The sensor responses of leucovorin and folic acid remained with in the base line noise and stastically siginificant fortunately.

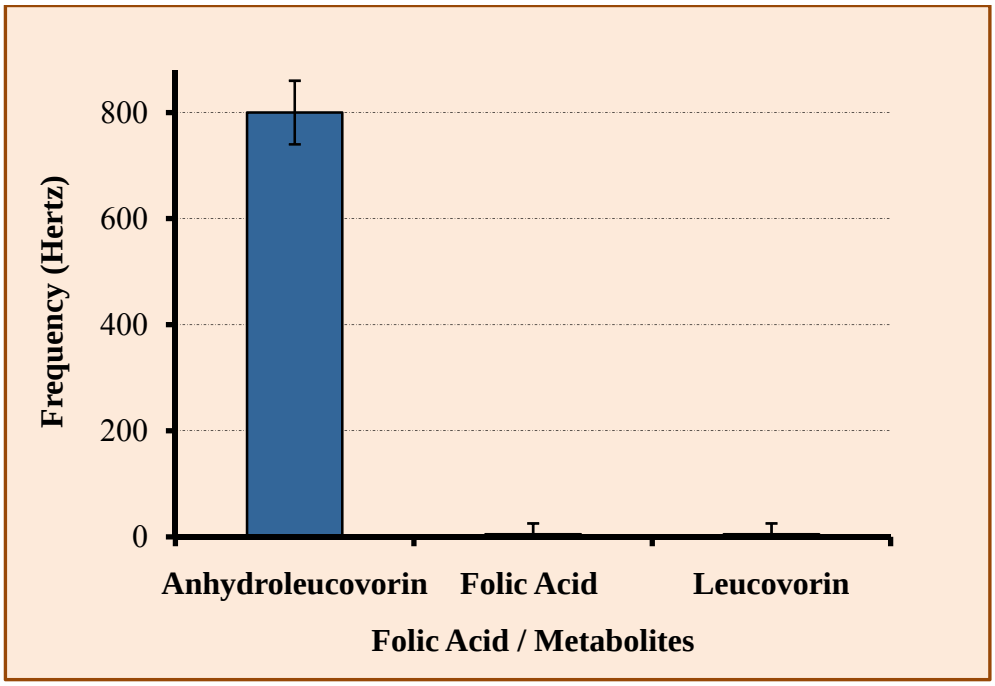

Figure 4.60 *Selectivity pattern at 100 ppm at anhydroleucovorin imprinted optimized MIP; 9 kHz MIP layer height achieved after drying and template removal*

Methanol, the only solvent for anhydrolecovorin makes imprinting for this molecule chellaging (because polymerization in 100% methanol turned out to be impossible). The problem was solved by using methanol : DMF (3:2) ratio for emulsion polymerization. The use of combination of different solvents for emulsion polymerization is unexplored area for MIP generation specifically as very little work has been reported in this respect.

4.4 Summary

Figure 4.61 summarizes selectivity and sensitivity pattern on different sensor thin films generated for sensing folic acid, leucovorin and anhydroleucovorin. 9 kHz layer height has been achieved for every sensor thin film and selectivity is measured at 100 ppm.

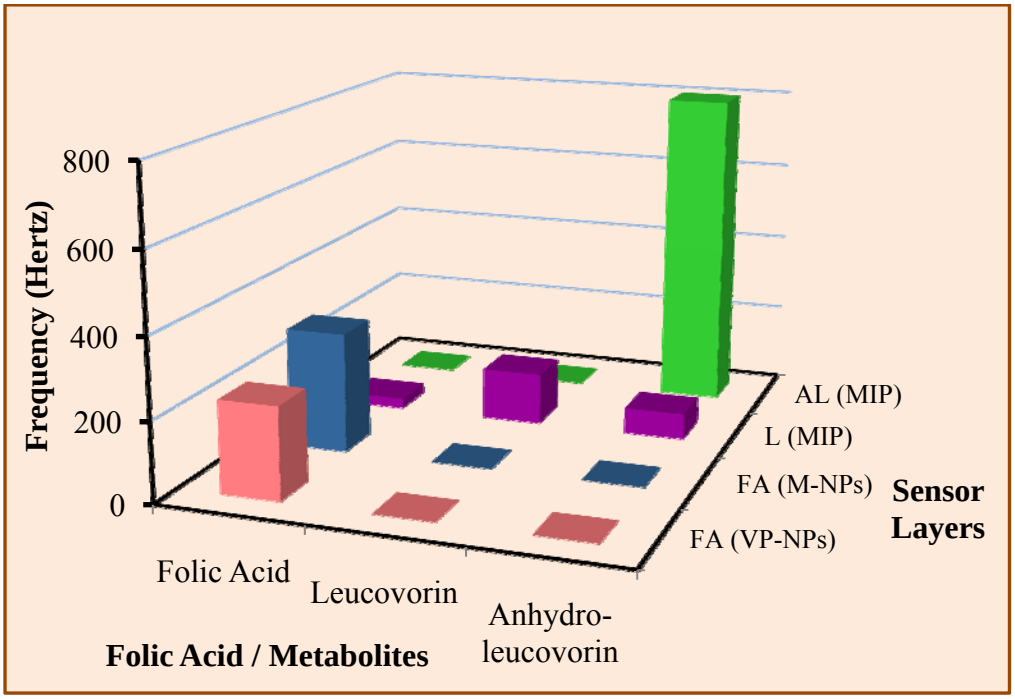

Figure 4.61 Selectivity patterns at 100 ppm at 9 kHz layer heights, folic acid and metabolites imprinting on different sensor layers, FA (VP-NPs) folic acid imprinted poly vinyl pyrrolidone particles, FA (M-NPs) folic acid imprinted poly methacrylate particles, L (MIP) Leucovorin MIP, AL (MIP) anhydroleucovorin MIP

Folic acid and anhydroleucovorin follow outclass selectivity pattern on their sensing thin films i.e. folic acid imprinted NPs and anhydroleucovorin MIP respectively. The sensor responses of counterparts remained within the base line without showing affinity to the sensor thin film. On the other hand, leucovorin cross sensitivity is five and two times as compared to that of anhydroleucovorin and folic acid respectively on leucovorin MIP thin film. The differences in selectivity can be traced back to the structural formulae which require different solvents for solubility comparatively. The different solvent (along with slight different chemical nature of template) needs modification in MIP system in the terms of cross linking monomer or initiator etc. The ultimate result is seen on differences in sensitivity and cross sensitivity patterns. Comparing the sensitivity of thin films, sensitiviy of anhydroleucovorin MIP is 2.5 and 5 times as compared to that of folic acid

imprinted NPs and leucovorin imprinted polymethacrylate MIP, respectivitely, at 100 ppm level. The enhanced sensitivity for anhydroleucovorin MIP, comparatively, can be attributed to emulsion polymerization factor (involving two solvents for MIP synthesis i.e. mehanol and DMF) which offers better surface accessiblility as compared to that of normal MIP thin film for template sensing. While the substantial lower sensitivity of leucovorin MIP is due to its the polymerization involving aqueous media which is incomparable with those of organic solvents like DMF or methanol.

Chapter 5
Phenyl Acetone Imprinting

5.1 Introduction

Phenyl acetone, IUPAC name 1-phenylpropan-2-one also called as phenyl-2-proponone (P2P), is colorless to pale yellow oil having a refractive index of 1.5168. Phenyl acetone is chemically similar in structure to that of coumarine or cinnamic acid for rodenticide anticoagulant and phenethylamine applications mainly involved in the sympathetic nervous system activity. It is employed for pesticides and anticoagulants production as an intermediate and active constituent as well as for sympathomimetic amines manufacturing. Furthermore it is employed in clandestine synthesis of 3, 4-methylenedioxymethamphetamine (MDMA), better known as ecstasy. Thus, it can only be shipped via import license, as it is a controlled substance.

Physical Properties

Molecular formula $C_9H_{10}O$, molar mass 134.18 g mol^{-1}, density 1.006 g / mL, melting point -15°C, specific gravity 1.015, boiling point 214 - 216 °C, flash point 83°C.

5.2 Phenyl Acetone Imprinting

Phenyl acetone imprinting is needed for rapid detection against drug trafficking in pharmaceutical industry. The imprinting technique has not yet been applied for this purpose.

5.2.1 Chemical Used in Imprinting

Chemical used in bulk imprinting of phenyl acetone are shown in figure 5.1

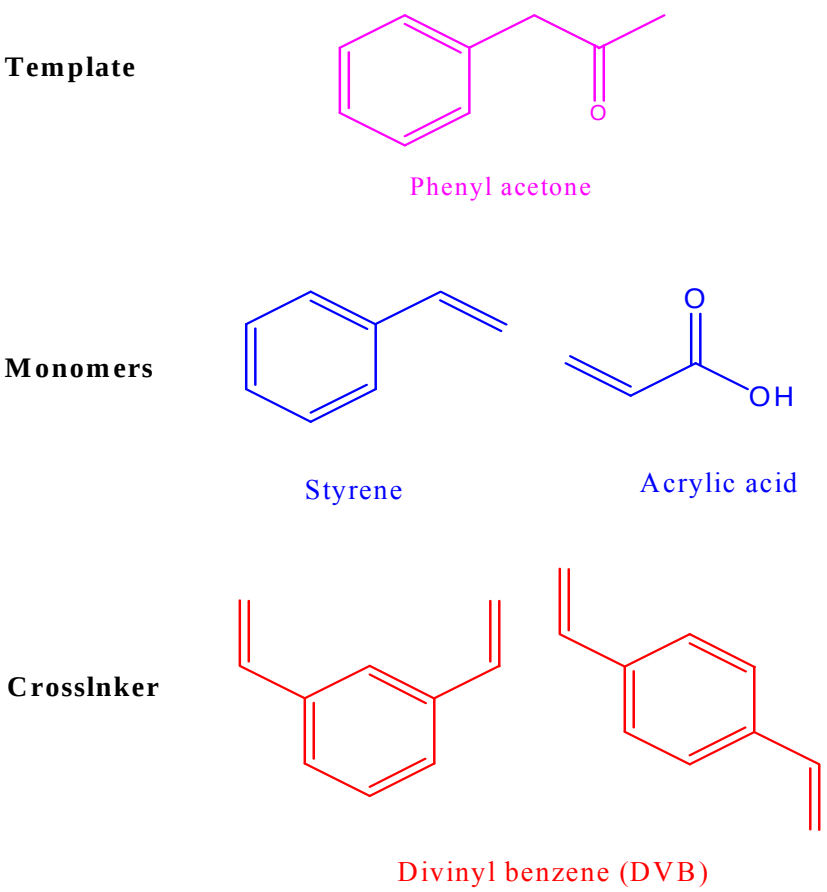

Figure 5.1 Chemicals used for phenyl acetone imprinting

5.2.2 Experimental

QCM gold printing, polymers coating and cell set up for mass sensitive measurements were carried out according to the procedures shown in chapter 3.3, 3.4, and 3.5.

a) Poly Styrene MIP

For initial MIP synthesis, 30 mg styrene along with 70 mg DVB (freshly extracted in 0.1 M NaOH) was mixed thoroughly after dissolving of 3 mg phenyl acetone in 500 µL DMF. In the end 5 mg AIBN was added to the homogenized mixture and reaction tube was kept under UV for 5 hours till the reach of gel point. The NIP was synthesized in the same way but without adding template. After MIP synthesis, 7 µL MIP oligomer solution was spin coated at 3000 rpm onto the measuring electrode of QCM while NIP was spin

coated onto the second electrode. The spin coated QCMs were kept overnight at room temperature for drying and hardening the MIP thin films. The dried QCMs were washed in methanol: water (1: 1) kept at 60ºC using water bath for one hour. After template washing, the dried QCMs were ready to be inserted into the measuring cell.

b) Poly Styrene MIP (modified)

In the optimal monomer to cross linker ratio MIP synthesis, 40 mg styrene along with 60 mg DVB (freshly extracted in 0.1 M NaOH) was mixed thoroughly via stirring after the dissolving 3 mg phenyl acetone in 500 µL DMF in a reaction tube. After homogenizing the mixture, 5 mg AIBN was added to initialize the polymerization. The reaction tube was kept for 6.5 hours under UV light to achieve the MIP till the reach of gel point.

c) Poly Styrene MIP (Acrylic Acid as Co-Monomer)

In the modified MIP synthesis, 4 mg phenyl acetone along with 20 mg styrene (freshly extracted with 0.1 M NaOH), 20 mg acrylic acid and 60 mg EGDMA was mixed thoroughly with 500 µL DMF in a reaction tube. After homogenized mixing of all the components, 6 mg AIBN was added to the initialize the polymerization. Then, reaction tube was kept under UV lamp for 2 hours at room temperature till the reach of gel point. The NIP was synthesized without adding template while keeping all the parameters constant. After MIPs synthesis, 10 µL MIP oligomer solution was used for spin coating at 3000 rpm on the measuring electrode of QCM while the second electrode was spin coated with NIP. The spin coated QCMs were kept overnight staying at room temperature for hardening and drying the thin films. Template was washed by keeping the QCMs in water at 50 ºC containing 15% ethanol and 5% methanol for two hours using magnetic stirrer on water bath. The template washing procedure has been adopted for the future experiments of phenyl acetone imprinting measurements in this chapter.

d) Poly Styrene MIP (Methacrylic Acid and Vinyl Pyrrolidone as Co-Monomer)

In modified MIP synthesis, 4 mg phenyl acetone along with 10 mg vinyl pyrrolidone, 15 mg methacrylic acid, 15 mg styrene (freshly extracted with 0.1 M NaOH) and 60 mg EGDMA was mixed thoroughly with 500 µL DMF in a reaction tube. In the end, 5 mg AIBN was added to the initialize the polymerization after homogenized mixing. The reaction tube containing mixture was kept under UV source for 70 minutes at room temperature till the reach of gel point. The NIP was synthesized keeping all parameters constant except the addition of phenyl acetone.

e) Optimized MIP

In the final optimized MIP synthesis, 4 mg phenyl acetone along with 20 mg styrene (freshly extracted with 0.1 M NaOH), 20 mg acrylic acid and 60 mg EGDMA was mixed with 167 µL ethyl acetate, 167 µL pyridine and 167 µL DMF in a reaction tube. After homogenized mixing, 6 mg AIBN was added to initialize the polymerization. The reaction tube containing mixture was kept under UV radiation lamp for 1 hour and 50 minutes at room temperature till the reach of gel point. While the NIP was synthesized keeping all the parameters constant except adding of template. After synthesis of polymers, 10 µL MIP oligomer solution was used for spin coating at 3000 rpm on the measuring electrode of QCM while the second electrode was coated with NIP. The spin coated QCMs were kept overnight stayed at room temperature for thin films drying and hardening. Template was washed by keeping the QCMs in water at 50 ºC containing 15% ethanol and 5% methanol for two hours using magnetic stirrer on water bath.

f) NPs Approach

For NPs synthesis, 500 µL MIP oligomer solution (generated from final MIP recipe) was poured into 10 mL water containing 25% / 50% / 75% acetonitrile, respectively. The suspensions were kept stirring for 24 hours by

using magnetic stirrer. The resulting NPs solution was centrifuged at 4000 rpm and solvent was removed to obtain the NPs. The NPs were resuspended in 500 µL acetonitrile in eppendorf tube. The NIP beads were generated in the same manner from NIP oligomer solution. 5 µL NPs were spin coated at 2000 rpm on the unhardened layer of acrylic acid and EGDMA (2:1) on one electrode of QCM while the second electrode was spin coated with NIP beads.

5.3 Results and Discussion

Phenyl acetone MIP design consisted of screening a variety of different monomers, cross linking monomers and solvents. In initial studies styrene has been used along with different co-monomers that offer stability, reproducibility and robustness for MIP systems e.g. methacrylic acid, vinyl pyrrolidone and acrylic acid. To achieve structural stability after template removal from MIP, DVB and EGDMA have been applied as cross linking monomers. To increase the porosity of MIP along with substructure and porogenic effects for better diffusion of phenyl acetone into MIP, solvents like DMF has been optimized along with pyridine and ethyl acetate. Finally phenyl acetone imprinting remained successful on poly styrene-acrylate emulsion polymerized in ethyl acetate, DMF and pyridine cross linked by EGDMA. All the MIPs and NIPs have been synthesized under UV source at room temperature.

5.3.1 Poly Styrene MIP

The purpose of using poly styrene system (styrene/DVB) is to target the aromatic ring of phenyl acetone as styrene or xylene polymer systems are expected to generate better MIPs for aromatic templates. To check the feasibility of poly styrene for phenyl acetone MIP design the first experiment was performed by keeping the 30 mg : 70 mg between the monomer (i.e. styrene) to cross linking monomer (i.e. DVB).

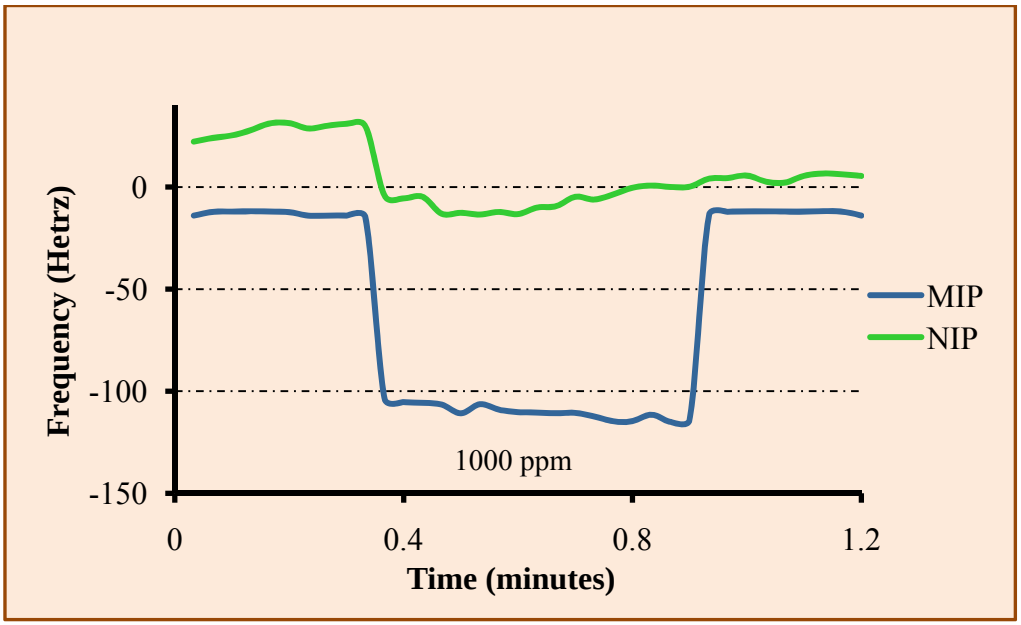

Figure 5.2 Sensor response at 1000 ppm phenyl acetone in 20% ethanol, 12 kHz MIP layer height achieved by MIP spin coating and after template removal

The above figure 5.2 demonstrates the very first the sensor response of phenyl acetone at 1000 ppm in 20% ethanol. The use of dilute ethanol for standards solutons of phenyl acetone has the advantage of better solubility as compared to water, thus mostly applied for pharmaceutical applications. On comparing the signals, 5 folds sensor response of MIP as compared to that of NIP suggests the success of phenyl acetone imprinting in poly styrene MIP. Higher concentration of crosslinker (i.e. 70% with respect to monomer) leads to very rigid layers leading to incomplete template removal. Therefore sensitivity of the thin film restricted to only 100 Hz at 1000. Highly sensitive sensor is possible through the optimization of parameters like monomer to crosslinking monomer. To improve the sensitivity of the MIP thin film, monomer to crosslinking monomer has been optimized in the next step. In the this experiment monomer to crosslinker ratio 40 mg : 60 mg was found to be effective in phenyl acetone imprinting. The layer height measured by network analyzer, was noted 12 kHz (480 nm) for MIP coated electrode after washing procedure. The lamp source distance with respect to reaction tube affects the

polymerization time as well as homogeneity and the extant of imprinting. The higher the distance the longer the polymerization time will be (and vice versa) due to the change in UV intensity as a function of distance. Increase and decrease of 1 cm distance between reaction tube and source with respect to optimum distance increases or decreases polymerization by 2.5 hours, respectively with respect to optimum time for this MIP. The polymerization by keeping reaction tube in plastic Petri dish under UV also gives these effects due to ultra violet radiations reflection from Petri dish walls. That is why the MIP prepared by keeping the reaction tube in plastic Petri dish lose homogeneity due to change in polymerization time ultimately giving poor or zero sensitivity in mass sensitive measurements.

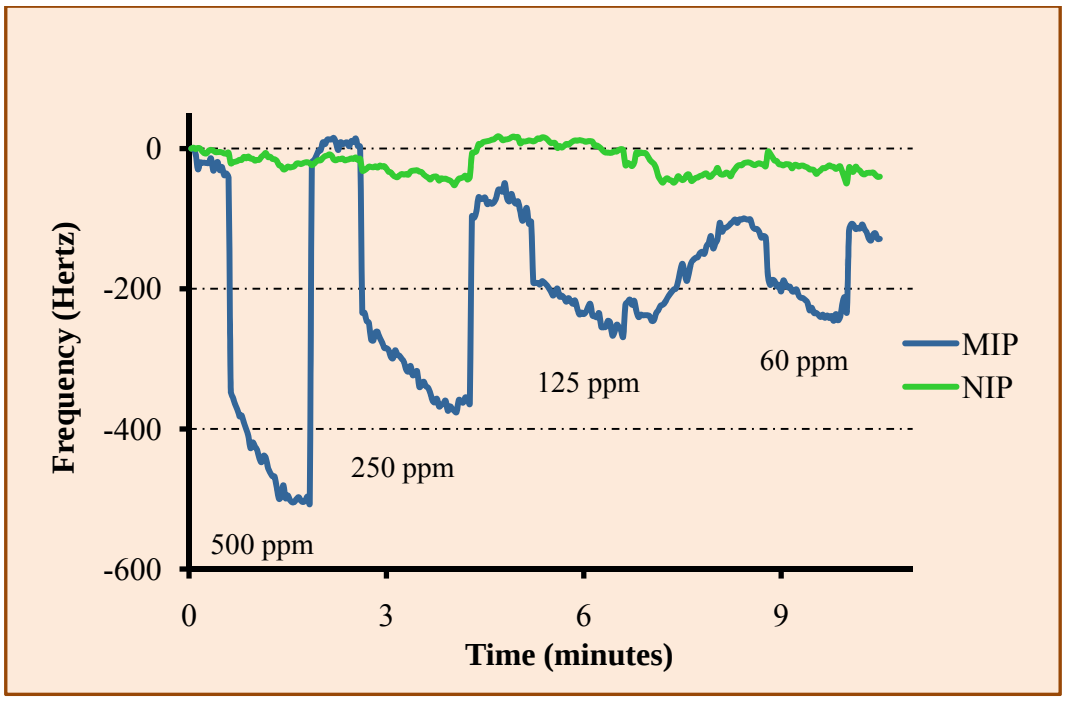

Figure 5.3 Sensor response in 20% ethanol, phenyl acetone imprinting in poly styrene, 12 kHz MIP layer height achieved after template washing

The figure 5.3 demonstrates MIP sensitivity at the parts per million levels with reproducible signals. 40:60 monomer to cross linking monomer ratio was found to be effective because of improvement in LoD to 60 ppm at S/N ratio ≥ 3 as compared to that of 30:70 ratio on comparing that gave 1000

ppm at S/N ratio ≥ 3. A drift in the base line and comparably low sensitivity in the range leading to LoD of 60 ppm are the main limitations of the sensor characteristics of these simple poly styrene based systems.

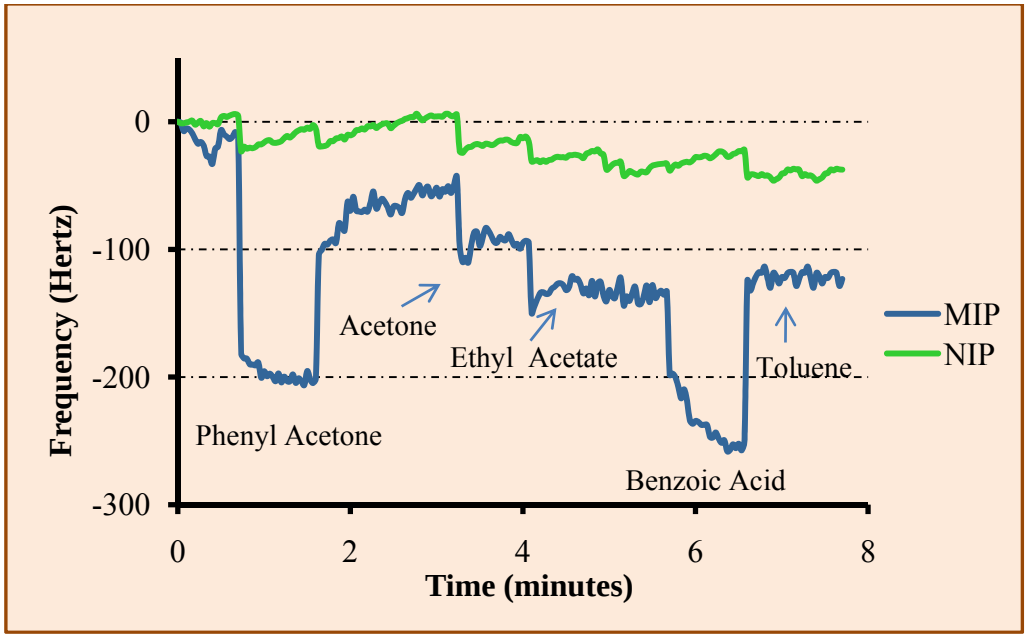

Figure 5.4 Selectivity pattern in 20% ethanol at 500 ppm, 12 kHz MIP layer height achieved after MIP spin coating, thin films drying and template washing

Although sensitivity of the material needs improvement, the previous results showed that the MIP and the NIP react differently. Figure 5.4, therefore, demonstrates a selectivity experiment to assess the quality of the imprinted cavities. As can be seen there, some drift in base line occurs due to non-polarity of styrene, therefore, somewhat impairing the outcome of selectivity measurements. Further improvements are possible by applying more polar monomers to have interaction possibilities with carbonyl group of phenyl acetone. This suggests applying methacrylic acid or acrylic acid or vinyl pyrrolidone would be interesting for the improvements in compactness and robustness of MIP. Thus modifications were done by adding more polar co-monomers in the next step for mass sensitive measurements.

5.3.2 Poly Styrene – Acrylate MIP

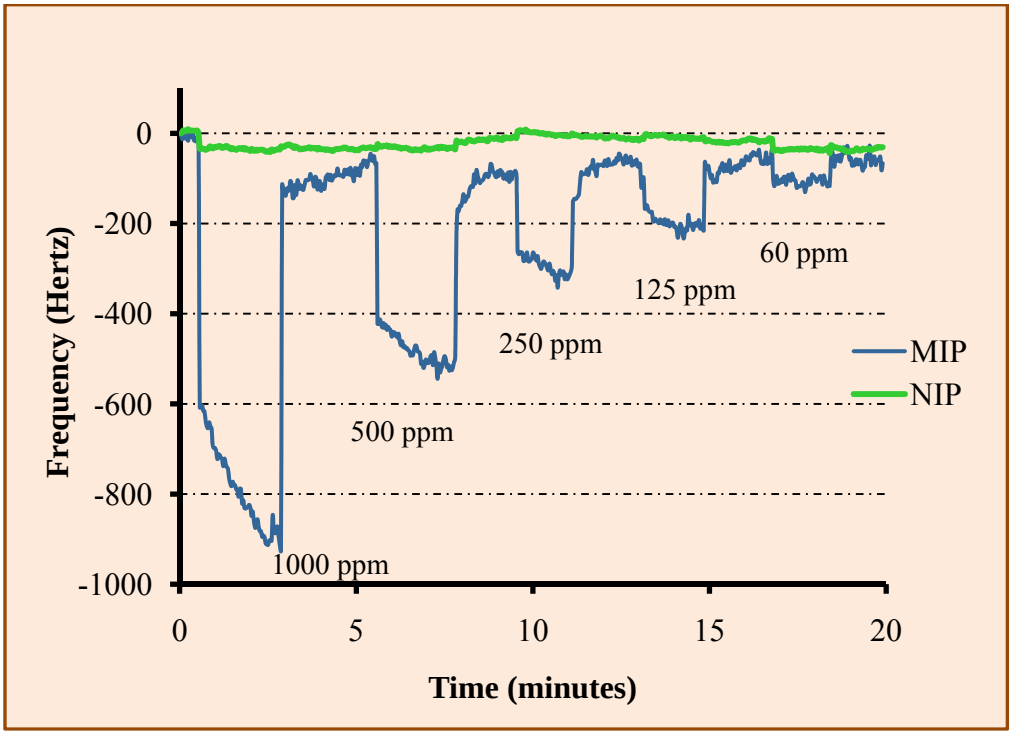

Figure 5.5 Sensor response in 30% ethanol, phenyl acetone imprinting in styrene: acrylic acid: EGDMA, 27 kHz MIP layer height achieved after MIP spin coating, thin films drying and template removal

Figure 5.5 demonstrates sensor response of phenyl acetone in 30% ethanol media for MIP containing poly styrene and acrylate. 27 kHz layer height was measured on network analyzer after spin coating and template washing step. This gives insight into suitability of the MIP for sensing phenyl acetone at higher ppm range with 60 ppm LoD at S/N ratio ≥ 3. Phenyl acetone imprinting in poly styrene: acrylic acid: EGDMA is advantageous over simple poly styrene MIP system because of fast and robust polymerization under UV. The further improvement in LoD and sensitivity is possible to meet the analytical requirements for sensing phenyl acetone. This can be done by changing solvent composition for generation of MIP with better porosity possessing porogenic and substructure effects from solvents.

This polymer composition also yielded optimal results for the solvent studies that are to follow in the next chapters

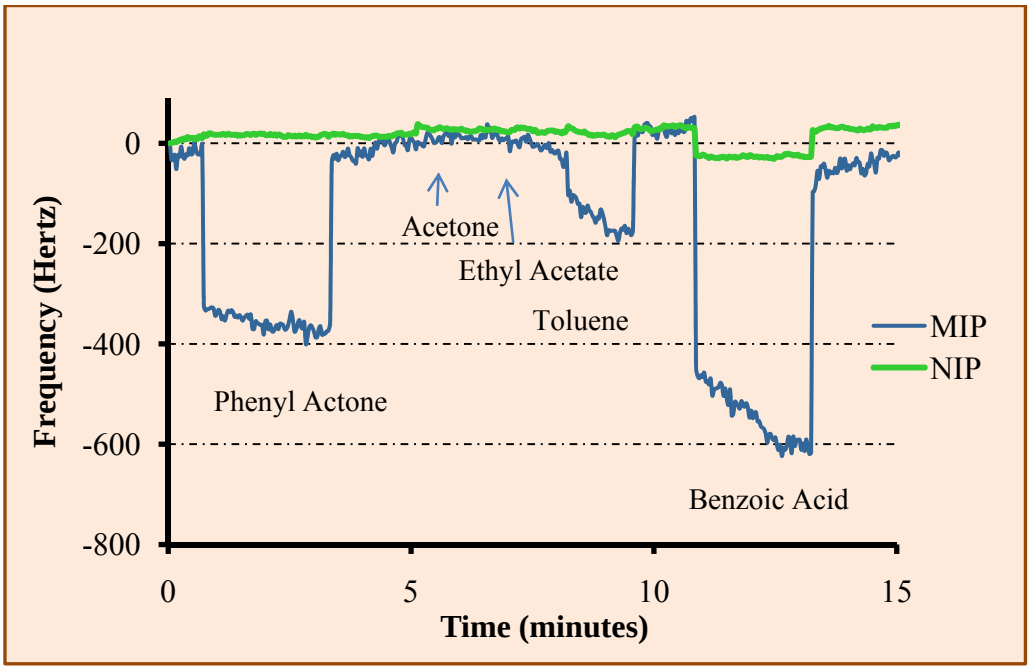

Figure 5.6 Selectivity pattern at 500 ppm in 30% ethanol, phenyl acetone imprinting in styrene: acrylic acid: EGDMA, 27 kHz MIP layer height achieved by MIP spin coating and template removal

Figure 5.6 demonstrates the selectivity pattern at 500 ppm between phenyl acetone and its structural analogs for poly styrene-acrylate-EGDMA MIP. Acetone and ethyl acetate gave no sensor response demonstrating appreciable results for phenyl acetone imprinting. Toluene also showed low response as compared to that of phenyl acetone while 1.5 times response of benzoic acid may be attributed to fitness into the cavities comparatively. Furthermore the comparatively more hydrophobic behavior of benzoic acid is also responsible for this higher response. To address not only the aromatic ring, but also the ketone functionality, MIP could be made slightly more polar by including methacrylate and vinyl pyrrolidone for MIP improvements.

5.3.3 Poly Styrene MIP (Methacrylic Acid and Vinyl Pyrrolidone as Co-Monomer)

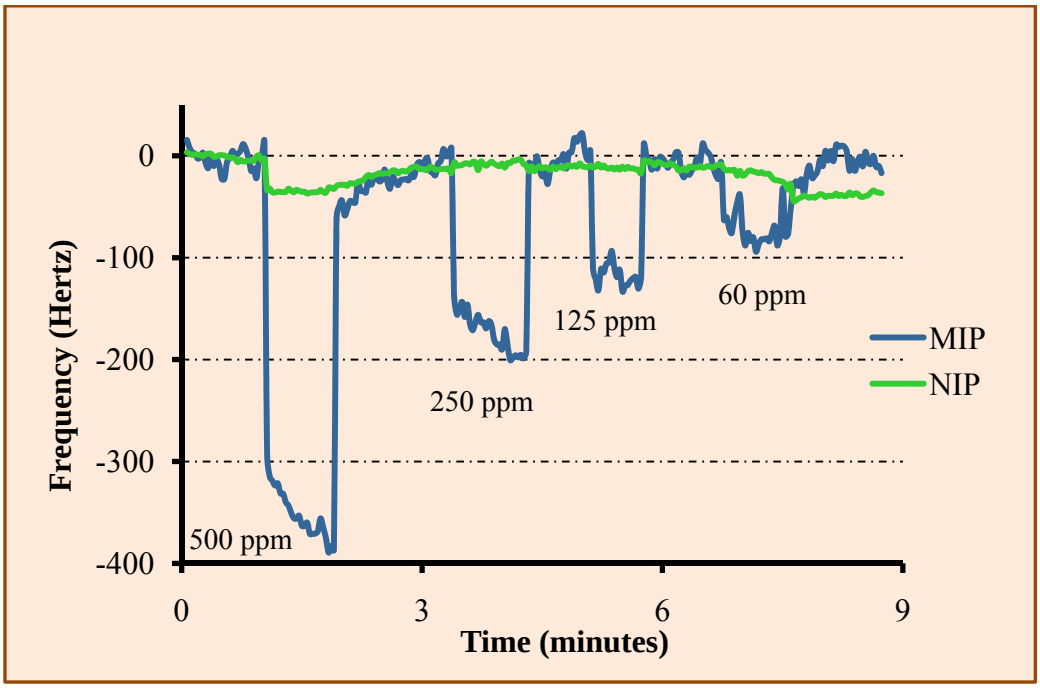

Figure 5.7 Sensor response in 30% ethanol, phenyl acetone imprinting in vinyl pyrrolidone: methacrylic acid: styrene: EGDMA, 25 kHz MIP layer height achieved by MIP after spin coating, MIP drying and template removal

Ketone reacts with both primary and secondary amines to form imine and enamine, respectively. Therefore one could expect affinity between carbonyl functionality of phenyl acetone and amine groups in the polymer by adding vinyl pyrrolidone in the MIP system. Figure 5.7 demonstrates the cumulative effect of methacrylate and vinyl pyrrolidone in poly styrene MIP system. For sensor measurement, 25 kHz layer height was measured on network analyzer after template washing step. The regeneration of the base line and signal shapes in the measurements has been improved by using vinyl pyrrolidone along with methacrylic acid in poly styrene system.

As it can be seen from figure 5.8, acetone, ethyl acetate and toluene lead to only minimal responses underpinning the high selectivity of the system at 500 ppm.

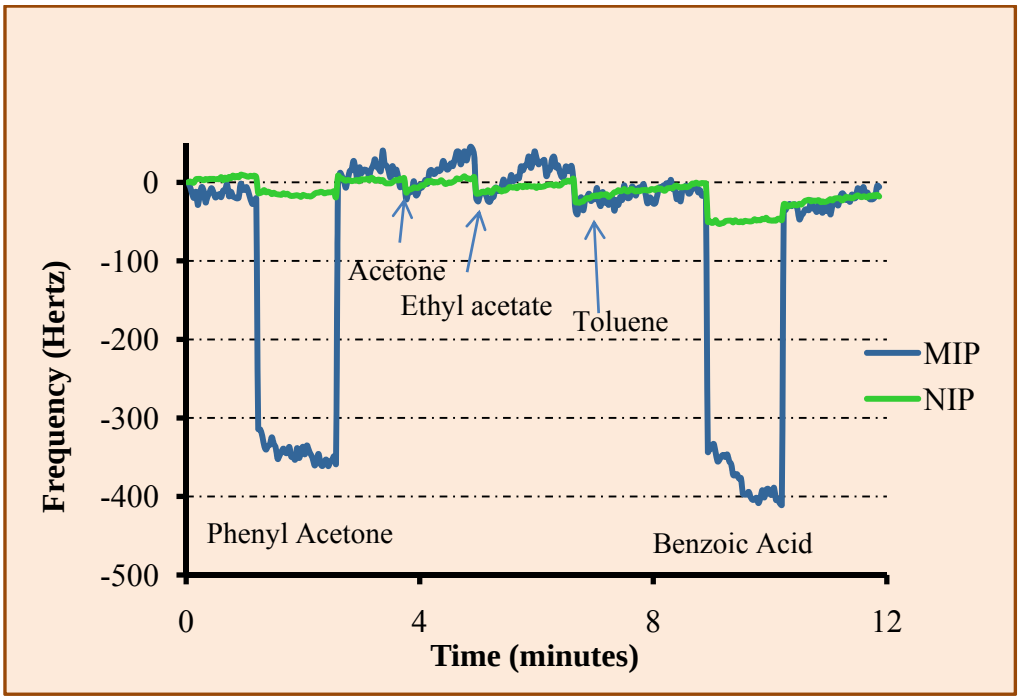

Figure 5.8 Selectivity pattern in 30% ethanol at 500 ppm, phenyl acetone imprinting in vinyl pyrrolidone: methacrylic acid: styrene: EGDMA, 25 kHz MIP layer height achieved by MIP spin coating and template removal

However, for benzoic acid the sensor response is the same as for phenyl acetone. The reasons behind selective behavior are contributed from the small structural differences among the structural analogs. Methacrylate-vinyl pyrrolidone co-polymerized in polystyrene yielded more appreciable results due to compactness of cavities for phenyl acetone diffusion. But the use of vinyl pyrrolidone was not carried out further. This also finally meant that the more straightforward system proved more useful, which is also favorable for MIP synthesis involving substructure or porogenic effect from solvents.

5.3.4 Modification of MIP Solvent Effect

The MIP sensitivity can be enhanced by increasing their porosity by adding porogen solvent and taking the edge of substructure imprinting by adding a solvent that is itself a substructure of the template. To increase the porosity of MIP along with substructure imprinting effects for better diffusion

of phenyl acetone into MIP, solvents like DMF can be optimized along with pyridine and ethyl acetate in emulsion polymerization. Addition of pyridine can contribute to the formation of cavities for aromatic ring for better inclusion of phenyl acetone molecule into MIP. On the other hand, ethyl acetate can contribute to the substructure imprinting of carbonyl moiety for phenyl acetone along with enhancing the porosity of MIP. Furthermore emulsion polymerization is a better alternative for MIP because of particles generation for enhancement of MIP surface area as compared to that of conventional MIP strategies.

MIP Surface Morphology

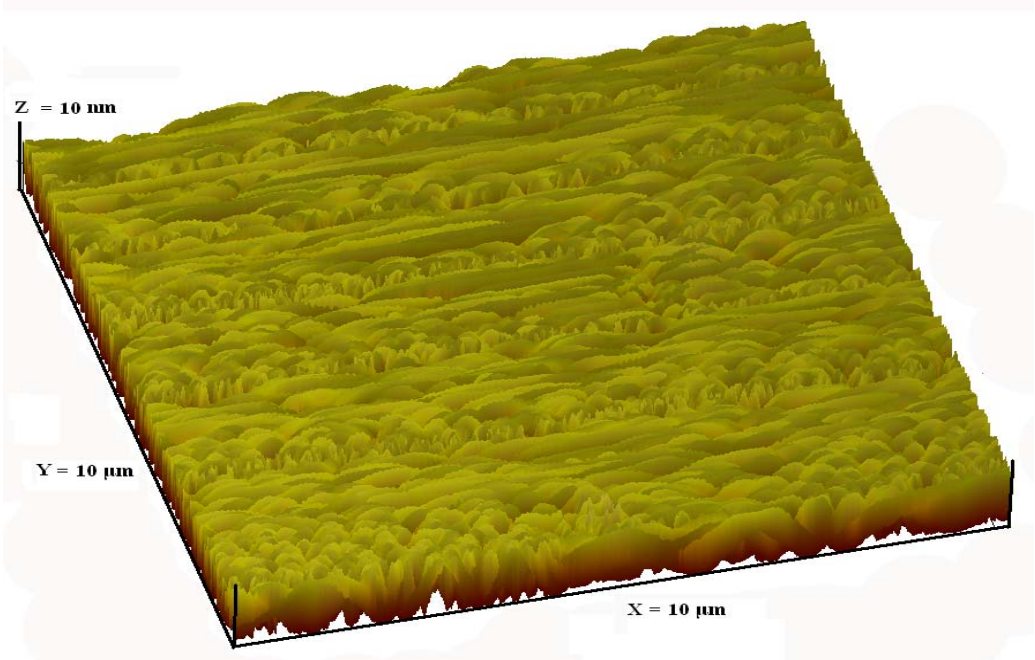

Figure 5.9 AFM image of optimized MIP layer, MIP solvent composition (ethyl acetate: DMF: pyridine 167:167:167 µL)

To check the feasibility of emulsion polymerization and enhancement in porosity and surface area AFM studies were done for MIPs having various compositions of solvents. Figure 5.9 demonstrates the MIP morphology containing optimal solvent composition i.e. ethyl acetate: DMF: pyridine

(167:167:167 µL). The MIP morphology demonstrates the formation of MIP particles from nano to micro levels with homogenous layout. The formation of particles suggests the enhancement of surface area ultimately an enhanced porosity and roughness for better diffusion of phenyl acetone. While MIPs having ethyl acetate: DMF: pyridine with ratios of (400:50:50), (50:400:50) and (50:50:400) µL showed noise in the AFM images indicating flat MIP surface (not shown here). All the MIPs were subjected to mass sensitive measurements to investigate into the sensitivity of each thin film. The target was to approach the high sensitive layer with appreciable detection limits for phenyl acetone sensing via generation of porosity, substructure imprinting effects and enhanced surface area. AFM images suggest 167:167:167 µL ratio could provide better sensitivity due to better surface morphology.

Ethyl Acetate Based Solvent Mixture

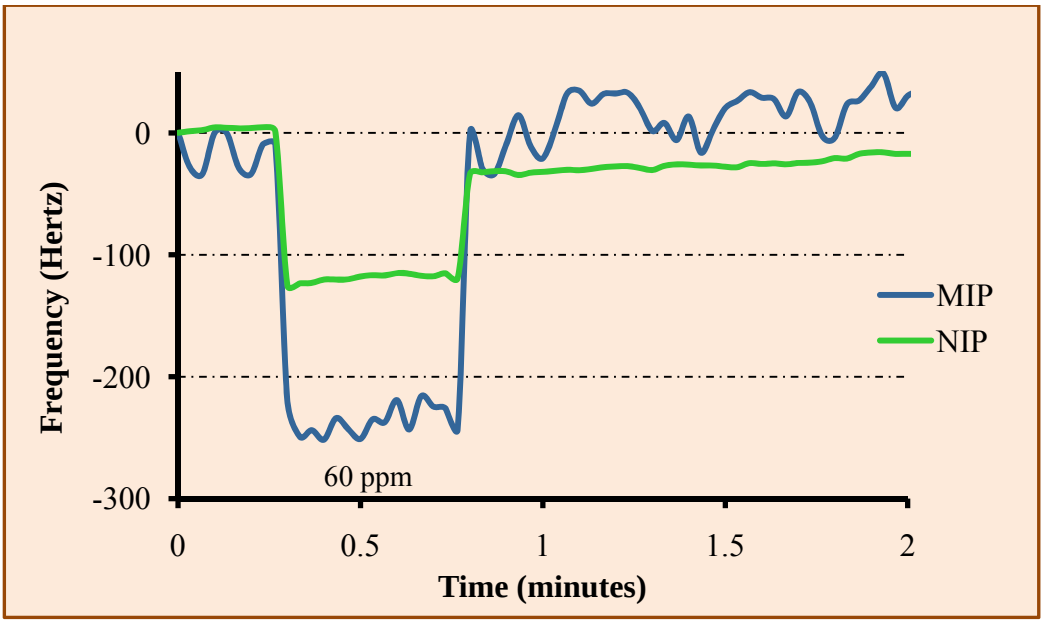

Figure 5.10 Solvent effect (ethyl acetate based solvent composition for polymerization), Sensor response at 60 ppm in H_2O, phenyl acetone imprinting in styrene: acrylic acid: EGDMA (20:20:60 mg), ethyl acetate: DMF: pyridine (400:50:50 µL), 6 mg AIBN, UV polymerization 1 hour 35 minutes. 12 kHz MIP layer height achieved by MIP spin coating at 4500 rpm and after template removal

For obtaining the results in figure 5.10, targeting appreciable sensitivity via taking the edge of substructure imprinting effects from ethyl acetate, ethyl acetate based mixture was used for MIP synthesis. The MIP was prepared in ethyl acetate: DMF: pyridine (400:50:50 µL) by keeping the mixture under UV for 1 hour and 35 minutes. 12 kHz layer height was measured on network analyzer for MIP after the template washing. The sensor response was measured by exposing the sensor to 60 ppm phenyl acetone in H_2O. The sensor signal is fully reversible in both cases of MIP and NIP while MIP signal exceeds the one of the NIP. However for reaching appreciable detection limits, further optimization is necessary.

DMF Based Solvent Mixture

To the figure 5.11, targeting sensitivity via substructure imprinting effects from ethyl acetate and pyridine cumulatively, DMF based mixture with small amounts of ethyl acetate and pyridine was used in the MIP.

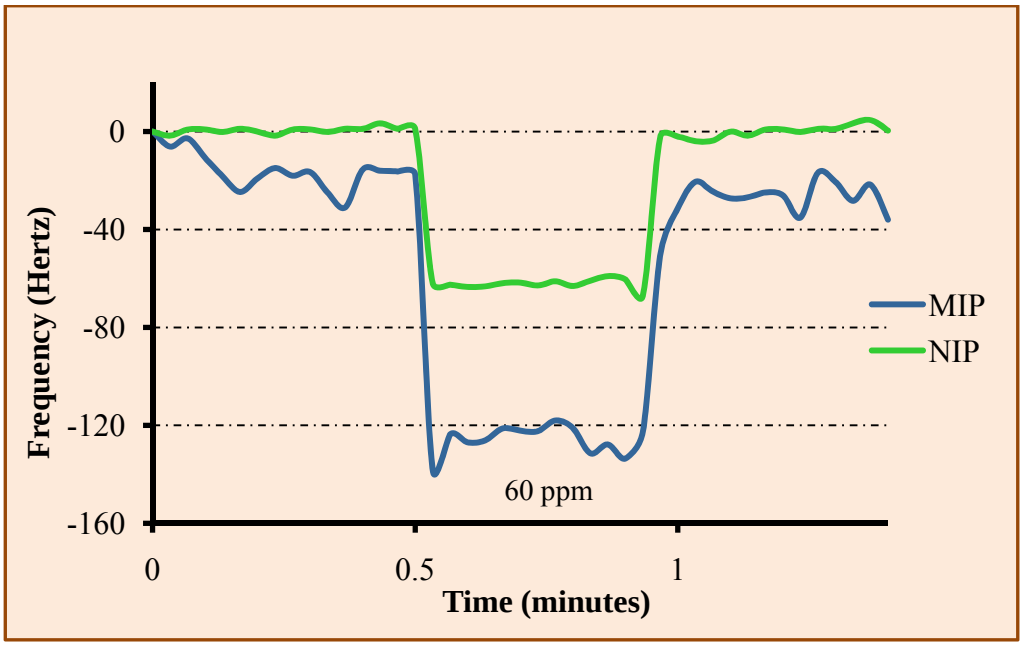

Figure 6.11 Solvent effect (DMF based solvent composition for polymerization), sensitivity (60 ppm in H_2O), phenyl acetone imprinting in styrene: acrylic acid: EGDMA (20:20:60 mg), ethyl acetate: DMF: pyridine (50:400:50 µL), 6 mg AIBN, UV polymerization 1 hour. 12 kHz MIP layer height achieved by MIP spin coating at 4500 rpm and after template removal

The MIP was prepared in ethyl acetate: DMF: pyridine (50:400:50 µL) by keeping the mixture under UV for 1 hour. 12 kHz layer height was measured on network analyzer for MIP after the template washing. The sensor response was measured by exposing the sensor to 60 ppm phenyl acetone in H_2O. The sensor signal is fully reversible in both cases of MIP and NIP while MIP signal leads slightly the one of the NIP. The MIP generated in ethyl acetate based solvent mixture gave two times sensitivity as compared to that of MIP generated in DMF based solvent mixture. Further optimization therefore should provide appreciable detection limits and sensitivity.

Pyridine Based Solvent Mixture

To the figure 5.12, targeting better sensitivity by taking substructure imprinting effects from pyridine, pyridine based mixture was used for MIP synthesis.

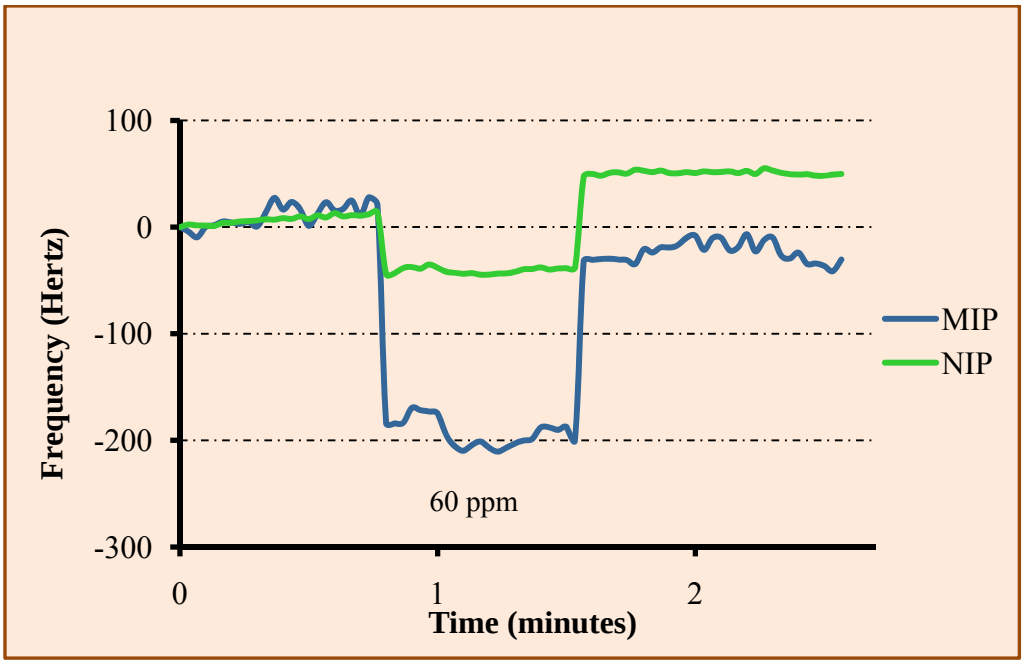

Figure 5.12 Solvent effect (pyridine based solvent composition for polymerization), sensitivity (60 ppm in H_2O), phenyl acetone imprinting in styrene: acrylic acid: EGDMA (20:20:60 mg), ethyl acetate: DMF: pyridine (50:50:400 µL), 6 mg AIBN, UV polymerization 1 hour 40 minutes. 13 kHz MIP layer height achieved by MIP spin coating at 4500 rpm and after template removal

The MIP was prepared in ethyl acetate: DMF: pyridine (50:50:400 µL) by keeping the mixture under UV for 1 hour and 40 minutes. 13 kHz layer height was measured on network analyzer for MIP after the template washing. The sensor response was measured by exposing the sensor to 60 ppm phenyl acetone in H_2O. The sensor response is similar as in the two cases hence demanding further optimization.

Optimum Solvent Composition

To achieve the goal of appreciable sensitivity and detection limits by taking the edge of porosity, substructure imprinting effects from ethyl acetate and pyridine the solvent composition was further optimized.

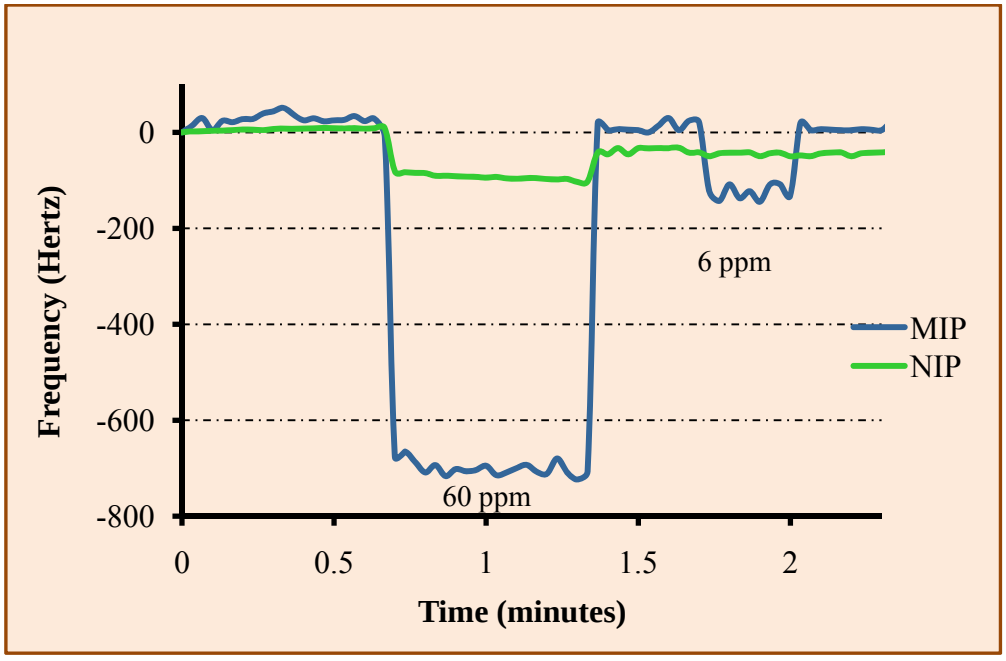

Figure 5.13 Sensitivity in H_2O, phenyl acetone imprinting in optimized solvent mixture (ethyl acetate: DMF: pyridine, 167:167:167 µL), 500 µL MIP was further diluted with 500 µL solvent (i.e. DMF: pyridine: ethyl acetate 1:1:1), 12 kHz MIP layer height achieved by (diluted) MIP spin coating at 4500 rpm and after template removal

Sensor response for optimized MIP has been shown in figure 5.13. Finally DMF based solvent composition was optimized using 33.3 % each of ethyl acetate, DMF and pyridine for emulsion polymerization. The sensor

response is reversible, robust and appreciable for phenyl acetone sensing at lower ppm range with 6 ppm LoD at S/N ratio ≥ 3. In MIP synthesis, increase and decrease of 1 cm distance between reaction tube and source with respect to optimum distance increases or decreases polymerization by 1 hour, respectively with respect to optimum time. MIP synthesized in shorter time remains unhardened gel and cannot be coated onto QCM electrodes. On the other hand, MIP batches synthesized in longer polymerization time become extremely rigid that template washing remains unsuccessful by any means giving either no sensor response at all or extremely low sensitivity.

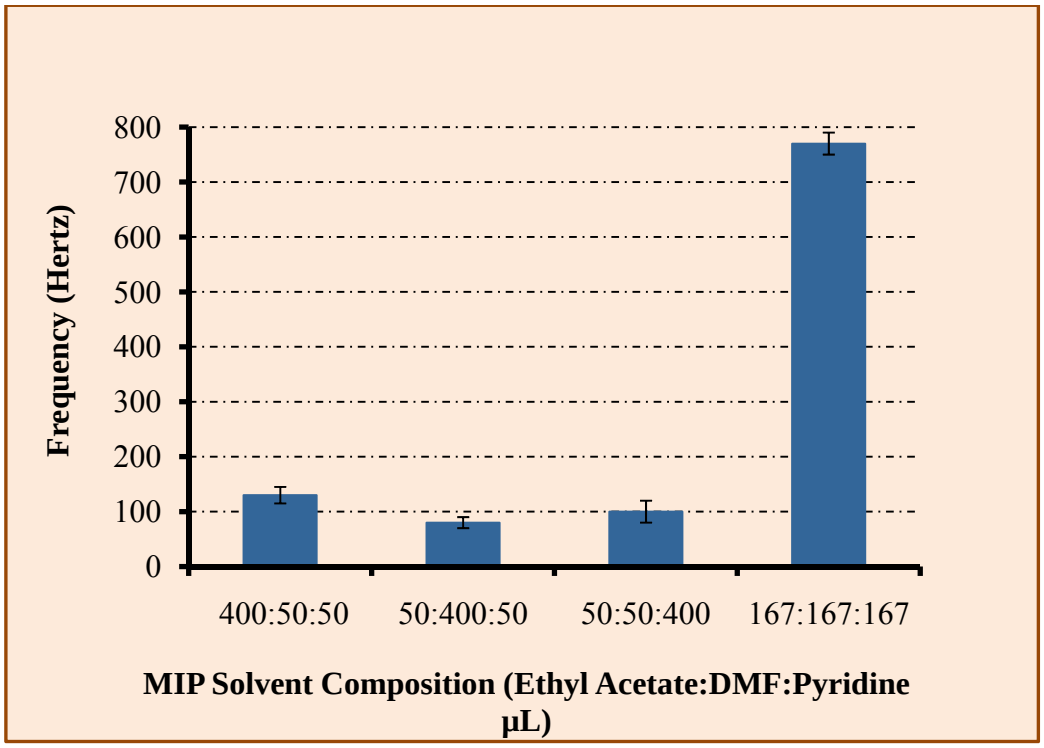

Figure 5.14 Solvent composition (polymerization) effect on MIP sensitivity (in H_2O), phenyl acetone imprinting in styrene: acrylic acid: EGDMA (20:20:60 mg), 6 mg AIBN, UV polymerization

Figure 5.14 demonstrates the solvent effect on MIP sensitivity at 60 ppm in aqueous media. Finally phenyl acetone imprinting remained successful on poly styrene-acrylate emulsion polymerized in ethyl acetate, DMF and pyridine (1:1:1) cross linked by EGDMA. Although ethyl acetate,

DMF and pyridine showed sensor responses when one solvent was kept in larger concentration in MIP synthesis, yet the 1:1:1 ratio composition enhanced the sensitivity 7 times as compared to that of single solvent based mixture. The enhanced sensitivity can be attributed to the substructure imprinting effects from ethyl acetate along with pyridine ring for sensing phenyl acetone. As shown in the beginning of solvent effect, AFM image of the optimized also supports the facts of formation of nano/micro structures leading to increasing the accessibility of individual interaction sites for phenyl acetone diffusion. The emulsion polymerization is uncommon and unexplored in molecular imprinting technology (also in polymer science) but the future applications can be wonderful for applied polymer science. The optimized recognition system is further subjected to mass sensitive measurements in 30% ethanol media and characterization in water media.

5.3.5 Optimized Recognition System (Measurements in 30% Ethanol)

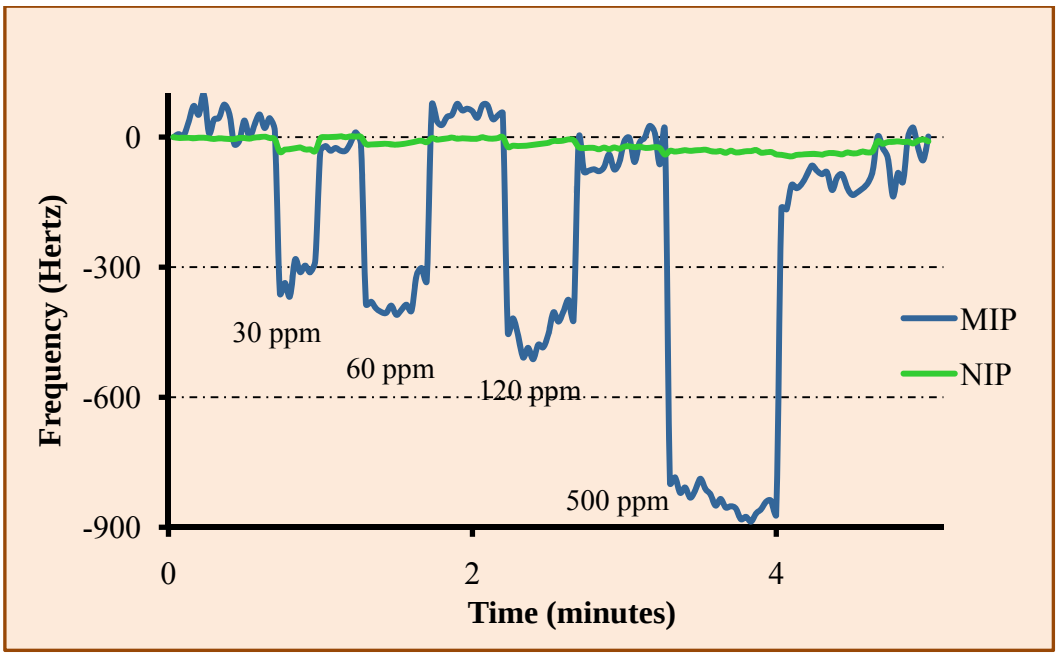

Figure 5.15 Sensor response in 30% ethanol for optimized MIP, 35 kHz MIP layer height achieved by MIP spin coating at 3000 rpm and after template removal

The optimized recognition system were subject to sensitivity and selectivity measurements in 30% ethanol media because of common applications of phenyl acetone in pharmaceutical industry in dilute ethanol media. Figures 5.15 and 5.16 show the sensitivity and LoD of optimized MIP measured in 30% ethanol media, respectively.

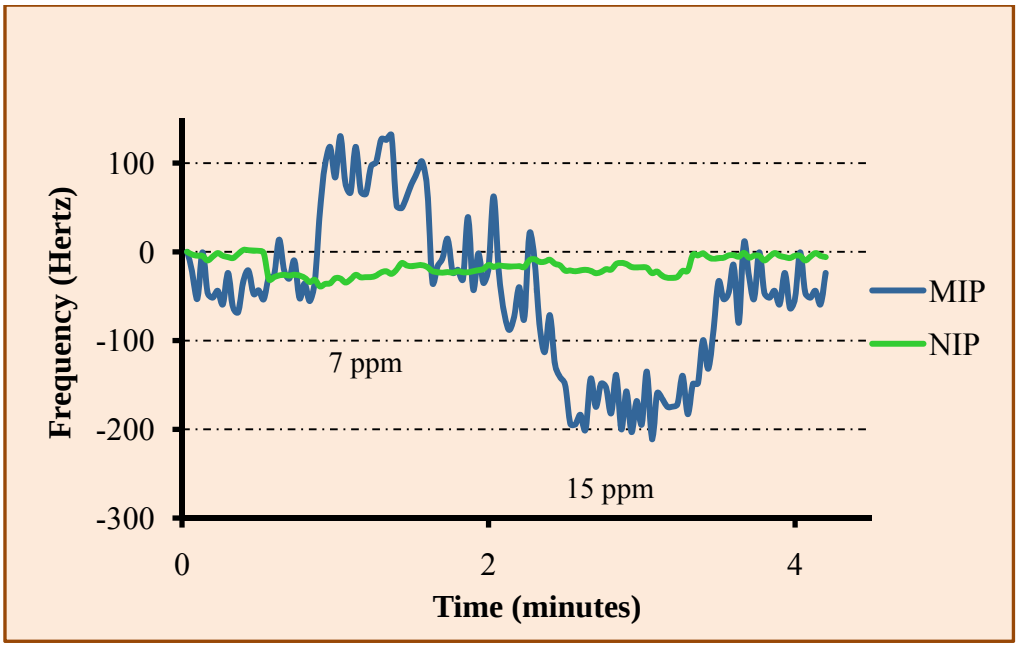

Figure 5.16 MIP sensitivity at low ppm range in 30% ethanol for optimized MIP, 35 kHz MIP layer height achieved by MIP spin coating and after template removal

The 35 kHz layer height was noted on network analyzer after spin coating, drying and template washing. The solvent composition in the optimized MIP has improved the sensitivity by the factor of three and LoD by a factor of ten from that of MIP generated in DMF on comparing with figure 5.5. Figures demonstrate the MIP sensitivity with reversible signals while the response in second figure shows anti Sauerbrey effect at 7 ppm due to fast moving of phenyl acetone molecules out of the MIP cavities generating low mass effect as compared to that of base line. LoD of 7 ppm at S/N ratio ≥ 3 has been achieved for the mass sensitive measurements using QCM as

transducer. The mass sensitive measurements in 30% ethanol media demonstrate good suitability of the MIP for sensing phenyl acetone for pharmaceutical applications in dilute ethanol media.

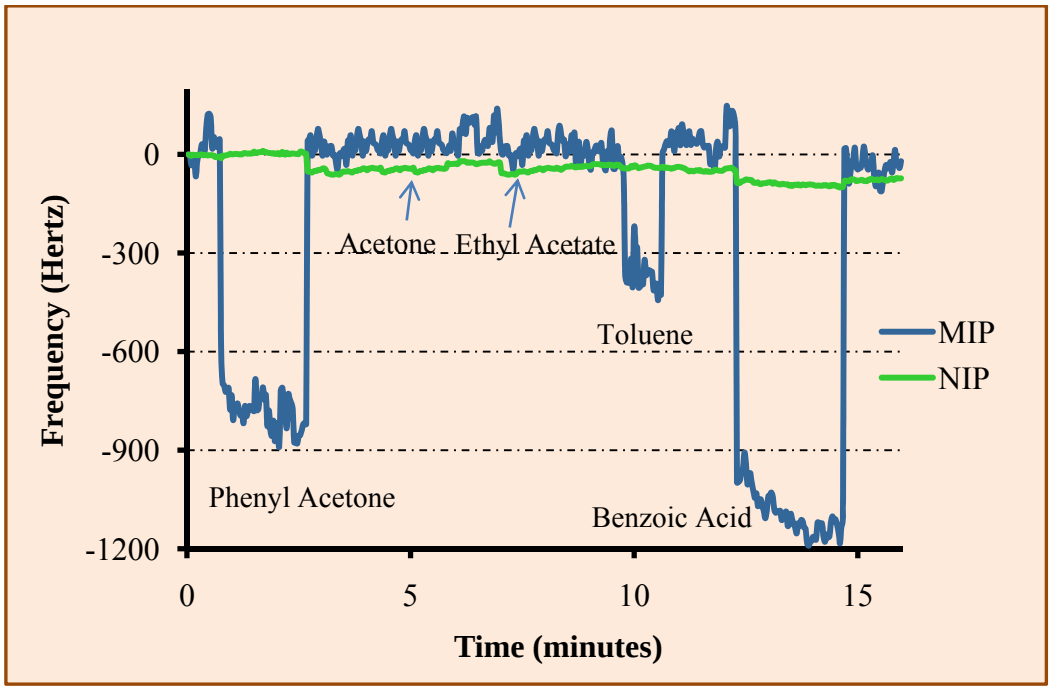

Figure 5.17 Selectivity pattern at 500 ppm in 30% ethanol for optimized MIP, 35 kHz MIP layer height achieved by MIP spin coating at 3000 rpm and template removal

Above Figure 5.17 demonstrates the selectivity pattern of phenyl acetone with its structural analogs. The optimized recognition system shows good selectivity for phenyl acetone at 500 ppm level in 30% ethanol media on comparing to that of acetone and ethyl acetate. While sensor response is two times for phenyl acetone as compared to that of toluene showing better fitness of phenyl acetone molecules into the cavities. On the other hand, comparatively ¾ times sensor response for benzoic acid may be attributed due to its more hydrophobic behavior.

5.3.6 Optimized Recognition System, Characterization in Aqueous Media

The optimized recognition system should be subjected to sensitivity and selectively measurements in aqueous media to investigate into the behavior of MIP on different layer height. The purpose of the studies is to look into the LoD, sensitivity and selectivity along with the noise levels for suitable layer height applications in the pharmaceutical industry. For this purpose, different layer heights were achieved by diluting the MIP with solvent composition (ethyl acetate: DMF: pyridine 1:1:1) and spin coating at higher rpm. The layer height 35, 23, and 12 kHz have been applied to investigate into the sensor characters and selectivity patterns.

35 kHz Layer Height

Figures 5.18 and 5.19 demonstrate the sensitivity of optimized MIP and sensor characteristics, respectively, at 35 kHz layer height in aqueous media. 35 kHz layer height was measured on network analyzer for MIP coated electrode after template removal.

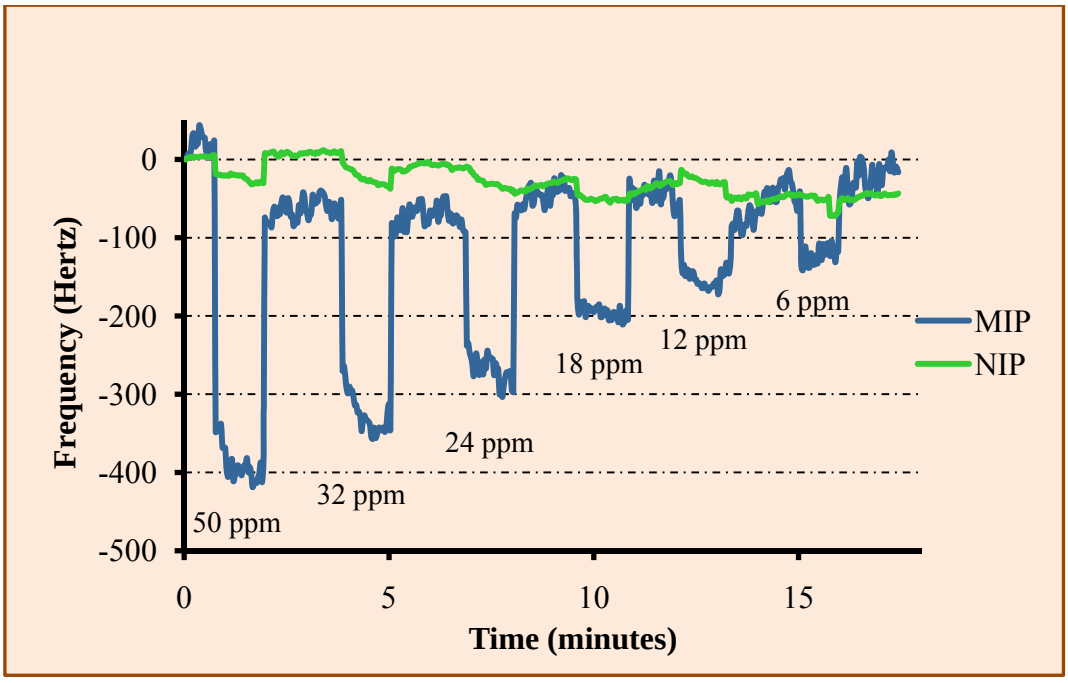

Figure 5.18 Sensor response in H_2O for optimized MIP, 35 kHz MIP layer height achieved by MIP spin coating at 3000 rpm and after template removal

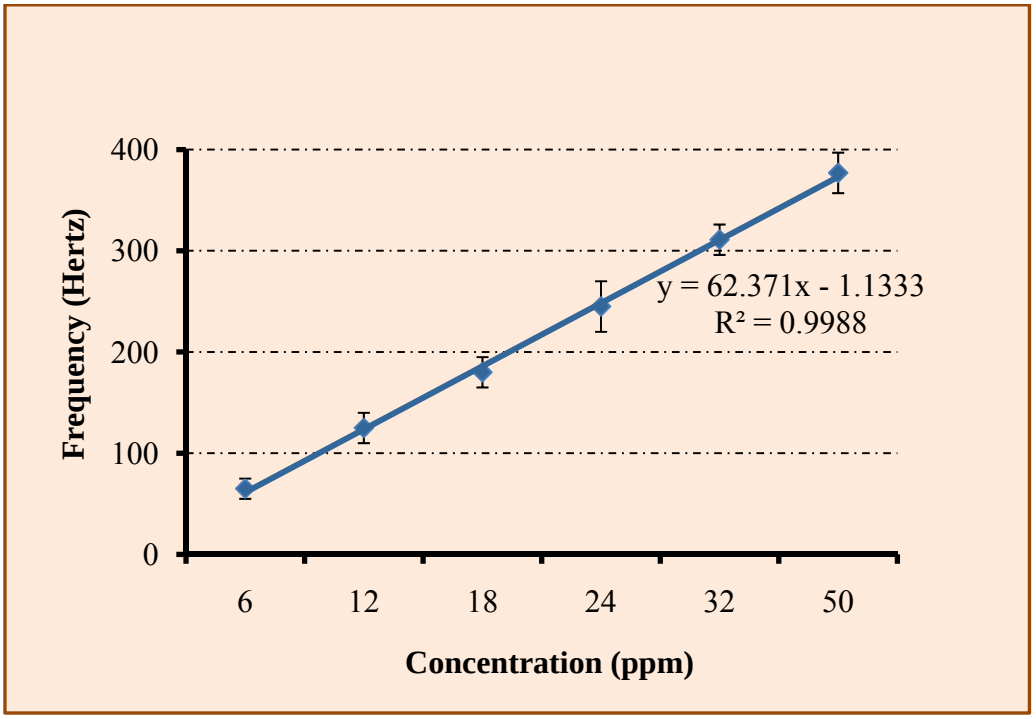

Figure 5.19 Sensor characteristics in H_2O for optimized MIP, 35 kHz MIP layer height achieved by MIP spin coating, drying and after template removal

The sensor response is linear leading to 6 ppm LoD at S/N ratio ≥ 3 in aqueous media. The measurements in aqueous media and in 30% ethanol gave LoDs, showing Sauerbrey effect, can be attributed due to phenyl acetone solubility differences both media at room temperature. The larger base line noise in the sensor characteristics may have a link towards the diffusion phenomena on the higher MIP thin film.

Figure 5.20 demonstrates outclass selectivity for phenyl acetone on comparing with that of structurally related compounds like acetone, ethyl acetate and toluene in aqueous media at 60 ppm. The astonishing selectivity of MIP can be attributed to the greater extant of phenyl imprinting in the optimized MIP. Although the benzoic acid gave net frequency changes of 200 Hz but still 3 times less as compared to that of phenyl acetone (600 hertz). While the effect of 200 Hz on the NIP electrode for benzoic acid indicate substantial non specific binding. The appreciable selectivity pattern is the

success story of phenyl acetone bulk imprinting. The higher noise level in the sensor response suggests investigating into the lower MIP heights for sensor characteristics and selectivity patterns.

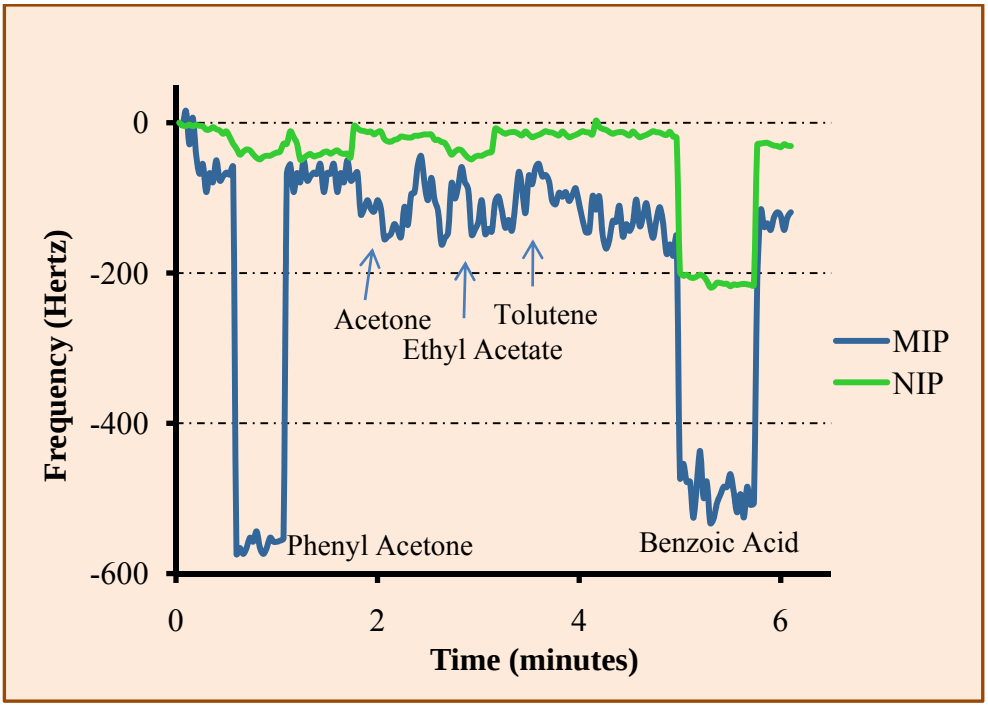

Figure 5.20 Selectivity pattern at 60 ppm in H_2O for optimized MIP, 35 kHz MIP layer height achieved by MIP spin coating and template removal

23 kHz Layer Height

Figures 5.21 and 5.22 demonstrate the sensor sensitivity and characteristics respectively on 23 kHz layer height in aqueous media. Although the LoD remained the same on 23 kHz layer height (i.e. 6 ppm LoD at S/N ratio ≥ 3), yet the sensitivity has been improved by a factor of two on comparing to that of 35 kHz layer height at 50 ppm (discussed earlier). The sensitivity differences can be attributed to the different diffusion behavior of MIPs layer heights in both cases. Furthermore improvement in S/N can be assigned to the compactness behavior for better diffusion pathways for MIP having 23 kHz as compared to that of 35 kHz. These improvements further

suggest investigating into selectivity pattern at 23 kHz for next mass sensitive measurement.

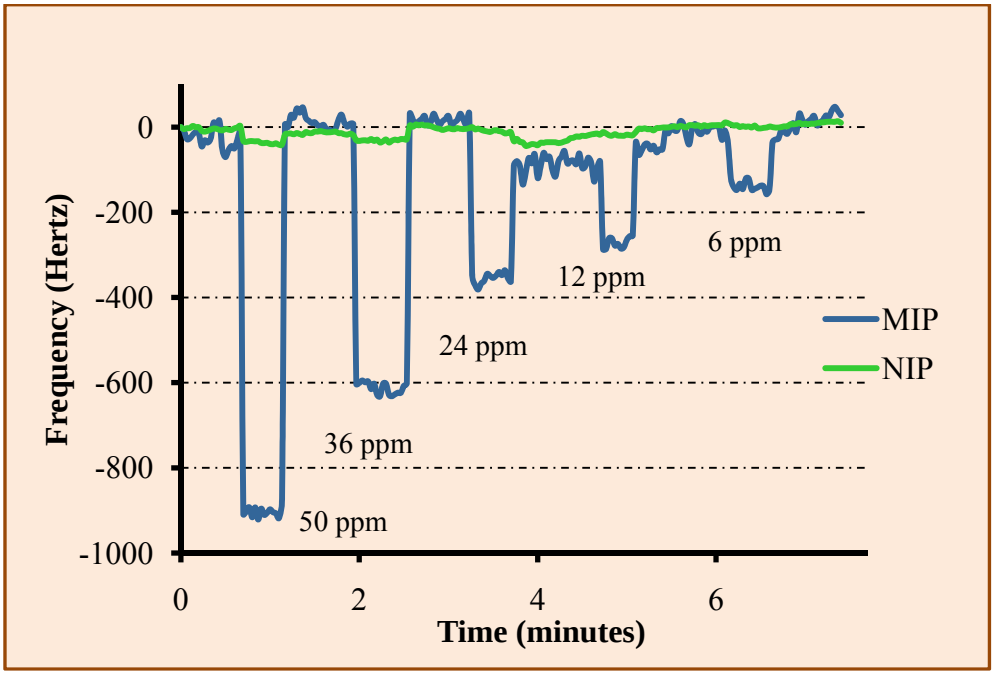

Figure 5.21 *Sensor response in H_2O for optimized MIP, 500 µL MIP was further diluted with 100 µL solvent (i.e. DMF: pyridine: ethyl acetate 1:1:1), 23 kHz MIP layer height achieved by (diluted) MIP spin coating at 4500 rpm and template removal*

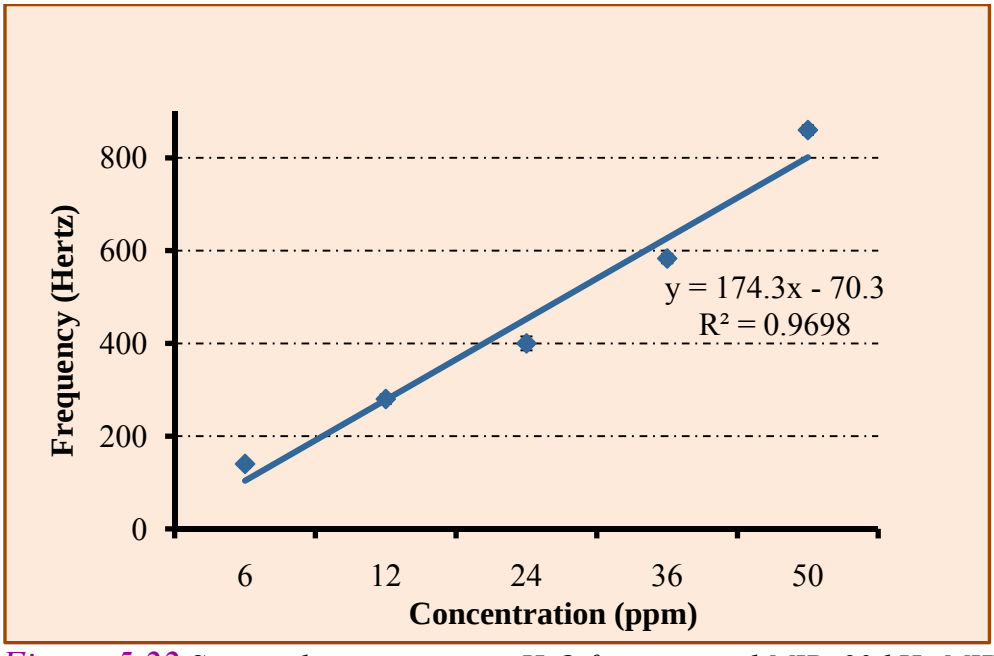

Figure 5.22 *Sensor characteristics in H_2O for optimized MIP, 23 kHz MIP layer height achieved after spin coating and template removal*

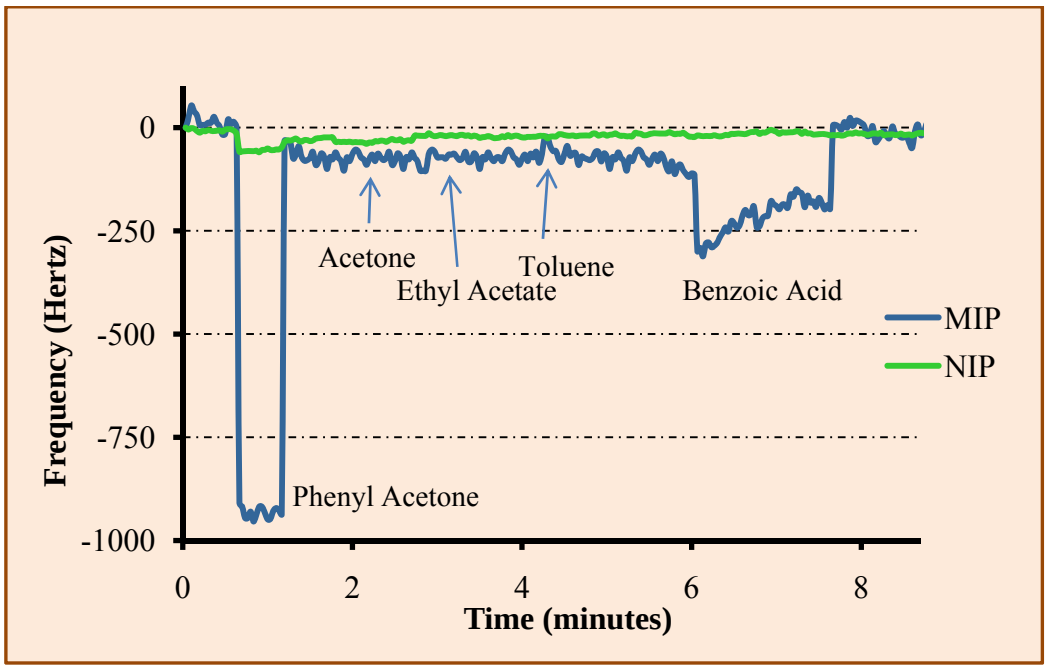

Figure 5.23 Selectivity pattern at 60 ppm in H_2O for optimized MIP 23 kHz MIP layer height achieved by MIP spin coating and after template removal

Figure 5.23 demonstrates the selectivity pattern for optimized MIP on layer height of 23 kHz in aqueous media. 23 kHz layer height was measured on network analyzer for MIP coated electrode after spin coating, MIP drying and template washing steps. The pattern follows the same outstanding selectivity as was achieved with layer height 35 kHz on comparing phenyl acetone with acetone, ethyl acetate and toluene in aqueous media at 60 ppm. The sensor responses of these structural analogs lead to zero response, underpinning the high selectivity of the system for phenyl acetone. The sensor response of phenyl acetone has been improved by a factor of two as compared to that of benzoic acid on 23 kHz layer height. While the benzoic acid response decreased kinetically from 300 Hz to 200 Hz demonstrating slightly different behavior as compared to that of 35 kHz layer height. The improved response has led to the difference of five times selectivity for phenyl acetone as compared to that of benzoic acid (the difference was 3 times on 35 kHz discussed earlier). The kinetically decreased sensor response of benzoic acid suggests improper or loose fitness of benzoic acid molecules in the cavities

giving the appreciable picture of bulk imprinting. Further mass sensitive measurements focusing lower layer height can be interesting regarding S/N ratio and selectivity pattern.

12 kHz Layer Height

Figure 5.24 demonstrates the selectivity pattern for phenyl acetone with structurally related compounds for optimized MIP at 12 kHz layer height. 12 kHz layer height was noted by using network analyzer for MIP coated electrode after MIP drying, hardening and template washing. The curve follows the same remarkable selectivity pattern as was achieved in the case of 23 kHz layer height in aqueous media at 60 ppm (discussed immediately above). The MIP sensitivity has been slightly decreased as compared to that of at 23 kHz, can be attributed due to decreased in longer diffusion path pathways as a function of decrease in the layer height.

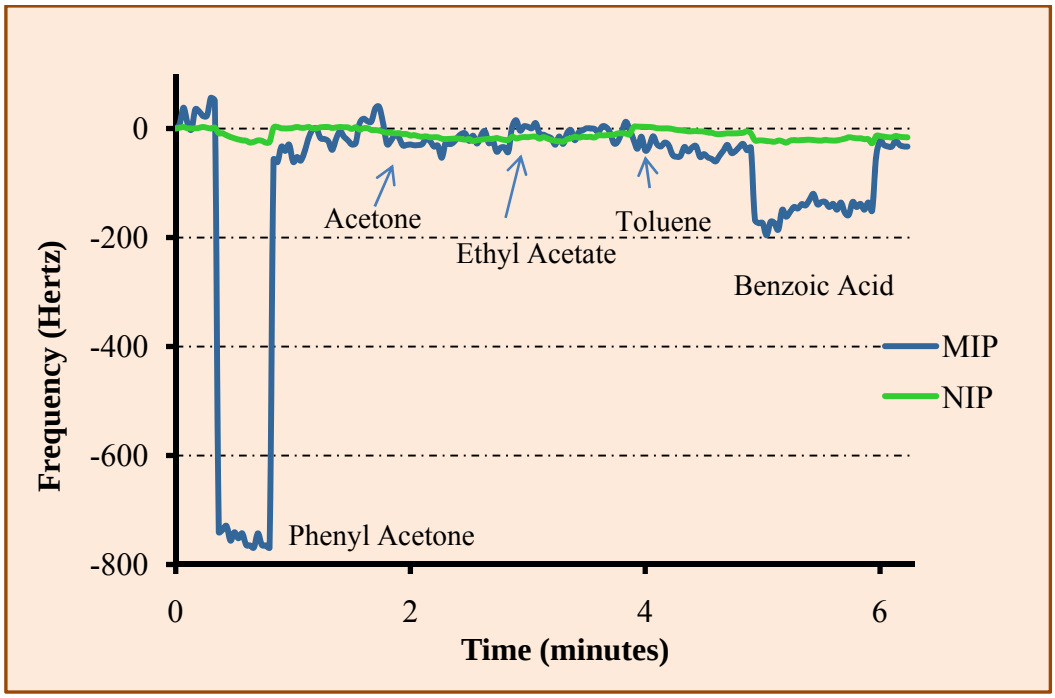

Figure 5.24 Selectivity pattern at 60 ppm in H_2O for optimized MIP, 500 µL MIP was further diluted with 500 µL solvent (i.e. DMF: pyridine: ethyl acetate 1:1:1), 12 kHz MIP layer height achieved by (diluted) MIP spin coating at 4500 rpm, MIP drying and after template removal

Layer Height Effect on Sensitivity

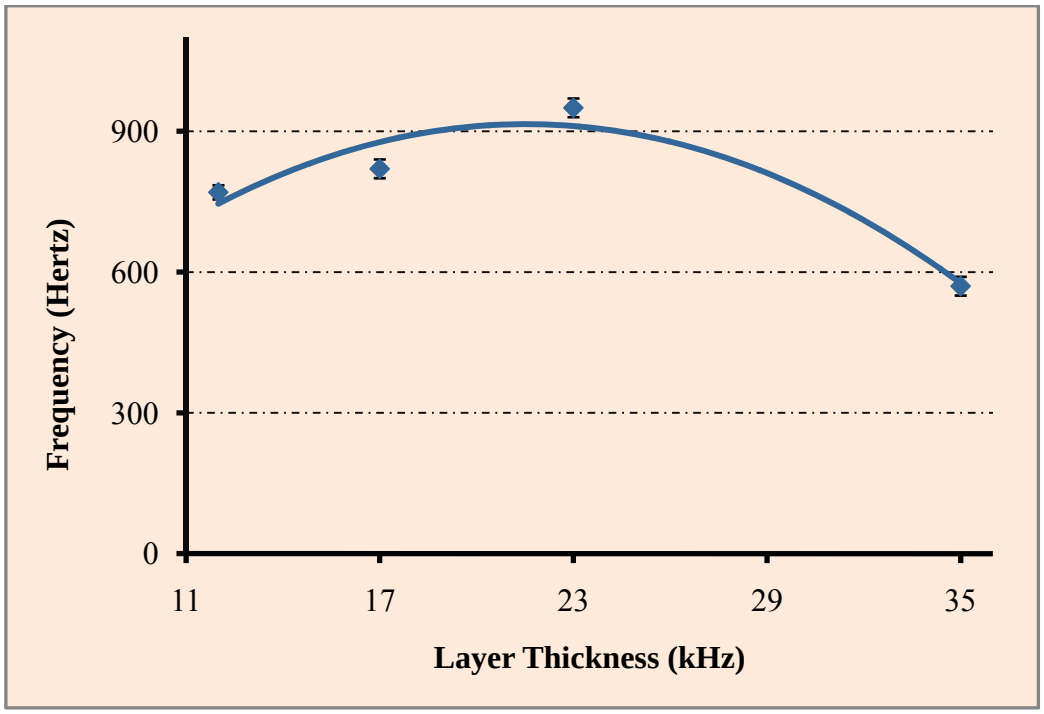

Figure 5.25 Layer height effect on sensitivity at 60 ppm phenyl acetone in aqueous media

Figure 5.25 summarizes the layer height effect on phenyl acetone sensitivity for optimized MIP at 60 ppm in aqueous media. Sensor response increases linearly as a function of increase in layer height from 12 kHz to 23 kHz due to increase in longer diffusion pathways for phenyl acetone. The sensor response measured in aqueous media at 60 ppm is peaks at 23 kHz MIP layer height as compared to that of other height. While astonishingly decrease in sensor response from layer height 23 kHz to 35 might be due to decrease in accessible diffusion pathways to cause the affective frequency shifts on electrode.

Layer Height Effect on Sensor Characteristics and Linearity

The figure 5.26 describes sensor characteristics and linearity on different layer height measured in aqueous media. Layer heights of 12, 23 and 35 kHz generated from optimized MIP have been subjected to phenyl acetone standards.

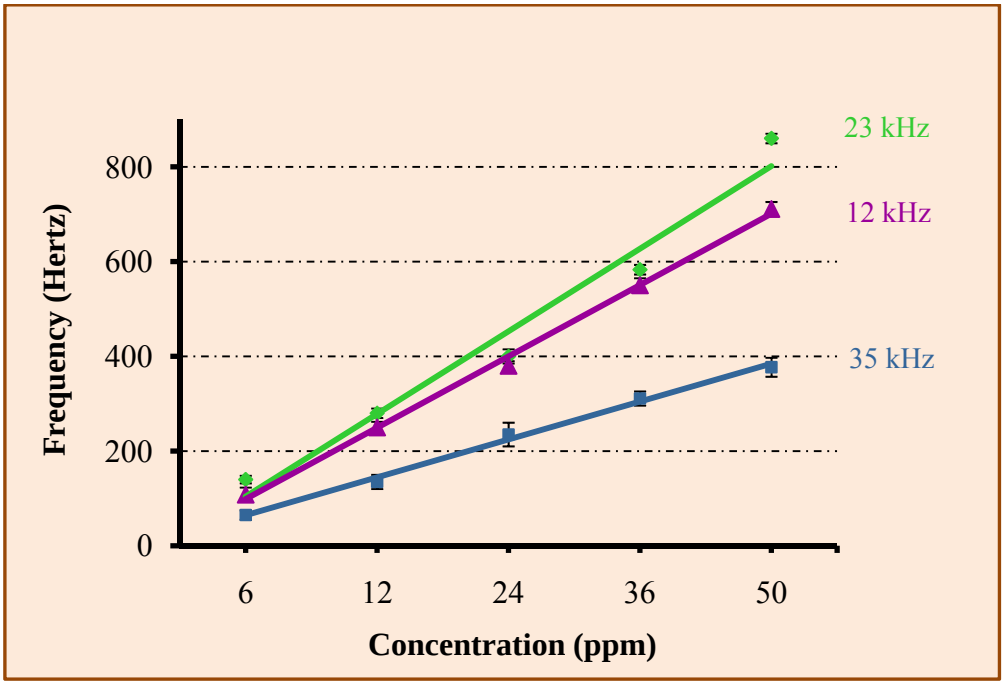

Figure 5.26 Sensor characteristics for different layer thickness for optimized MIP in aqueous media, 35 kHz layer height achieved by spin coating of MIP at 3000 rpm, 23 kHz layer height achieved by MIP diluted with 100 µL of ethyl acetate: DMF: pyridine (167:167:167 µL) and after spin coating at 4500 rpm, 12 kHz MIP layer height achieved by (2x diluted) MIP spin coating at 4500 rpm

The response is monotonous and not exactly linear on every layer showing sensitivity with 6 ppm LoD at S/N ratio ≥ 3. The differences in sensor responses at lower concentrations are not significant as compared to that of at higher concentrations. The difference in sensor response peaks at 60 ppm that is two times on comparing 35 kHz to that of 12 or 23 kHz layer heights. Furthermore the noise is greater on 35 layer height as compared to that of 12 and 23 kHz layer heights.

Layer Height Effect on Selectivity

Figure 5.27 summarizes the selectivity pattern for imprinted phenyl acetone with structurally related compounds on different layer heights measured in aqueous media at 60 ppm.

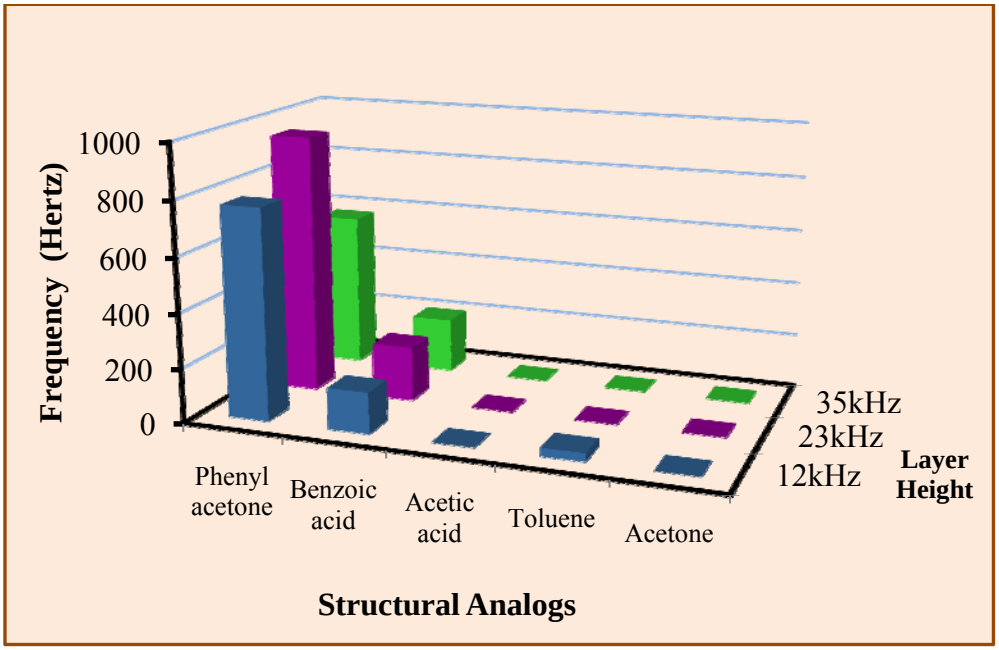

Figure 5.27 Selectivity pattern (60 ppm in H_2O) on different layer heights, phenyl acetone imprinting in styrene: acrylic acid: EGDMA

The pattern follows outstanding selectivity on every layer height on comparing phenyl acetone with acetone, ethyl acetate and toluene. Phenyl acetone response is five times as compared to its closest counterpart benzoic acid on 12 and 23 kHz layer height while 3 times on 35 kHz. The sensor response of benzoic acid is independent of layer height because the benzoic acid molecule is combination of aromatic and more hydrophilic parts comparatively different from phenyl acetone. Acetone and acetic acid have the lowest cross sensitivity in general that can be traced back to their molecular structures. Both molecules do not possess aromatic ring to be penetrated into the cavities designed for phenyl acetone. While toluene also follows the same cross sensitivity on higher layer heights i.e. at 23 and 35 kHz except appearance of slight response at 12 kHz. This can be ascribed to the chemical structure of toluene that lacks of hydrophilic moiety giving it low hydrophilic or non hydrophilic characteristics comparatively.

5.3.7 Air Contamination Effect

The air contamination effect on the sensor response can be helpful to validate optimized recognition system for applications of real life samples. Phenyl acetone sampling can be done by filtering after specific intervals through sieve with continuous air flushing (so that the samples could be contaminated). The sensor applications to artificially contaminated samples could further be interesting for understanding the sensor applications/characteristics to the real pharmaceutical samples. Figures 5.28, 5.29 and 5.30 explain the optimized recognition system applications to the artificially contaminated phenyl acetone samples. The study was done to investigate into air contaminated samples (by filtering after specific intervals through sieve with continuous air flushing).

Sample 1

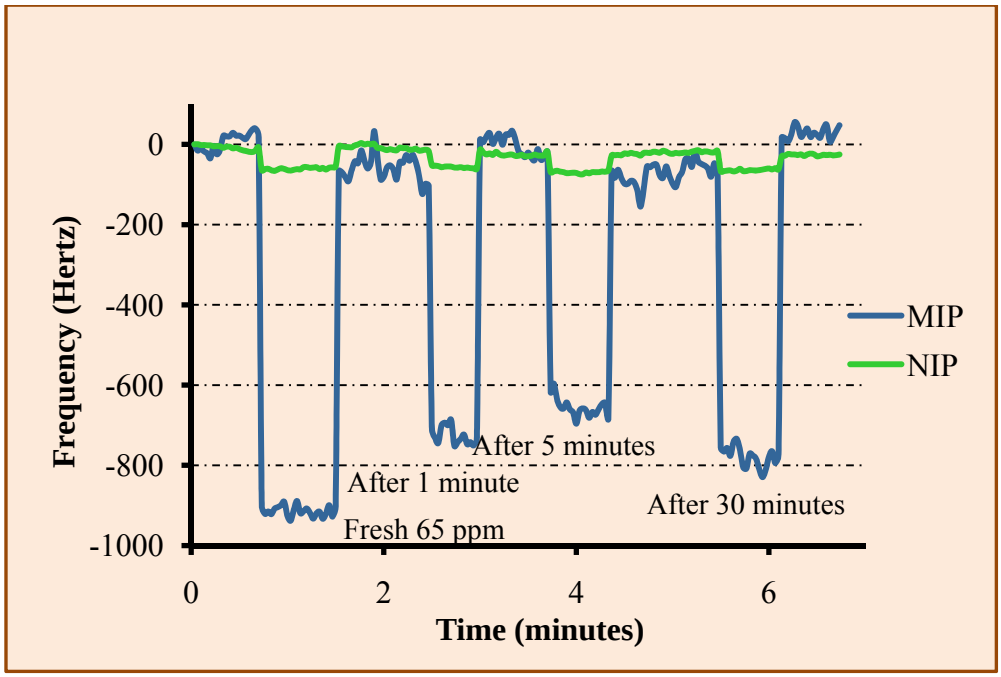

Figure 5.28 Air contamination effect on 65 ppm phenyl acetone (filtering after specific intervals through sieve with continuous air flushing), 19 kHz layer height achieved by MIP diluted with 200 µL of ethyl acetate: DMF: pyridine (167:167:167 µL) and spin coating at 4500 rpm and after template washing

Sample 2

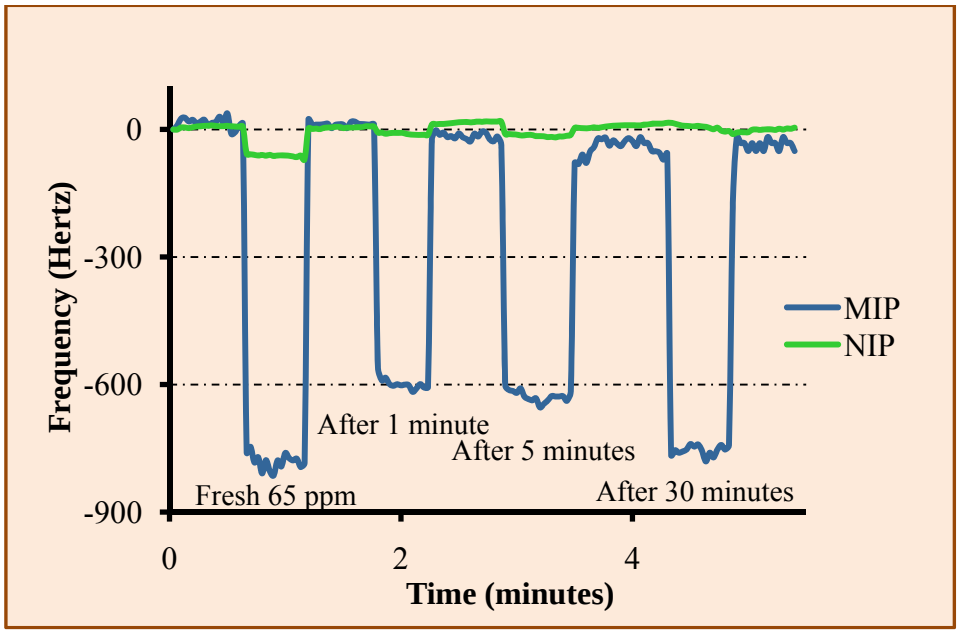

Figure 5.29 Air contamination effect on 65 ppm phenyl acetone (filtering after specific intervals through sieve with continuous air flushing), 17 kHz layer height achieved by MIP spin coating and after template washing

Sample 3

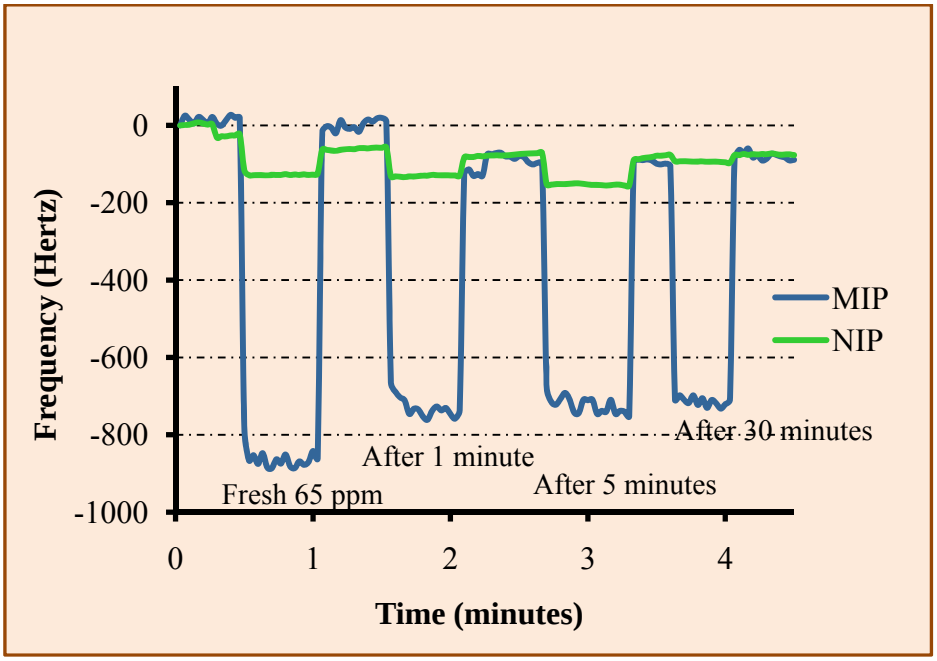

Figure 5.30 Air contamination effect on 65 ppm phenyl acetone (filtering after specific intervals through sieve with continuous air flushing), 19 kHz layer height achieved by MIP spin coating and after template washing

Although the dust was visible on the filter, yet the sensor response only changed by 25% in extreme cases while the analyte was only present in 65 ppm. The reason could be contributed by the factor of clogging of the MIP surface ultimately leading to decreased sensor signal. Furthermore a drift in baseline supports the factor of clogging of the MIP surface by dust particles. The clogging of MIP surface can be washed away by means of suitable cleaning solutions (e.g. HF) for dust and can be applied to real samples. Phenyl acetone molecules might have attached to the dust particles ultimately leading to decreased affective concentration in the media. The dust particles in the solution can further be removed by filtering through a clean filter.

5.3.8 NPs Approach

NPs can be generated from MIP to enhance the surface area for sensitivity improvements. NPs strategy is widely used for simple MIPs systems but currently no well defined information is found regarding NPs generation from emulsion MIP. The purpose of the NPs is to investigate either emulsion MIP or NPs (generated from emulsion MIP) can be preferred option for phenyl acetone sensing.

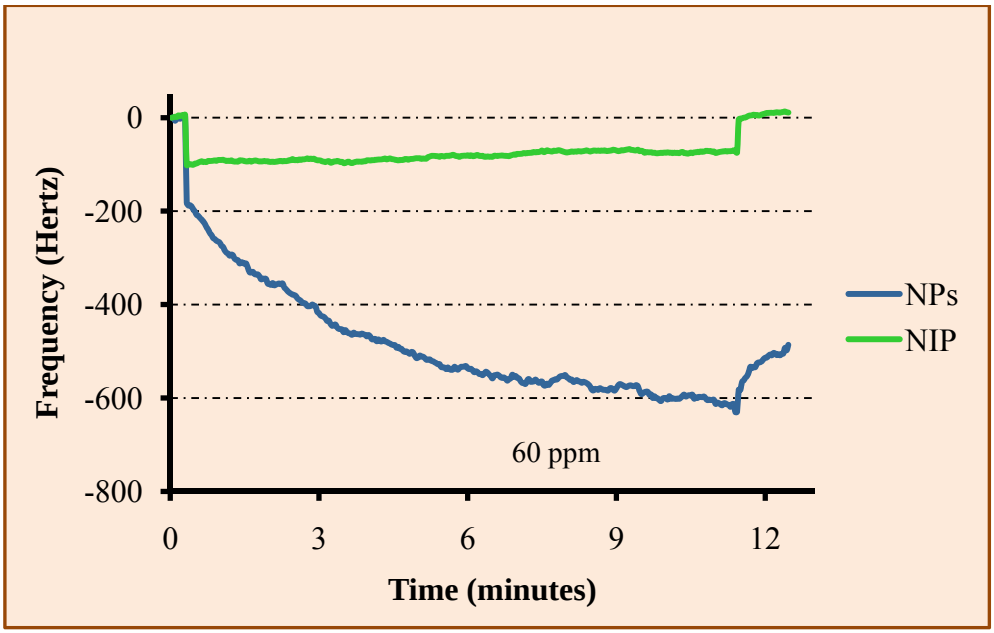

Figure 5.31 NPs generated from MIP in 25% acetonitrile, sensitivity at 60 ppm in aqueous media, 14 kHz layer height achieved after spin coating

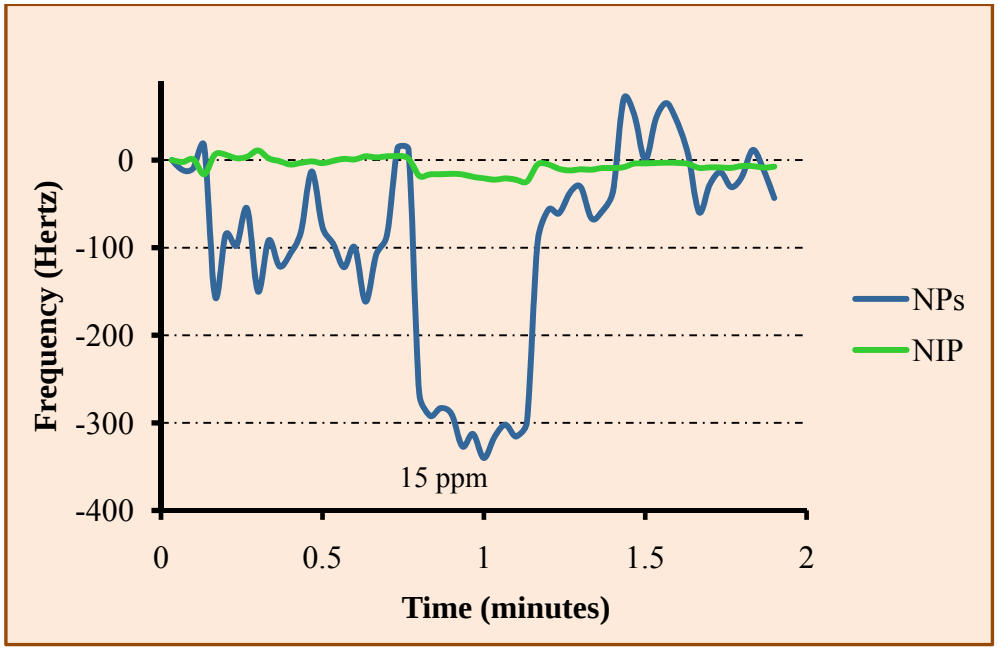

Figure 5.32 NPs generated from MIP in 50% acetonitrile, sensitivity at 15 ppm in aqueous media, 13 kHz layer height achieved after spin coating

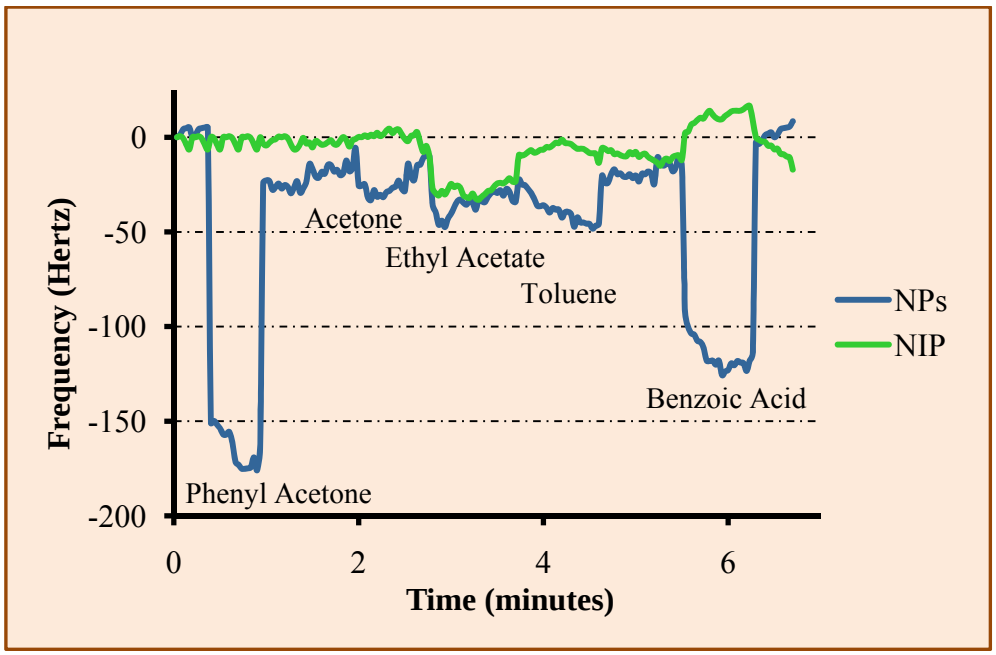

Figure 5.33 NPs generated from MIP final in 75% acetonitrile, selectivity at 60 ppm in aqueous media. 12 kHz layer height achieved after spin coating

To investigate into the NPs approach, NPs were generated from MIP in different acetonitrile concentrations (i.e. 25%, 50% and 75% acetonitrile in

H_2O). For NPs generated in 25% acetonitrile shown above in figure 5.31, 14 kHz layer height gave 600 Hz sensor response at 60 ppm in aqueous media apparently slight less than that of MIP. The sensor response is not as reversible and robust as compared to that of MIP. On the other hand, although NPs generated in 50% acetonitrile gave reversible sensor response, yet the base line noise is dominant. (See above Figure 5.32) While NPs generated in 75% acetonitrile (as sensor response shown above in figure 5.33) gave reversible and robust response but the results are not comparable with MIP in the terms of sensitivity and selectivity. Over all, emulsion MIP keeps inherent advantages over tedious and time consuming NPs approach in the terms of sensor reversibility, robustness, sensitivity and selectivity. The possible reasons can be contributed from generation of particles at micro and nano levels during polymerization. The presence of three solvents (i.e. ethyl acetate, DMF and pyridine) used in emulsion MIP restrict the NPs morphology by compromising sensor efficiency. The simple and straightforward emulsion MIP synthesis is advantageous over tedious and time consuming NPs approach for phenyl acetone sensor applications.

5.4 Summary

Phenyl acetone imprinting remained successful on poly styrene-acrylate emulsion polymerized in ethyl acetate, DMF and pyridine (1:1:1) cross linked by EGDMA. For optimized recognition system, sensor response peaked at 23 kHz layer height (900 Hz at 60 ppm). The sensor response is linear on different layer height (i.e. 12 kHz to 35 kHz) demonstrating appreciable sensitivity with 6 ppm LoD at S/N ratio ≥ 3. The cross sensitivity measurements follow remarkable selectivity on different layer heights on comparing sensitivity of phenyl acetone to that of structural analogs i.e. acetone, ethyl acetate and toluene. Phenyl acetone response is five times as compared to its closest counterpart benzoic acid. Acetone and acetic acid have

the lowest cross sensitivity in general that can be traced back to their molecular structures. Both molecules do not possess aromatic ring to be penetrated into the cavities designed for phenyl acetone. While toluene also follows the same cross sensitivity as was observed in the cases of acetone and acetic acid. This can be ascribed to the chemical structure of toluene that lacks of hydrophilic moiety giving it low hydrophilic or non hydrophilic characteristics comparatively.

Abstract (English)

Within the present thesis, novel molecularly imprinted thin films and nanoparticles have been developed for sensing biologically active compounds by the means of mass-sensitive detection. The first task has been determination of folic acid and its metabolites, the second to design a phenyl acetone sensor. Folic acid (to the best of our knowledge the largest molecule for bulk imprinting till now) bulk imprinting remained successful in poly methacrylate demonstrating 60 ppm limit of detection (LoD) on quartz crystal microbalances (QCM) at S/N ratio ≥ 3 with broad band selectivity on comparing with that of its metabolites. In further improvement MIP NPs gave 5 ppm LoD at S/N ratio ≥ 3 and 6 times enhanced sensitivity as compared to that of MIP at 500 ppm due to better accessibility. Demonstrating remarkably improved selectivity in NPs, sensor responses of counterparts remained within base line level without showing affinity to the sensor at 100 ppm. Further optimization were achieved on poly vinyl pyrrolidone MIP demonstrating 7 times enhanced sensitivity at 500 ppm and 2 times improved LoD as compared to that of poly methacrylate MIP. Poly vinyl pyrrolidone MIP NPs gave 0.7 ppm LoD at S/N ratio ≥ 3. In NPs selectivity measurements, metabolites did not show sensor responses at the 100 ppm demonstrating the outcome of NPs approach. Similar effects could be obtained with the two metabolites leucovorin and anhydroleucovorin as templates. The MIP demonstrated remarkable selectivity for anhydroleucovorin at 100 ppm, which was the only compound to yield a QCM signal.

Phenyl acetone imprinting, giving 6 ppm LoD at S/N ratio ≥ 3 in aqueous media, was successful on poly styrene-acrylate emulsion polymerized in a mixture of ethyl acetate, DMF and pyridine. The MIP follows remarkable selectivity pattern on comparing phenyl acetone with structural analogs i.e. acetone, ethyl acetate and toluene at 60 ppm in aqueous

media. Phenyl acetone sensor response is five times as compared that of its closest counterpart benzoic acid. Solvent mixtures yield patterned MIP surfaces and this increase sensitivity.

Zusammenfassung (Deutsch)

Im Rahmen der vorgelegten Arbeit wurden neuartige molekular geprägte Dünnfilme und Nanopartikel für die Detektion biologisch Aktiver Verbindungen mittels massensensitiver Sensoren entwickelt. Der erste Aufgabenbereich umfaßte dabei die Sensorik von Folsäure und einiger ihrer Metabolite, der zweite die Entwicklung eines Meßfühlers für Phenylaceton. Es ist möglich, molekular geprägte Polymere für die Wiedereinlagerung von Folsäure in ihrem gesamten Volumen herzustellen. Nach bestem Wissen ist dieses Molekül das zur Zeit größte, mit dem ein derartiger Ansatz gelungen ist. Die entsprechenden, auf der Quarzmikrowaage (quartz crystal microbalance – QCM) beruhenden Sensoren erreichen ein Detektionslimit von 60 ppm Folsäure bei einem Signal-/Rauschabstand von 3 und breitbandiger Selektivität gegenüber Metaboliten. Dies läßt sich durch die Verwendung molekular geprägter Nanopartikel um einen Faktor von 6 verbessern. Grund dafür ist die wesentlich vergrößerte Oberfläche und damit Erreichbarkeit der Bindungsstellen im Material. Ebenso erhöht sich dadurch die Selektivität, 100 ppm der Metaboliten Leukovorin und Anhydro-leukovorin führen beispielsweise zu keinen meßbaren Änderungen des Sensorsignals. Ersetzt man das verwendete Polymethacrylat durch ein Copolymer mit Vinylpyrrolidon (VP), verbessern sich Sensitivität und Detektionslimit um Faktoren von sieben bzw. zwei. Die entsprechenden PVP-nanopartikel erreichen auf QCM Detektionslimits von 0,7 ppm bei einem Signal-Rauschabstand von 3. Ebenso zeigten die Partikel keine Signale für die Metaboliten. Ähnliche Effekte konnten für Leukovorin und Anhydroleukovorin erzielt werden. Teilweise erreichen die Systeme erstaunliche Selektivität: ein Anhydroleukovorin-geprägtes Polymer zeigte beispielsweise keinerlei Reaktion auf 100 ppm Folsäure bzw. Leukovorin.

Molekulares Prägen mit Phenylaceton ermöglicht Detektionslimits von 6 ppm bei einem Signal-/Rauschabstand von drei auf der Basis von emulsionspolymerisierten Styren-/Acrylatsystemen in einer Mischung aus Ethylazetat, Dimethylformamid und Pyridin. Die entstehenden MIP sind erstaunlich selektiv: Strukturanaloga, wie beispielsweise Azeton, Ethylazetat und Toluen ergeben bei 60 ppm Konzentration in Wasser keinerlei Sensoreffekte. Der gewünschte Analyt (Phenylaceton) wird immer noch fünfmal stärker eingelagert, als die nächststärker meßbare Verbindung, nämlich Benzoesäure. Die Verwendung von Lösungsmittelgemischen resultiert in strukturierten Oberflächen der Filme und erhöht damit die Sensitivität.

Abbreviations

AFM	**Atomic Force Microscope**
AIBN	Azobisisobutyronitrile
BAW	Bulk Acoustic Wave devices
DMF	Dimethylformamide
DMSO	Dimethyl sulfoxide
DVB	Divinylbenzene
EGDMA	Ethylene glycol dimethylacrylate
FET	Field Effect Transistor
GCMS	Gas Chromatography Mass Spectrometry
HPLC	High Performance Liquid Chromatography
LOD	Limit of Detection
MIP	Molecularly Imprinted Polymer
MIPs	Molecularly Imprinted Polymers
NIP	Non Imprinted Polymer
NPs	Nano Particles
QCM	Quartz Crystal Microbalance
QCMs	Quartz Crystal Microbalances
QMB	Quartz Microbalance
SAW	Surface Acoustic Wave devices
THF	Tetrahydrofuran
UV	Ultra-Violet

References

[1] R. Kellner, J. M. Mermet, M. Otto, H. M. Widmer, *Anal. Chem.* **1998,** 359-373

[2] A. Hulanicki, S. Glab, F. Ingman, *Chemical Sensors Definitions and Classifications, Pure Appl. Chem.* **1991**, 63, 1247–1250

[3] R. Schirhagl, P. A. Lieberzeit, F. L. Dickert, *Adv.Mater.* **2010**, 22, 18, 2078-2081

[4] R. Schirhagl, A. Seifner, F. T. Husain, M. Cichna-Markl, P. A. Lieberzeit, F. L. Dickert, *Sensor Lett.* **2010**, 8, 399-404

[5] P. A. Lieberzeit, A. Afzal, D. Podlipna, S. Krassnig, H. Blumenstock, F. L. Dickert, *Sens. Actuators B*. **2007**, 126, 153–158

[6] F. L. Dickert, P. A. Lieberzeit, *Enc. Anal. Chem.* **2000**, P. 3831-3855

[7] P. A. Lieberzeit, S. G. Miarecka, K. Halikias, C. Schirk, J. Kauling, F. L. Dickert, *Sens. Actuators B*. **2005**,111–112

[8] F. L. Dickert, P. A. Lieberzeit, O. Hayden, *Anal. Bioanal. Chem.* **2003**, 377

[9] B. Pejcic, P. A. Lieberzeit, F. L. Dickert, *Anal. Bioanal. Chem.* **2007**, 387, 237–247

[10] F. L. Dickert, P. A. Lieberzeit, M. Tortschanoff, *Sens. Actuators B*. **2000**, 65 (1-3), 186-189

[11] P. A. Lieberzeit , A. Afzal, A. Rehman, F. L. Dickert, *Sens. Actuators B*. **2007**, 127

[12] F. L. Dickert, O. Hayden, P. A. Lieberzeit, C. Palfinger, D. Pickert, U. Wolff, G. Scholl, *Sens. Actuators B*. **2003**, 95, 20

[13] P. A. Lieberzeit, A. Rehman, S. Yaqub, F. l. Dickert, *NANO.* **2008,** 3, 4, 205–208

[14] M. Yang, M. Thompson, *Anal. Chem*. **1993**, 65, 1158–1168

[15] J. C. Love, L. A. Estroff, J. K. Kriebel, R. G. Nuzzo, G. M. Whitesides, *Chem. Rev*. **2005**, 105, 1103–1169

[16] S. Zhang, C. C. Cardona, L. Echegoyen, *Chem. Comm.* **2006**, 4461–4473

[17] T. P. Delaney, V. M. Mirsky, M. Ulbricht, O. S. Wolfbeis, *Anal. Chim. Acta,* **2001**, 435, 157–162

[18] C. Alexander, H. S. Andersson, L. I. Andersson, R. J. Ansell, N. Kirsch, I. A. Nicholls, J. O'Mahony, M. J. Whitcombe, *J. Molec. Recogn.* **2006**, 19, 106–180

[19] N. Pe´rez-Moral, A. G. Mayes, *Langmuir.* **2004**, 20, 3775–3779

[20] S. Q. Liu, J. H. Yu, H. X. Ju, *Electroanal. Chem.* **2003**, 540, 61–77

[21] K. Haupt, *Nat. Biotechnol*. **2002,** 20, 881–885

[22] B. Sellergren, *Trends Anal. Chem.* **1999**, 18, 164–174

[23] C. Lubke, M. Lubke, M. J. Whitcombe, E. N. Vulfson, *Macromol.* **2000**, 33, 5098–5105

[24] A. J. Hall, P. Manesiotis, M. Emgenbroich, M. Quaglia, E. De Lorenzi, B. Sellergren, *J. Org. Chem.* **2005**, 70, 1732–1736

[25] M. Kempe, K. Mosbach, *Tetrahedron Lett*. **1995**, 36, 3563–3566

[26] B. R. Hart, K. J. Shea, *J. Am. Chem. Soc*. **2001**, 123, 2072–2073

[27] F. Lanza, A. J. Hall, B. Sellergren, A. Bereczki, G. S. Horvai, P. A. G. Cormack, D. C. Sherrington, *Anal. Chim. Acta.* **2001**, 435, 91–106

[28] W. T. Nicholas, I. H. Clovia, W. D. Scott, A. McCluskeya, C. B. Michael, *New J. Chem.* **2010,** 34, 686–692

[29] T. Kobayashi, T. Fukaya, M. Abe, N. Fujii, *Langmuir.* **2002,** 18, 2866–2872

[30] C. H. Lim, C. D. Ki, T. H. Kim, Y. J. Chang, Macromol. **2004,** 37, 6–8

[31] H. Shi, T. Wei-Bor, D. Michael, G. S. Ferrari, B. D. Ratner, *Nature.* **1999,** 398, 593–597

[32] E. Yilmaz, K. Haupt, K. Mosbach, *Angew Chem. Int.* **2000,** 39, 2115–2118

[33] M. M. Titirici, B. Sellergren, *Anal. Bioanal. Chem.* **2004,** 378, 1913–1921

[34]V. T. Remcho, Z. J. Tan, *Anal. Chem.* **1999,** 71, A248–A255

[35] A. Molinelli, R. Weiss, B. Mizaikoff, *J. Agric. Food Chem.* **2002,** 50, 1804–1808

[36] S. N. Zhou, E. P. C. Lai, J. D. Miller, *Anal. Bioanal. Chem*. **2004,** 378, 1903–1906

[37] Q. Z. Zhu, P. Degelmann, R, Niessner, D. Knopp, *Envir. Sci. Technol*. **2002,** 36, 5411–5420

[38] Y. Yu, L. Ye,V. D. Biasi, K. Mosbach, *Biotechnol. Bioeng.* **2002,** 79, 23–28

[39] M. Emgenbroich, G. Wulff, *Chem. Eur. J.* **2003,** 9, 4106–4117

[40] C. Sulitzky, B. Ruckert, J. Andrew, A. J. Hall, F. Lanza, K. U. Kand, B. Sellergren, *Macromolecules.* **2002,** 35, 79–91

[41] L. Zhu, L. Chen, X. Xu, *Anal. Chem.* **2003,** 75, 6381–6387

[42] K. Mosbach, Y. Yu, J. Andersch, L. Ye, *J. Am. Chem. Soc.* **2001,** 123, 12420–12421

[43] R. Shoji, T, Takeuchi, I. Kubo, *Anal. Chem.* **2003,** 75, 4882–4886

[44] M. L. Mena, L. Agui, P. M. Ruiz, P. Y. Sedeno, A. J. Reviejo, J. M. Pingarron, *Anal. Bioanal. Chem*. **2003,** 376, 18–25

[45] S. A. Piletsky, E. V. Piletska, B. Chen, K. Karim, D. Weston, G. Barrett, P. Lowe, A. P. F. Turner, *Anal. Chem.* **2000,** 72, 4381–4385

[46] F. L. Dickert, O. Hayden, R. Bindeus, K. J. Mann, D. Blaas, E. Waigmann, *Anal. Bioanal. Chem.* **2004,** 378, 1929–1934

[47] M. K. P. Leung, B. K. W. Chiu, M. H. W. Lam, *Anal. Chim. Acta*. **2003,** 491, 15–25

[48] S. Gao, W. Wang, B. Wang, *Bioorg. Chem.* **2001,** 29, 308–320

[49] D. Lee, Y. K. Choi, M. J. Kim, *Org. Lett.* **2000,** 2, 2553–2555

[50] Z. Meng, T. Yamazaki, K. Sode, *Biotechnol. Lett.* **2003,** 25, 1075–1080

[51] H. K. Mitchell, E. E. Snell, R. J. Williams, *J. Am. Chem. Soc*. **1944,** 66, 267–268

[52] P. M. Finglas, A. J. A. Wright, C. A. Wolfe, D. J. Hart, D. M. Wright, J. R. Dainty, *Proc. Nutr. Soc.* **2003,** 62, 591–598

[53] D. Chippel, K. G. Scrimgeour, *Can. J. Biochem*. **1970,** 48 (9), 999–1009

[54] C. W. Suitor, L. B. Bailey, *J. Am. Diet. Assoc.* **2000,** 100 (1), 88–94

[55] L. B. Bailey, *Folate Requirements and Dietary Recommendations, in Folate in Health and Disease, Bailey, L. B. Ed. Marcel Dekker, New York.* **1995,** 123–151

[56] W. B. Freire, C. P. Howson, J. F. Cordero, *Nutr. Rev.* **2004,** 62 (6 Pt 2), S1–S2

[57] C. M. Pfeiffer, S. P. Candill, E. W. Gunter, J. Osterloh, E. J. Sampson, *Am. J. Clin. Nutr.* **2005,** 82 (2), 442–450

[58] J. G. Ray, M. J. Vermeulen, S. C. Boss, D. E. Cole, *Epidemiology.* **2002,** 13 (2), 238–240

[59] J. Arcot, J. Shrestha, *Trends Food Sci. Technol.* **2005,** 16, 253–66

[60] T. Tamura, *J. Nutr. Biochem.* **1998,** 9 (5), 285–293

[61] S. K. Tomar, N. Srivatsa, R. Iyer Singh, *Milchwissenschaft.* **2009,** 64(3), 260–3

[62]J. Koontz, K. Phillips, K. Wunderlich, J. Exler, J. Holden, S. Gebhardt, D. Haytowitz, *J. AOAC Int.* **2005,** 88 (3), 805–813

[63] G. Varela-Moreiras, E. Seyoum, J. Selhub, *J. Nutr. Biochem.* **1991,** 2 (1), 44–53

[64] E. P. Quinlivan, A. D. Hanson, J. F. Gregory, *Anal. Biochem.* **2006,** 348 (2), 163–184

[65] C. M. Pfeiffer, Z. Fazili, L. McCoy, M. Zhang, E. W. Gunter, *Clin. Chem.* **2004,** 50 (2), 423–432

[66] E. W. Gunter, B. A. Bowman, S. P. Caudill, D. B. Twite, M. J. Adams, E. J. Sampson, *Clin. Chem.* **1996,** 42 (10), 1689–1694

[67] H. Said, T. Nguyen, D. Dyer, K. Cowan, S. Rubin, *Biochim. Biophys. Acta.* **1996,** 1281, 164–172

[68] M. A. Caudill, A. C. Cruz, J. F. Gregory, A. D. Hutson, L. B. Bailey, *J. Nutr.* **1997,** 127 (12), 2363–2370

[69] J. T. Hjelle, E. I. Christensen, F. A. Carone, J. Selhub, *Am. J. Physiol. Cell Physiol.* **1991,** 260 (2), C338–C346

[70] J. R. Suh, E. W. Oppenheim, S. Girgis, P. J. Stover, *J. Biol. Chem.* **2000,** 275 (45), 35646–35655

[71] B. Shane, *Folate Chemistry and Metabolism, in Folate in Health and Disease, Bailey, L. B. Ed. Marcel Dekker, New York.* **1995,** pp. 1–22

[72] M. A. Caudill, J. F. Gregory, A. D. Hutson, L. B. Bailey, *J. Nutr.* **1998,** 128 (2), 204–208

[73] J. R. Suh, A. K. Herbig, P. J. Stover, *Annu. Rev. Nutr.* **2001,** 21 (1), 255–282

[74] P. J. Stover, *Nutr. Rev.* **2004,** 62 (6 Pt 2), S3–S13

[75] V. M. Whitehead, *Pharmacokinetics and Physiological Disposition of Folate and its Derivatives, in Folates and Pterins, Blakley, R. L. and Whitehead, V. M. Eds. John Wiley & Sons, New York,* **1986,** 177–205

[76] R. J. Cook, *Folate Metabolism, in Homocysteine in Health and Disease, Carmel, R. and Jacobsen, D. Eds. Cambridge University Press, Cambridge, UK.* **2001,** 113–134

[77] P, Stover V. Schirch, *TIBS.* **1993,** 18, 102–106

[78] G. P. Kauwell, B. L. Lippert, C. E. Wilsky, K. Herrlinger-Garcia, A. D. Hutson, D. W. Theriaque, G. C. Rampersaud, J. J. Cerda, L. B. Bailey, *J. Nutr.* **2000,** 130 (6), 1584–1590

[79] J. Selhub, P. F. Jacques, P. W. Wilson, D. Rush, I. H. Rosenberg, *JAMA.* **1993,** 270 (22), 2693–2698

[80] K. Rasmussen, J. Moller, *Methodologies of Testing, in Homocysteine in Health and Disease, Carmel, R. and Jacobson, D. Eds. Cambridge University Press, Cambridge, UK.* **2001,** 199–211

[81] D. C. McCabe, M. A. Caudill, *Nutr. Rev.* **2005,** 63 (6), 183–196

[82] J. Lindenbaum, R. Allen, *Clinical Spectrum and Diagnosis of Folate Deficiency, in Folate in Health and Disease, Bailey, L. B. Ed. Marcel Decker, New York, NY.* **1995,** 43–73

[83] S. E. Vollset, H. Refsum, L. M. Irgens, B. M. Emblem, A. Tverdal, H. K. Gjessing, A. L. Monsen, P. M. Ueland, *Am. J. Clin. Nutr.* **2000,** 71 (4), 962–968

[84] J. S. Lopez-Camelo, I. M. Orioli, M. D. Dutra, J. Nazer-Herrera, N. Rivera, M. E. Ojeda, A. Canessa, E. Wettig, A. M. Fontannaz, C. Mellado, E. E. Castilla, *Am. J. Med. Genet. A.* **2005,** 135 (2), 120–125

[85] S. Daly, A. Cotter, A. Molloy, J. Scott, *Semin. Vasc. Med.* **2005,** 5, 190–200

[86] S. P. Rothenberg, M. P. da Costa, J. M. Sequeira, J. Cracco, J. L. Roberts, J. Weedon, E. V. Quadros, *N. Engl. J. Med.* **2004,** 350 (2), 134–142

[87] G. M. Shaw, E. J. Lammer, H. Zhu, M. W. Baker, E. Neri, R. H. Finnell, *Am. J. Med. Genet.* **2002,** 108 (1), 1–6

[88]L. B. Bailey, R. J. Berry, *Am. J. Clin. Nutr.* **2005,** 81 (5), 1213S– 1217S

[89] L. D. Botto, J. Mulinare, J. D. Erickson, *Am. J. Med. Genet.* **2003,** 121A (2), 95–101

[90] B. V. Guelpen, *Scand. J. Clin. Lab. Invest*. **2007,** 67, 459

[91] C. M. Pfeiffer, S. P. Caudill, E. W. Gunter, J. Osterloh, E. J. Sampson, *Am. J. Clin. Nutr.* **2005,** 82 (2), 442–450

[92] G. J. Hankey, J. W. Eikelboom, K. Loh, M. Tang, J. Pizzi, J. Thom, Q. Yi, *Cerebrovasc. Dis.* **2005,** 19 (2), 110–116

[93] J. P. Casas, L. E. Bautista, L. Smeeth, P. Sharma, A. D. Hingorani, *Lancet.* **2005,** 365 (9455), 224–232

[94] E. Giovannucci, *J. Nutr.* **2002,** 132 (8 Suppl), 2350S–2355S

[95] Y. I. Kim, *Cancer Epidemiol. Biomarkers Prev.* **2004,** 13 (4), 511–519

[96] T. A. Sellers, L. H. Kushi, J. R. Cerhan, R. A. Vierkant, S. M. Gapstur, C. M. Vachon, J. E. Olson, T. M. Therneau, A. R. Folsom, *Epidemiology.* **2001,** 12 (4), 420–428

[97] H. S. Feigelson, C. R. Jonas, A. S. Robertson, M. L. McCullough, M. J. Thun, E. E. Calle, *Cancer Epidemiol. Biomarkers Prev.* **2003,** 12 (2), 161–164

[98] A. M. Treon, M. Shea-Budgell, B. Shukitt-Hale D. E. Smith J. Selhub I. H. Rosenberg. *PNAS.* **2008,** 105(34), 12474–9

[99] B. Levin, *Environmental Nutrition: Understanding the Link between Environment, Food Quality and Disease. In. Levin B, Editor. Hinge Pin Integrative Learning Materials. Vashon Island, Wash. Hinge Pin Press.* **1999,** p 220–2

[100] J. Durga, M. P. V. Boxtel, E. G. Schouten, *Lancet.* **2007,** 369 (9557), 208–16

[101] E. C. Mastsue, W. M. Matsui, *J. Allergy Clin.* **2009,** 123 (6), 1253-1259

[102] S. L. Morgan J. E. Baggott, W. H. Vaughn, J. S. Austin, T. A. Veitch, J. Y. Lee, W. J. Koopman, C. L. Krumdieck, G. S. Alarcón, *Ann. Intern. Med.***1994,** 121(11), 833-841

[103] I. M. Ebisch, C. M. Thomas, W. H. Peters, D. D. Braat, R. P. Steegers-Theunissen *Hum. Reprod. Update.* **2007,** 13 (2), 163–74

[104] W. G. Christen, R. J. Glynn, E. Y. Chew, C. M. Albert, J. E. Manson, *Arch. Intern. Med.* **2009,** 169 (4), 335–41

[105] A. J. Hall, L. Achilli, P. Manesiotis, M. Quaglia, E. D. Lorenzi, B. R. Sellergren, *J. Org. Chem.* **2003,** *68*, 9132-9135

[106] A. J. Hall, M. Quaglia, P. Manesiotis, E. D. Lorenzi, B. R. Sellergren, *Anal. Chem.* **2006,** 78, 8362-8367

[107] Z. Song, X. Zhou, *Spectrochim. Acta. Part A.* **2001,** 57, 2567–2574

[108] H. E. Indyk, *Int. Dairy J.* **2010**, 20, 106–112

[109] A. Lermoa, S. Fabianoc, S. Hernándezc, R. Galveb, M. P. Marcob, S. Alegret, M. I. Pividoria, *Biosen. Bioelectron.* **2009,** 24, 2057–2063

[110] P. Kalimuthu, S. A. John, *Biosen. Bioelectron.* **2009,** 24, 3575–3580

[111] A. A. Ensafi, H. K. Maleh, *J. Electroanal. Chem.* **2010,** 640, 75–83

[112] M. M. Ardakania, H. Beitollahi, M. A. S. Mohsenia, H. N. N. Taghavinia, *Appl.Cata. A.* **2010,** 378, 195–201

[113] B. B. Prasad, M. P. Tiwari, R. Madhuri, P. S. Sharma, *Anal. Chim. Acta.* **2010,** 662, 14–22

[114] B. B. Prasad, R. Madhuri, M. P. Tiwari, P. S. Sharma, *Sens. Actuators B*. **2010,** 146, 321–330

[115] B. B. Prasad, R. Madhuri, M. P. Tiwari, P. S. Sharma, *Biosen. Bioelectron.* **2010,** 25, 2140–2148

[116] A. Ellwanger, C. Berggren, S. Bayoudh, C. Crecenzi, L. Karlsson, P. K. Owens, K. Ensing, P. Cormack, D. Sherrington, B. Sellergren, *Analyst.* **2001,** 126, 784–792

[117] K. Yoshimatsu, K. Reimhult, A. Krozer, K. Mosbacha, K. Sode, L. Ye, *Anal. Chim. Acta.* **2007,** 584 112–121.

Curriculum Vitae

Munawar Hussain

Assistant professor, Department of Chemistry, Islamia University

Bahawalpur, Punjab, Pakistan

Email: munawar_arif@hotmail.com

DATE OF BIRTH	NATIONALITY	N.I.C. NUMBER
23-03-1976	Pakistani	31103-1110477-1

Ph.D Thesis (Analytical Chemistry) University of Vienna, Austria (January 2009-Continued)

M.Sc. (Chemistry) 1999, Islamia University Bahawalpur, Pakistan

B.Sc. (Pre-Medical) 1996, Govt. College Bahawal Nagar, Pakistan

F.Sc. (Pre-Medical) 1994, Govt. College Bahawal Nagar, Pakistan

S.S.C. 1992, Govt. High School Fort Abbas, Pakistan

Awards / Distinction Certificates / Medals

1) Distinction Certificate and Silver Medal in matriculation presented by Board of Intermediate and Secondary Education Bahawalpur, Pakistan, (1992)

2) Talented Student of Punjab Certificate presented by Punjab Boards Committee of Chairmen, Pakistan, (1993)

3) Merit and Distinction Certificate in M.Sc Chemistry presented by Islamia University Bahawalpur, Pakistan, (1999)

4) PhD scholarship for Austrian University awarded by Higher Education Commission of Pakistan, (2008)